Drug repurposing against the store-operated calcium entry (SOCE) pathway and subsequent exploration of SOCE in oligodendrocyte progenitor cells

Md Saifur Rahman

Wolfson College

Department of Pharmacology

University of Cambridge

The dissertation is submitted for the degree of

Doctor of Philosophy

January 2020

Declaration

This dissertation is the result of my own work and includes nothing which is the outcome of work done in collaboration except where specifically indicated in the text.

My dissertation is not substantially the same as any that I have submitted for a degree or diploma or other qualification at any other University. I further state that no part of my dissertation has already been or is being concurrently submitted for any such degree, diploma or other qualification. Chapter 3 of this thesis has been published as 'Rahman Saifur and Rahman Taufiq. 2017. "Unveiling some FDA-approved drugs as inhibitors of the store-operated Ca^{2+} entry pathway." *Sci Rep* 7(1):12881.'

I hereby declare that my dissertation does not exceed the limit of length of 60,000 words prescribed in the Special Regulations of the PhD examination for which I am a candidate.

Abstract

Name: Md Saifur Rahman

Thesis title: Drug repurposing against the store-operated calcium entry (SOCE) pathway and subsequent exploration of SOCE in oligodendrocyte progenitor cells

The store-operated calcium entry (SOCE) pathway is an important route for generating cytosolic Ca^{2+} signals that regulate a diverse array of biological processes. Abnormal SOCE seem to underlie several diseases that notably include allergy, inflammation, acute pancreatitis and cancer. Therefore, any modulator of this pathway is likely to have significant impact in cell biology under both normal and abnormal conditions. In this study, the FDA-approved drug library was screened for agents that share significant similarity in 3D shape and surface electrostatics with few, hitherto best-known inhibitors of SOCE. This has led to the identification of five drugs that showed dose-dependent inhibition of SOCE in cell-based assay, probably through blocking SOCE pathway extracellularly. Of these drugs, leflunomide and teriflunomide could suppress SOCE significantly at clinically-relevant doses and this provides for an additional mechanism towards the therapeutic utility of these drugs as immunosuppressants.

Few more compounds from each of the 4 different pharmacological classes were further tested using cell-based methods to find agents with more potent SOCE-inhibitory potency. Three candidates with better potency namely trequinsin, roflumilast N-oxide and vidofludimus, were identified. Of these compounds, vidofludimus which is known to be an inhibitor of the dihydroorotate dehydrogenase (DHODH) enzyme, proved to be the most potent (IC_{50}~1.4μM) SOCE inhibitor among all the drugs tested, inhibitor of SOCE as it could suppress SOCE significantly at nanomolar dose.

Next, selected drugs identified with SOCE suppressive ability were evaluated against the proliferation of different lung cancer cells namely H520, H1752, and LK2. In agreement with previous studies with bona fide SOCE inhibitors, the chosen drugs significantly reduced proliferation of those lung cancer cells.

Although the possible contribution of the inhibition of the known targets of these drugs towards their anti-proliferative activity could not be ruled out, it was nevertheless indicative of the fact that their SOCE-inhibitory property was definitely implicated.

This, in agreement with existing literature, hinted towards the fact that SOCE can be targeted to achieve potential therapeutic benefit against lung cancer and other cancer cells of epithelial origins.

Of the drugs identified at the early phase of the present work to possess SOCE suppressive ability, teriflunomide is approved for multiple sclerosis (MS) which is believed to be autoimmune origin. The pro-drug of teriflunomide is leflunomide which is approved for managing rheumatoid arthritis. Since oligodendrocytes progenitor cells (OPCs) play important role in MS due to their myelin forming ability upon differentiation, SOCE was characterized in OPCs using single cell Ca^{2+} imaging approach and effect of some SOCE inhibitory compounds were then evaluated for any role in OPC differentiation. Employing different biochemical and imaging methods, AnCoA4, a known SOCE blocker was found to promote differentiation of OPCs. This finding could help to identify new target to develop therapeutic for demyelinating diseases like MS.

Acknowledgements

I would like to thank my supervisor Dr. Taufiq Rahman for his guidance, constant support and encouragement during my PhD. I am also grateful to Prof. Robin Franklin at Cambridge Stem cell Institute for his laboratory support to get primary training on OPCs isolation and culture. Many thanks to Dr. Graham ladds lab for the assistance with cell proliferation assay.

I would also like to express my gratitude and appreciation to all the members of the Department of Pharmacology, Cambridge for their help and kindness. Special gratitude to my family members those who supported me throughout my PhD.

Finally, special gratitude to Yousef Jameel Cambridge Trust for their studentship to support my PhD.

Table of contents

Page Number

List of Figures

Page Number

List of Tables

Page Number

List of Abbreviations

2-APB	2-Aminoethoxydiphenyl borate
ANOVA	Analysis of variance
ATF	Activating transcription factor
BSA	Bovine serum albumin
bFGF	Basic fibroblast growth factor
$[Ca^{2+}]_i$	Intracellular free Ca^{2+} concentration
CCE	Capacitative Ca^{2+} entry
CCh	Carbachol
CICR	Ca^{2+}-induced Ca^{2+} release
CNPase	2',3'-Cyclic-nucleotide 3'-phosphodiesterase
CRACM1	Ca^{2+} release-activated Ca^{2+} modulator 1 (also known as Orai1)
CREB	cAMP response element-binding
DAG	Diacylglycerol
DIC	Differential interference contrast
DMEM	Dulbecco's Modified Eagle's Medium
DMSO	Dimethyl sulfoxide
ER	Endoplasmic reticulum
Fura-2/AM	Fura-2 acetoxymethyl
GFAP	Glial fibrillary acidic protein
I_{CRAC}	Ca^{2+} release-activated Ca^{2+} current
IP_3	Inositol 1,4,5-trisphosphate
IP_3Rs	Inositol 1,4,5-trisphosphate receptors
LEDs	light-emitting diodes

MBP Myelin basic protein

mRNA messenger RNA

MS Multiple sclerosis

Non-SOCE Non-store-operated Ca^{2+}entry

NG2 Neural/glial antigen 2

OAG 1-oleoyl-2-acetyl-sn-glycerol

OLGs Oligodendrocytes

Olig2 Oligodendrocytes 2

OPCs Oligodendrocyte progenitor cells

PCNA Proliferating cell nuclear antigen

PDGF Platelet-derived growth factor

PIP_2 Phosphatidyl inositol 4,5-bisphosphate

PKC Protein kinase C

PLC Phospholipase C

PM Plasma membrane

PMCA Plasma membrane Ca2+-ATPase

PKC Protein kinase C

PLC Phospholipase C

PM Plasma membrane

ROCE Receptor-operated Ca^{2+}channel entry

RR-MS Relapse remitting multiple sclerosis

RYRs Ryanodine receptors

SAM Sterile-motif

SCID Severe combined immunodeficiency disorder

SERCA Sarco/endoplasmic reticulum Ca^{2+}-ATPase

SOC Store-operated Ca^{2+}channel

SOCE Store-operated Ca^{2+}entry

STIM1 Stromal-interaction molecule 1

Tg Thapsigargin

TRPC Transient potential receptor channel

VGCC Voltage-gated Ca^{2+}channel

Chapter 1

Introduction

1.1 Store operated calcium entry pathway

Ca^{2+} is a versatile an intracellular messenger that controls a diverse range of biological processes including fertilisation, differentiation, growth and proliferation, gene transcription, contraction, exocytosis and cell death (Berridge et al. 2000; Carafoli 2002). With the help of various pumps and transporters which are often energized, cytosolic free Ca^{2+} concentration ($[Ca^{2+}]_i$) is maintained at low (100-300nM) level under resting condition. A Ca^{2+} signal is effectively switched on with the transient increase of $[Ca^{2+}]_i$ from the resting nanomolar level to a global maximum of ~1μM (Berridge et al. 2003). In order to generate such signals, cells secure the 'extra' Ca^{2+} from the internal stores (notably the sarcoplasmic or endoplasmic reticulum, SR or ER respectively but also from some other organelles such as lysosome, mitochondria, nucleoplasm etc.) as well as from the extracellular space. In excitable cells such as neurons, Ca^{2+} entry across the plasma membrane (PM) occurs mainly through voltage gated Ca^{2+} channels (VGCCs) following depolarisation of the PM. Non-excitable cells such as smooth muscle cells and immune cells essentially lack such VGCC-mediated Ca^{2+} entry. Instead, these cells employ several non-voltage-gated Ca^{2+} influx mechanisms that notably include the store operated Ca^{2+} entry (SOCE) pathway (Parekh 2010).

SOCE, originally termed as the 'capacitative calcium entry (CCE)' (Putney et al. 2001), is triggered by the depletion of endoplasmic reticulum (ER) Ca^{2+} stores either by physiological or pharmacological means (Prakriya and Lewis 2015). Ca^{2+} entry via this pathway replenishes the depleted stores but emerging evidence suggests that it also can couple to specific biological processes (Kar and Parekh 2013; Putney 2005).

Physiologically, activation of SOCE occurs in the wake of agonist stimulation of $G_{q/11}$ protein-coupled receptors (for example, muscarinic M_1 or M_3 receptor) or certain growth factor receptors in the PM and this in turn activates phospholipase C isoforms (PLC_β, PLC_γ). The latter then catalyses the hydrolysis of phosphatidylinositol 4,5-bisphosphate (PIP_2), a membrane bound phospholipid, into the second messengers, inositol 1, 4, 5- trisphosphate (IP_3) and diacylglycerol (DAG). The latter is well-known to trigger the receptor-operated Ca^{2+} entry (ROCE) pathway through activation of members of the transient receptor potential family C (TRPC) channels and also known to activate protein kinase C (PKC) (Hofmann et al. 1999; Martin 2006). IP_3 diffuses through the cytosol and binds to and activates inositol 1, 4, 5-trisphosphate receptors (IP_3Rs) located within the membrane of the endoplasmic reticulum (ER). Opening of these channels allows Ca^{2+} to move down its concentration gradient from lumen of the ER into the cytosol and this leads to depletion of the ER luminal Ca^{2+} stores

(Bootman et al. 2001). The latter which is often termed as 'the store depletion' in turn triggers SOCE, thereby allowing a slow and sustained Ca^{2+} entry across the PM. As Ca^{2+} store becomes replenished, SOCE is terminated (Smyth et al. 2010).

Activation of SOCE surely requires depletion of internal Ca^{2+} stores but it appears to be independent of how stores are depleted. Thus apart from physiological means (for instance, stimulating cell surface receptors that produce IP_3), SOCE can be triggered pharmacologically by using tools that directly (for example, ionomycin, a Ca^{2+} ionophore or TPEN, a luminal Ca^{2+} chelator) or passively (for example, thapsigargin - an inhibitor of the the sarco/endoplasmic reticulum Ca^{2+}-ATPase (SERCA) pump) deplete the internal Ca^{2+} stores (Parekh and Putney 2005) (**Fig. 1.1**).

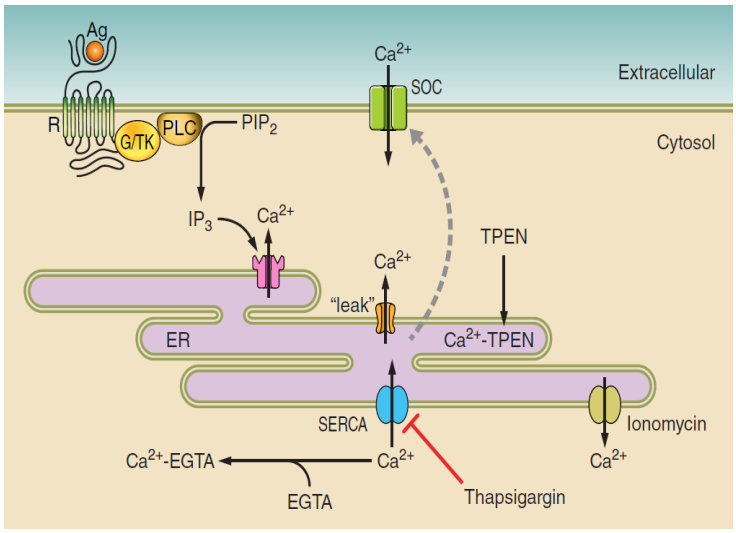

Figure 1.1 Store-operated calcium entry. Binding of an agonist (Ag) to receptor (R) activates phospholipase C (PLC) that hydrolyzes PIP_2 and produces IP_3. The latter then open IP_3Rs within the ER membrane, via which Ca^{2+} is rapidly drained into the cytosol from the lumen of the ER. The latter becomes emptied and thereby leads to the activation of SOCE in the PM. SOCs are also activated by the consequent reduction of ER luminal $[Ca^{2+}]_i$. SOCE can be activated by chelating intracellular Ca^{2+} with EGTA, inhibiting SERCA pumps with thapsigargin, releasing Ca^{2+} from the ER with ionomycin, or chelating intraluminal Ca^{2+} with TPEN. Figure is taken from Prakriya and Lewis 2015.

1.1.1 Proteins underlying the SOCE pathway

Since the first proposal of SOCE pathway (Putney 1986), its molecular mechanism including the identity of the channel protein(s) that mediate the Ca^{2+} entry and how the channels underlying SOCE sense and respond to the store depletion remained elusive for many years. Till 2006, some Ca^{2+}-permeable members of the mammalian transient receptor protein (TRP) family (notably TRPC1, TRPC3 and TRPV6) were among the most widely-proposed candidates to mediate the SOCE, although none of them when expressed heterologously fully match the biophysical properties of I_{CRAC} (Ca^{2+} release-activated Ca^{2+} current) and for some of the candidates, it was even not clear whether their activation was truly store-dependent (Prakriya and Lewis 2015). The mechanism coupling ER Ca^{2+} depletion to CRAC channels activation, despite over a dozen proposed schemes, also remained largely unknown for a long time till 2005.

In 2005, a real breakthrough happened in the SOCE field with two research groups led by Meyer (Liou et al. 2005) and Stauderman (Roos et al. 2005) independently establishing the same protein namely STIM1(stromal interaction molecule 1) as an ER membrane protein that senses the change in ER Ca^{2+} levels. Another breakthrough occurred in the following year with the identification of a protein namely Orai1 (Prakriya et al. 2006) or CRACM1 (Ca^{2+} release-activated Ca^{2+} modulator 1) (Vig et al. 2006) as the pore-forming subunit of the CRAC channel in two independent studies. With the discovery of STIM and Orai, the molecular mechanism of CRAC channel activation has been extensively studied worldwide and we now have a basic understanding of the choreography of molecular events that begins with Ca^{2+} release in ER and culminates in Ca^{2+} entry through CRAC channels.

STIM1

STIM1is a 77kDa type 1 membrane protein, the majority of which is located in the ER membrane though up to 25% of STIM1 expression can be identified in the PM (Lewis 2007; Zhang et al. 2005). In vertebrates there are two STIM homologues; STIM1 and STIM2 (Liou et al. 2005). STIM1 is composed of multiple domains that include an unpaired EF-hand and sterile α-motif (SAM) domain that reside within the ER lumen at the N-terminal region of the protein and a coiled-coil (CC)/ezrin-radixin-moesin (ERM), serine/proline-rich and lysine-rich domain residing within the cytosol at the C-terminal region of the protein. Several amino acids from both EF hands come together to form a hydrophobic cleft that interacts with, and stabilizes, the hydrophobic, helix-rich SAM domain (Stathopulos et al. 2008).

STIM1 is predicted to sense the level of Ca^{2+} within the ER through its unpaired EF-hand domain (Zhang et al. 2005).

STIM2

STIM2 is also a type 1 membrane protein that shares 66% sequence homology with STIM1 (Williams et al. 2001). This protein also has an EF hand and SAM domain within the ER and a CC, serine/proline and lysine-rich domain reside within the cell cytosol at the C-terminal region of the protein (Williams et al. 2001; Zheng et al. 2008). Unlike STIM1, STIM2 is mainly expressed in ER membrane whereas the former also expresses in the PM (Zheng et al., 2008). Likewise, STIM1, STIM2, also can be translocated to ER-PM junctions in response to ER depletion and can activate SOCE through interaction with Orai1. However, STIM2 only respond to little decreases in ER-Ca^{2+} level (Brandman et al., 2007).

Orai1

Orai1 is a 33kDa protein with four transmembrane domains (TM1-TM4) located within the PM with both N- and C-termini facing towards the cytosol (Prakriya et al. 2006). In vertebrates there are three Orai homologues namely Orai1, Orai2 and Orai3 (Feske et al. 2006). In 2006, Orai1 was first identified as an essential component of SOCE (Feske et al. 2006; Zhang et al. 2006). T cells from patients with severe combined immunodeficiency (SCID) syndrome failed to activate SOCE following store depletion (Feske et al. 2005) which was later attributed to a single point mutation (R91W) in Orai1 (Feske et al. 2006). Furthermore, transfection with wild-type Orai1 in cells derived from SCID patients restored SOCE.

Orai2

Orai2 forms complex with STIM1 in HEK293 cells to enhance SOCE though to a lesser extent than Orai1 (Mercer et al. 2006).

Orai3

Unlike Orai1 and Orai2, Orai3 usually does not involve in SOCE pathway (Mercer et al. 2006; DeHaven et al. 2007). Mutation of Orai3 gene in HEK293 cells had no effect on SOCE (Mignen et al. 2008). However, Orai3 may be involved in SOCE in some extent as Orai3 expression in Orai1 knockdown cells rescued SOCE (Mercer et al. 2006).

Figure 1.2 demonstrates the activation of the STIM proteins, the subsequent coupling of STIM1 to Orai1, and the consequent structural rearrangements that gate the Orai channels into the open state to allow Ca^{2+} permeation into the cell.

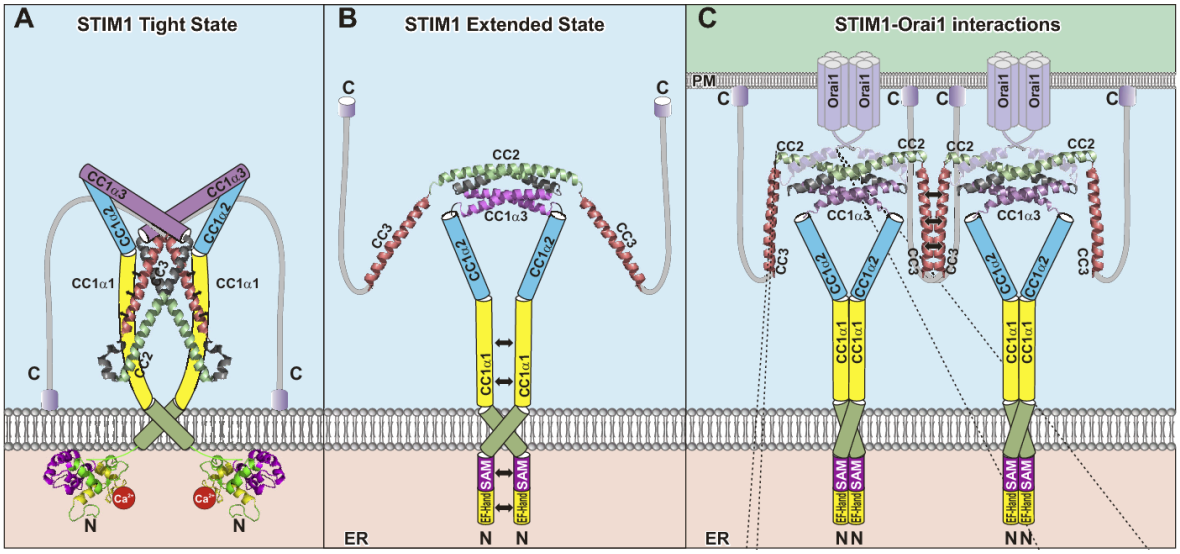

Figure 1.2 Hypothetical model for the coupling of STIM1 and Orai1. After store depletion, STIM1 proteins lose the Ca^{2+} bound to the luminal EF-hand and undergo a conformational change from the inactive, tight state **(A)** to the active, extended state **(B)**. Thereby, the crossing angle of the TM helices alters and the inhibitory, intramolecular clamp between CC1α1 and CC3 is released. **(C)** Extension of STIM1 proteins leads to the interaction with Orai1, is accompanied by oligomerization of STIM1 proteins to larger aggregates than dimers and involves the CC3 domains. Image is taken from Derler et al. 2016.

TRPC1

TRPC1, a 90kDa PM protein, has been implicated in SOCE in many cell types (Parekh and Putney 2005). For instance, knockout of TRPC1 in submaxillary acinar mouse cells caused an 80% reduction in SOCE (Liu et al. 2007). However, role of TRPC in SOCE pathway is still unclear as several studies have shown that TRPC1 is not involved in SOCE.

Most of the controversy surrounding the role of TRPC1 as a SOCE is due to its well-established role as receptor-operated calcium channel (ROCC), a non-voltage gated Ca^{2+} permeable channel activated by agonists acting on a range of G-protein-coupled receptors. However, studies showed TRPC1 can function as both a ROCE and a SOCE in a STIM1 dependent manner (Alicia et al. 2008). TRPC1 activates SOCE by interacting with STIM1 and this interaction disrupted upon knockdown of STIM1, which indicated TRPC1 is STIM1 dependent (Yuan et al., 2007). TRPC1 forms complex with STIM1 in ER-PM junction area when ER-

Ca^{2+} is depleted (Huang et al. 2006). Studies also have shown that following store depletion, the interaction between STIM1 and TRPC1 is increased (Huang et al. 2006; Lopez et al. 2006; Alicia et al. 2008; Ng et al. 2009).

1.1.2 SOCE channel vs CRAC channel

Now its substantially evident that STIM1 acts as the ER Ca^{2+} sensor that signals store depletion to Orai1, the pore forming subunit of the SOCE channel, together forming the elementary unit of SOCE (Luik et al. 2006). However, before these discoveries, TRPC1 was a sole candidate for SOCE channel although its role in SOCE still remains controversial (Alicia et al. 2008).

Variants of SOCE channels have been described in different cell types, based on the distinct biophysical properties of the Ca^{2+} current that underlies SOCE (Roos et al. 2005; Cheng et al. 2008). For instance, a popular notion exists in this field that the I_{CRAC}, which is highly selective to Ca^{2+} current, can be interceded through Orai1 channels (Prakriya et al. 2004; Parekh and Putney 2005), on the other side, the store-operated Ca^{2+} current (I_{SOC}), a non-selective Ca^{2+} current is mediated through TRPC1 channels (Liu et al. 2007). Moreover, in some cases, cells could form a 'complex of STIM1, Orai1 and TRPC1' to constitute SOCE (Ong et al. 2007; Liao et al. 2009; Cheng et al. 2008).

However, till now the best characterised current representing the SOCE is the I_{CRAC} which was first recorded in T lymphocytes (Lewis and Cahalan 1989) and mast cells (Matthews et al. 1989) following physiological stimulation with antigen or agonists. Subsequently, similar currents were recorded following pharmacological (e.g. thapsigargin (Tg)), IP_3 or ionomycin mediated) depletion of intracellular Ca^{2+} stores in Jurkat T cells (Zweifach and Lewis 1993) and RBL cells (Hoth and Penner 1992) establishing store-depletion as the proximal stimulus for channel activation. I_{CRAC} is characterized by its high selectivity for Ca^{2+}, an inwardly rectifying current-voltage relationship, and an extremely small single-channel conductance in the sub-pico siemens range (Hoth and Penner 1993; Prakriya and Lewis 2015).

1.1.3 Mechanism underlying CRAC channels activation

Under resting condition, STIM1 is homogeneously distributed within the ER membrane. Cell surface stimulation of the PLC-coupled receptors or pharmacological manipulation (for e.g. Tg, ionomycin or TPEN) causes loss of Ca^{2+} from the ER lumen and this results in Ca^{2+} dissociation from the luminal EF hand (helix loop helix structural domain) of STIM1 (Liou et al. 2005; Zhang et al. 2005). This reduces the intramolecular interactions between the EF hands and the SAM domain leading to the partial unfolding of STIM1 (Stathopulos et al. 2008). STIM1 oligomers form due to the homotypic interaction between exposed hydrophobic SAM domains (Stathopulos et al. 2008). The oligomers then migrate to specialized endoplasmic reticulum–plasma membrane (ER-PM) junctions (Liou et al. 2007), which are located within 10-25 nm of the PM (Wu et al. 2006). Olimerization alone leads the STIM1 accumulation at ER-PM junction regardless of the presence of a full Ca^{2+} store, however, this is not enough to activate Orai1 (Park et al. 2009). Although it is still not clear what precisely pushes clustered STIM1 proteins to the cell periphery but surely this does not require Orai1 (Wu et al. 2006). Nevertheless Orai1–STIM1 interactions stabilize STIM1 at the PM (Park et al. 2009). A cytosolic region of STIM1 (the CRAC activation domain, CAD; also known as the STIM1 Orai1-activating region, SOAR) has been established to be essential for CRAC channel activation (Muik et al. 2009). This domain is probably exposed on STIM1 oligomerization and binds directly to both the N and C termini of Orai1 to open the channels (Park et al. 2009). CRAC channel activation is briefly shown in **Fig. 1.3**.

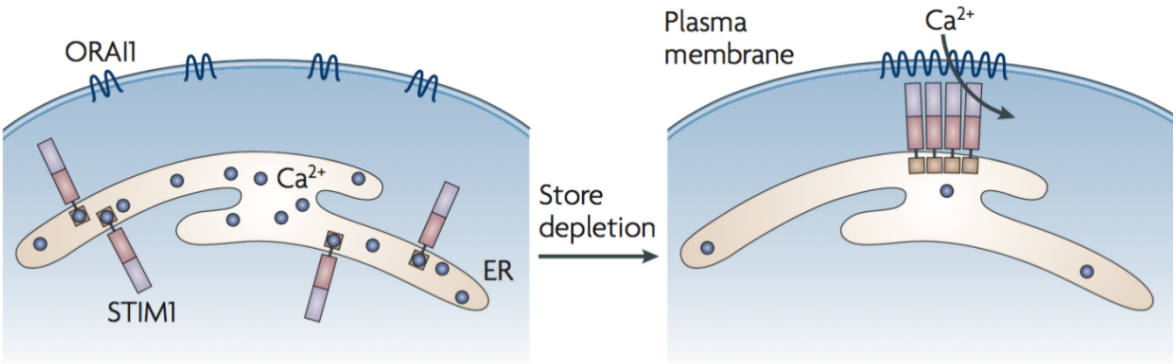

Figure 1.3 Possible gating mechanism of CRAC channels. In cells with full Ca^{2+} stores, STIM1 is homogenously distributed in the ER with its EF hand occupied with Ca^{2+}. Orai1 is dispersed throughout the PM. Upon stimulation with physiological or pharmacological means, the Ca^{2+} content of the store falls. Ca^{2+} dissociates from STIM1 and this results in STIM1 oligomerization and subsequent migration to ER-PM junctions. At this point, STIM1 captures diffusing Orai1 channels. Interaction between the amino and carboxyl termini of Orai1 with the CAD of STIM1 leads to CRAC channel opening. The figure has been taken from Parekh 2010.

1.1.4 Physiological role of SOCE pathway

SOCE in non-excitable cells provides for a means to replenish the internal Ca^{2+} stores for next round of Ca^{2+} release. This mechanism holds true for the excitable cells such as neurones as well (Wu et al. 2011). However, apart from this fundamental role, Ca^{2+} emanating from the open CRAC channels form microdomains near the vicinity of the open pore of these channels, largely due to poor diffusibility of Ca^{2+} in cytosol. Intriguingly, interesting links have been established with the store depletion and cAMP signalling where interplays between STIM1/Orai1 and Ca^{2+} sensitive adenyl cyclases have been reported (Lefkimmiatis et al. 2009).

The 'local' Ca^{2+} signals generated by SOCE pathway seem to couple to specific biological processes such as regulation of various Ca^{2+}-sensitive enzymes as well as activation of certain genes. The notable example of the latter includes activation and nuclear translocation of the nuclear factor of activated T cells (NFAT) (Parekh 2008; Ng et al. 2009).

In resting cells, NFAT proteins are phosphorylated and reside in the cytoplasm; on stimulation, during a sustained elevation of Ca^{2+}, they are dephosphorylated by calcineurin and translocated to the nucleus. Once in the nucleus, NFAT proteins become transcriptionally active and bind to consensus DNA sites, therein controlling the transcription of target genes (**Fig. 1.4**). On cessation of Ca^{2+} signalling, NFAT proteins are re-phosphorylated and translocated back to the cytoplasm, resulting in the termination of their activities (Macián et al. 2002).

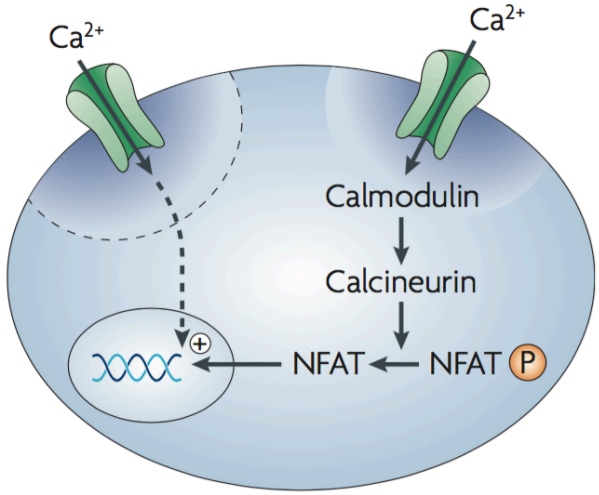

Figure 1.4 SOCE drives NFAT translocation into nucleus.

The figure is taken from Parekh 2010.

1.1.5 Abnormal SOCE pathway in diseases

Aberrant SOCE pathway over the years has been implicated in several diseases including severe combined immunodeficiency (SCID) disorders, allergy, inflammatory bowel disease, neurodegenerative diseases, and cardiovascular disorders (Parekh 2010; Roberts-Thomson et al. 2010). STIM/ORAI-mediated SOCE plays important roles in the proliferation and metastasis of cancer cells. The exact function and mechanism are complicated and context-dependent (Mukherjee and Brooks 2014; Roberts-Thomson et al. 2010), such complications are summarized in **table 1.1**.

SOCE in severe combined immunodeficiency (SCID)

In severe combined immunodeficiency SCID diseases, I_{crac} is absent and T cell activation is severely impaired (Feske et al. 2005). SCID patients have the genetic defect to a region of approximately 74 genes on chromosome 12. ORAI1 was mapped to the SCID defect region in chromosome 12. The SCID sufferers had a single point mutation (R91W) in ORAI1 within the coding region (figure 03). This mutation led to the complete loss of I_{CRAC} (Feske et al. 2006).

SOCE in allergic disorders

Excursive mast cells activation is linked to a range of allergic disorders including asthma, rhinitis, eczema and nasal polyposis (Peters-Golden et al. 2006). Nasal polyposis is an inflammatory disease of the upper respiratory tract. The polyps are rich in mast cells and eosinophils (Di Capite et al. 2009). However, presence of I_{crac} in polyps has been demonstrated. Partial blocking of CRAC channel has been proven as effective in dampening down mast-cell activation (Di Capite et al. 2009).

SOCE in antitumor immunity regulation

SOCE regulates antitumor immunity by inducing the activation of Ca^{2+}-dependent transcription factors, such as NFAT, cAMP response element-binding protein (CREB) or activating transcription factor (ATF) 2. These factors are essential for the development and normal function of immune cells (Kreideweiss et al. 1999). SOCE also promotes the production of cytokines and chemokines that can directly kill cancer cells.

SOCE in apoptotic cell death, proliferation and metastasis of cancer cells

Inhibition of SOCE through STIM1 knockdown shows the upregulation of p21 and the downregulation of Cdc25C, cyclin E, cyclin D, CDCK2 and CDCK4, which eventually elicits cell cycle arrest (Chen et al. 2011) . STIM1 and Orai1 knockdown impair adhesion turnover and cell migration (Yang et al. 2013; Chen et al. 2011; Yang et al. 2009). Due to deviant SOCE, Ca^{2+}-regulated protease calpain and the cytoplasmic kinase Pyk2 become activated, which essentially regulate the focal adhesion dynamics of migratory cervical cancer cells (Chen et al. 2011). STIM1 over expression enhances the colorectal cancer cells migration via an increase in the expression of cyclooxygenase-2 (COX-2) and the production of prostaglandin E2 (PGE2) (Wang et al. 2015).

SOCE in tumour angiogenesis

SOCE promotes the recruitment of new blood vessels, or angiogenesis through regulating the production of vascular endothelial growth factor (VEGF), which is critical for the formation of new blood vessels (Chen et al. 2011). Ca^{2+}-dependent activation of NFAT also regulates the expression of key molecules such as tissue factor (TF) and COX-2. These molecules are very important for endothelial cell migration, tube formation and angiogenesis (Armesilla et al. 1999; Hernández et al. 2001).

Table 1.1 below provides some evidence implicating SOCE and its underlying protein players in promoting cancerous features in various cell types.

Table 1.1 Aberrant SOCE in different cancer cells

Ca^{2+} channel	Cancer cell type	Possible mechanisms	Major effects	Reference
STIM1-Orai1	Cervical cancer SiHa and Caski cell	STIM1 knockdown induces cell cycle arrest and tumorigenesis	Promotion of tumour cell growth, migration and invasion	Chen et al. 2011
STIM1-Orai1	Ovarian cancer A2780 cells	ORAI1/STIM1 enhances AKT activity	Contribution to cisplatin resistance	Schmidt et al. 2014
STIM1-Orai1	Breast cancer 4T1 cells	SOCE impairs focal adhesion turnover	Promotion of tumour metastasis	Yang et al. 2009
STIM1-Orai1	Colorectal cancer cells	STIM1 overexpression promotes EMT	Promotion of cell motility	Wang et al. 2015
STIM1-Orai1	Hepatocarcinoma HCC-LM3 cells	STIM1 impairs focal adhesion turnover	Promotion of cell migration and invasion	Yang et al. 2013
STIM1-Orai1	Glioblastoma U251 cells	STIM1 suppression induces cell cycle arrest	Promotion of cell proliferation and migration	Li et al. 2013
STIM1-Orai1	Epidermoid carcinoma A431 cells	STIM1 knockdown inhibits DNA synthesis and decreases EGFR phosphorylation	Promotion of cell and tumour growth	Yoshida et al. 2012
STIM1-Orai1	Melanoma cells	SOCE activates the ERK signalling pathway	Promotion of cell proliferation and migration	Umemura et al. 2014
Orai3	Breast cancer MCF-7 cells	ORAI3 knockdown reduces c-Myc expression and activity	Promotion of cell growth, invasion and tumorigeneses	Faouzi et al. 2013
TRPC3	Ovarian cancer SKOV-3 cells	TRPC3 inhibition dephosphorylates Cdc2 and	Promotion of cell proliferation	Yang et al. 2009

		induces G2/M phase arrest.	and tumour formation	
TRPC6	Gastric cancer AGS cells	TRPC6 blockade induces G2/M phase and arrest	Increase cell growth and tumour formation in mice	Cai et al. 2009
TRPC6	Glioblastoma U373 cells	TRPC6 activates NFAT pathway	Promotion of cell growth, invasion and angiogenesis	Chigurupati et al. 2010

1.1.6 Pharmacology of SOCE/CRAC channels

The complexity of CRAC channel activation process, such as protein-protein and ER-PM interactions, opens up potential scopes for pharmacological modulation of the SOCE pathway (Luik and Lewis 2007). Historically, few inhibitors have been widely used for the characterisation as well as evaluating the biological roles of CRAC channels in various tissues. However, their precise mechanisms of action on CRAC channel remains largely unclear (Jairaman and Prakriya 2013).

Given the emerging roles of the CRAC channels in the pathogenesis of various diseases mentioned earlier (Parekh 2010), there have been interests by academics as well as pharmaceutical companies to develop specific inhibitors of these channels and in recent time, there have been few synthetic small molecules with improved potency and selectivity towards CRAC channels (Putney 2010; Prakriya and Lewis 2015). Few of these molecules are claimed to be selective for particular proteins like Orai1. Nevertheless, even for most of these new generation CRAC modulators, the precise mechanism of action remains insufficiently understood. Most common modulators of SOCE or CRAC channels are summarised in **table 1.2**, based on what is known about them (Jairaman and Prakriya 2013; Parekh 2010).

Table 1.2 Common modulators of SOCE/CRAC channels

Category	Compound	Effect	Mechanism	IC_{50}	Reference
Ions	La^{3+}	Inhibition	Pore blockade	3358nM, (SOCE), 240nM,(Orai1), 470nM,(Orai3)	(Ross and Cahalan 1995; Yamashita and Prakriya 2014)
	Gd^{3+}	Inhibition	Pore blockade	18–28 nM, (SOCE) 46 nM, (I_{CRAC})	(Ross and Cahalan 1995; Yeromin 2004)
	2-APB	Enhance STIM activated current	Unknown	3μM, (I_{CRAC}), 4μM, (Orai1)	(Peinelt et al. 2008; Prakriya and Lewis 2001)
	2-APB	Inhibition	Unknown	10μM, (I_{CRAC}) 8μM, (Orai1)	(Prakriya and Lewis 2001;Peinelt et al. 2008)
	2-APB	Activation	Direct channel activation?	24μM, (Orai3, I_{CRAC}) 15μM, (Orai3,SOCE)	(Peinelt et al. 2008; Yamashita and Prakriya 2014)
	2-APB analogues	Inhibition	Unknown	90–170 nM (I_{CRAC})	(Goto et al. 2010)
Small molecules	ML-9	Inhibition	Inhibits STIM translocation	16μM (SOCE)	(Smyth et al. 2008)
	BTP2 (YM58483)	Inhibition	Unknown	100-150nM (SOCE; acute), 6–12nM (SOCE; 24 h pre-incubation) 0.5–2.2μM (I_{CRAC}; acute)	(Ishikawa et al. 2003; Takezawa et al. 2006; Zitt et al. 2004)
	Synta66	Inhibition	Unknown	3μM (I_{CRAC})	(Ng et al. 2008)
	Econazole	Inhibition	Unknown	0.6–14μM (I_{CRAC})	(Franzius et al. 1994)
	SK&F96365	Inhibition	Unknown	4μM (I_{CRAC})	(Franzius et al. 1994)
	GSK-7975A GSK-5503A	Inhibition	Unknown	4μM (Orai1)	(Derler et al. 2013)
	RO2959	Inhibition	Unknown	25nM (Orai1) 530nM (Orai3)	(Chen et al. 2013)
	AnCoA4	Inhibition	Inhibits Orai1	1–10μM (Orai1)	(Sadaghiani et al. 2014)
Antibodies	monoclonal Ab	Inhibition	Inhibits Orai1	1nM (Orai1)	(Lin et al. 2013)
	Anti-Orai1 mAb	Inhibition	Inhibits Orai1	<1nM (SOCE)	(Cox et al. 2013)

1.2 Virtual Screening

Virtual screening is a cost-efficient and time-efficient high-throughput method used to select promising lead candidates from a vast chemical space based on information from either a) the structure of the ligand binding site (LBS) of a receptor or b) the chemical structure of known ligands. The former is termed as structure-based virtual screening (SBVS) while the latter is called as ligand-based virtual screening (LBVS). Virtual screening methods have been widely used in the industry as well as in the academia, parallel to wet high throughput screening for finding new chemical scaffolds as hits/leads towards developing new therapeutic entities.

Since SOCE channel is implicated in various diseases mentioned above, there has been legitimate interest in pharmaceutical and academic communities towards developing selective inhibitors of this pathway. In recent time, there have been developed few synthetic small molecules with improved potency and selectivity towards CRAC channels (Putney 2010; Prakriya and Lewis 2015).

Rational ligand-based *in silico* approach (Yan et al. 2015) approach can be utilised to find new molecules as SOCE inhibitor through exploiting the structures of few existing CRAC inhibitors. Since the database of the officially approved drugs is publicly available therefore whether any drug with hitherto no known effect on SOCE pathway can be identified through such *in silico* ligand-based approach. The latter thus essentially entails a drug repositioning (Langedijk et al. 2015) endeavour against the SOCE pathway.

1.3 Primary aims and objectives

Based on the studies done by various groups so far, it is perhaps fair to say that SOCE/CRAC channels are valid therapeutic targets against some diseases that notably include some cancer and few that stem from autoimmunity (Parekh 2010; Feske 2019). Although to date, there are several small molecule inhibitors of SOCE developed with few being in early phase of clinical trial (Stauderman 2018), most of the existing molecules suffer from the lack of adequate selectivity, potency as well as clear mechanism of actions. Few such molecules also have effects on other channel, transporters and pumps and cytoskeleton (Prakriya and Lewis 2015), and thus only useful as tool compounds whilst those in early phase of clinical trials may or may not succeed in successfully completing final phase of clinical trials. Therefore, the need for identifying new scaffolds against SOCE/CRAC channels remains still valid for future developing of more specific inhibitors with greater potency and with the mechanism of action deciphered. In recent time, drug repurposing has been an attractive theme towards finding novel use of approved or investigational drugs at substantially reduced cost, time and risk (Schein 2019). Besides, such approach can also potentially reveal any beneficial or unwanted off target effect of a known agent. Apart from phenotypic screening, virtual screening and other in silico approaches have been proving to be useful techniques for drug repurposing endeavours.

The primary aims of the present work include:

(a) To find whether any of the existing drug(s) possess comparable similarities in 3D shape and surface electrostatics with those of few known SOCE modulators and verifying through bioassay the possible SOCE modulatory effect of few of the best hits from the virtual screening.

(b) If any drug candidate(s) available from (a) then exploring more drugs/analogues of similar class against SOCE pathway.

(c) Testing the best performing SOCE modulatory drugs or compounds in biological functioning aspect.

Chapter 2

Methods and materials

2.1 Materials

2.1.1 cell culture

Cell lines and their sources

Cell lines were kindly provided by different institute across the globe: rat basophilic leukemia-1 (RBL-1) cells (passage 11) from Professor Anant B. Parekh, Oxford University, Oxford, UK; SH-SY5Y cells (passage 20) from Professor Robin Irvine, University of Cambridge, Cambridge, UK; human jurkat T cells (passage 2) from Dr Heike Laman, University of Cambridge, Cambridge, UK; HEK293 cell line with an inducible mCherry-STIM1-T2A-Orai1-eGFP from Dr. Chan Young Park, UNIST, South Korea; HeLa cells stably expressing the NFAT1(1-460)-GFP fusion protein from Professor Patrick Hogan, La Jolla Instiute for Allergy and Immunology, CA, USA; and lung cancer cell lines from Dr. Graham Ladd, University of Cambridge, Cambridge, UK.

Cell medium and other elements

Dulbecco's Modified Eagle Medium (DMEM), Ham's F 12 media with L-Glutamine, 0.25% trypsin media, RPMI medium, fetal bovine serum, fetal calf serum and antibiotic antimycotic 100X mix, were used and bought from Life Technologies Ltd (Paisley, UK). Glass bottom petri-dishes (10mm) from MatTek corporation were used to culture the cells for confocal and Ca^{2+} imaging.

2.1.2 Drugs and compounds

Table 2.1 List of drugs and compounds tested against SOCE

Name	Supplier	Name	Supplier
Leflunomide	Tocris, UK	Terazosin	Sigma-Aldrich
Teriflunomide	Tocris, UK	Flutamide	Sigma-Aldrich
Tolvaptan	Tocris, UK	Roflumilast	Sigma-Aldrich
Omeprazole	Sigma-Aldrich	Conivaptan	Selleckchem
Lansoprazole	Sigma-Aldrich	Lixivaptan	Cayman Chemical
Rufinamide	Sigma-Aldrich	Mozavaptan	Cayman Chemical
Prazosin	Sigma-Aldrich	OPC 21268	Tocris, UK
STK485210	Selleckchem	Piclamilast	Sigma-Aldrich
PF 3716556	Tocris, UK	3,4-Bis Roflumilast	Biosynth Carbosynth
Roflumilast N-oxide	MedChemExpress	Trequinsin	Tocris, UK
BR1138	Tocris, UK	Cilostamide	Tocris, UK
BRL 50481	Tocris, UK	Rolipram	Tocris, UK
SR 49059	Sigma-Aldrich	ML390	Selleckchem
Brequinar	Tocris, UK	Atovaquone	Tocris, UK
Vidofludimus	Selleckchem	9090672	Selleckchem
9099120	Selleckchem	SCH 28080	Tocris, UK
Apremilast	MedChemExpress	Bay736691	Sigma-Aldrich
Milrinone	Tocris, UK		

2.1.3 Oligodendrocyte progenitor cells (OPCs) isolation and culture

2.1.3.1 Animals

For the experiments, timed pregnancies of the inbred Sprague-Dawley rats from Charles River UK, Ltd (Kent) were used. The rats were kept in the local animal facility (Dept. of Veterinary Medicine, University of Cambridge, UK) in a 12h light/dark cycle until the pups reached an age of postnatal day (P) 2.

2.1.3.2 Medium and solutions

Dissociation solution Hibernate media (Gibco) Papain (Worthington Biochem): 40µl/ml DNase I Type IV (Sigma): 10µl/ml L-Cysteine (Sigma): 2mM	**Ovomuccoid** L-15 media (Gibco) soybean trypsin inhibitor (Sigma): 1 mg/ml BSA V (Sigma): 50µg/ml DNase I Type IV (Sigma): 40 µg/ml
Dissection media DMEM/F-12 (Gibco) 10µl/ml of Penicillin/Streptomycin (Sigma)	**Mixed Glia Medium (MGM)** DMEM/F-12 (Gibco) 10% FCS (BioSera) Penicillin/Streptomycin (Gibco): 10µl/ml
OPC Medium DMEM with L-Glutamine and high Glucose BSA fraction V (Sigma): 330µg/ml Sodium selenite (Sigma): 0.25mg Progesterone (Sigma): 60ng/ml Sodium selenite (Sigma): 40ng/ml Putrescine (Sigma): 16µg/ml Insulin (Gibco):10µg/ ml Sodium pyruvate (GIBCO): 1mM Penicillin/Streptomycin (Gibco): 10µl/ml Apo-transferrin (Sigma): 50µg/ ml	**Milteny washing buffer (MWB)** BSA (Sigma): 0.5% EDTA (ThermoFisher): 2mM Sodium pyruvate (GIBCO): 2mM PBS (Gibco): 10% pH: 7.3 Deionized water **Trituration solution** Hibernate media supplemented with 2% B27 Sodium-pyruvate: 2mM Pluronic™ F-68 (Gibco): 1%
Differentiation medium OPC medium supplemented with daily addition of 40ng/ml tri-iodothyroxine (T_3) (Sigma)	**Proliferation medium** OPC medium supplemented with daily addition of 10ng/ml PDGF-AA and bFGF (Peprotech).

2.1.3.3 Immunocytochemistry

Table 2.2 Primary antibodies

Antigen	Host	Dilution	Supplier
Olig2	goat	1:500	R&D system
Olig2	rabbit	1:500	Millipore
GFAP	rabbit	1:1000	DAKO
CD11b	mouse	1:200	Abcam
NG2	rabbit	1:200	Millipore
MBP	rat	1:500	Serotec
PCNA	mouse	1:500	Santa Cruz
CNPase	mouse	1:500	Thermo Scientific

Table 2.3 Secondary antibodies

Conjugate	Reactivity	Dilution	Supplier
Alexa Fluor 488	goat	1:500	Invitrogen
Alexa Fluor 568	rabbit	1:500	Invitrogen
Alexa Fluor 568	rat	1:500	Invitrogen
Alexa Fluor 647	mouse	1:500	Invitrogen

2.1.4 Other chemicals and compounds

Fura-2/AM (Molecular Probes), Ionomycin (Calbiochem Darmstadt, Germany), MnCl2 (Sigma-aldrich), thapsigargin (Sigma-aldrich), Hank's Balanced Salt Solution (HBSS, with or without Ca^{2+}), carbachol (Sigma-aldrich), nifedipine (Tocris), SKF96365 (Tocris), potassium chloride (Sigma-aldrich), and Ca^{2+} solution (Sigma-aldrich), BTP2 (Tocris), 1-Oleoyl-2-acetyl-sn-glycerol (OAG) (Cayman Chemical) and AnCoA4 (Calbiochem).

2.2 Methods

2.2.1 Ligand-based screening of database of officially-approved drugs

The method reported by Naylor et al. 2019 was largely followed. Latest version of the eDrugs3D database were used that contains 1822 molecular structures comprising of 3D representations along with isomers of total 1557 FDA-approved drugs (Pihan et al. 2012). For each drug, up to 100 conformers were generated using OMEGA33 (version 2.5.1.4, OpenEye Scientific Software, Santa Fe, NM, USA). The query molecules (SOCE inhibitors) such as BTP2, Synta66, Pyr6 and AnCoA4 were drawn and energy-minimized with the Merck Molecular Force Field 94 using the ChemBioOffice Ultra 11.0 (Cambridge Soft Corporation, Cambridge, MA, USA). The energy-minimized structures of the query molecules were then used for generating the 3D queries. Each of the queries was then utilized to scan the above-mentioned conformer library generated from eDrugs3D by using Rapid Overlay of Chemical Screens (ROCS)35 (version 3.2.1.4, OpenEye Scientific Software, Santa Fe, NM) and all resulting hits were ranked with Tanimoto Combo (TC) score that represents a numerical sum of the shape Tanimoto (maximum value = 1) and scaled colour Tanimoto score (maximum value = 1).

The size of the screening output was limited to 500 molecules. The ROCS output was then used as an input to EON (version 2.2.0.5, OpenEye Scientific Software, Santa Fe, NM) for re-ranking the aligned molecules on the basis of their electrostatic similarity with the cognate query ligand. For this, the EON Tanimoto combo (ET combo) score was used which is the sum of the EON Poisson-Boltzmann and EON Shape Tanimoto scores. Default parameters were used throughout. VIDA (version 4.3.0.4, OpenEye Scientific Software, Santa Fe, NM) was used to visualize and analyze the outputs from screening done with ROCS and EON. VIDA and MacPyMol (version 1.7.2.1) were used for molecular representations.

For each query molecule, each hit molecule was visually inspected using VIDA and shortlisted 10 candidates on the basis of several aspects including their similarity in electrostatic isopotential contour surfaces (EON-generated) with the cognate bait, their TC score and ET_pb score, their rank and frequency of appearing within the top 100 hits in ROCS as well as EON based screening, previous reported activity on calcium signalling and availability. The chosen molecules were purchased for bioassay. The drugs were dissolved in Ca^{2+}-free Hank's balanced salt solution (HBSS) or 10% DMSO.

All computational works were done in a Dell™ Precision Tower 7810 workstation (Intel® Xeon® Processor E5-1650 V3, 6 core, 3.5 GHz, 32GB RAM) run with 64-bit Windows 7 Professional as the operating system.

2.2.2 Cell culture

RBL-1 cells, SHSY-5Y cells, HEK-293 cells and lung cancer cells were cultured in high glucose DMEM medium with the F-12 nutrients mixture, supplemented with 10% (v/v) fetal bovine serum, 2 mM L-glutamine and 1% (v/v) antibiotic/antimycotic mixture in humidified atmosphere with 5% CO2 and 95% air at 37°C. Cells were kept in 75cm^2 flask and passaged at least once in a week after reaching ~90% confluence. In preparation for the passage of the cells, DMEM and trypsin media were pre-warmed at 37°C. Cell medium from the flask was aspirated and cells were detached from the flask through addition of 2/3ml of trypsin. After 2/3 min, the flasks were gently shaken to allow complete detachment of adhered cells and then trypsin was neutralized by adding 8-10ml of DMEM. The cell suspension was then gently pipetted few times before it was centrifuged at 800 rpm for 5 minutes after which the supernatant was discarded, and the cell pellet was re-suspended in DMEM (10ml). The resultant cell suspension was used for seeding of cells into flasks and onto glass bottom dishes (10mm) as required for Ca^{2+} and confocal imaging.

Human jurkat T cells were cultured in RPMI-1640 medium supplemented with 10% (v/v) fetal calf serum. Cells were kept in 75cm2 flask and passaged at least once in a week after reaching ~90% confluence. Glass bottom petri-dishes (10mm) were coated with PDL before seeding the cells for Ca^{2+} imaging.

2.2.3 Confocal Microscopy

STIM1-Orai1 oligomerization assay

HEK293 cells with an inducible mCherry-STIM1-T2A-Orai1-eGFP were plated onto sterilized cover slips and maintained in complete DMEM. STIM1-mCherry and Orai1-GFP protein were induced through tetracycline (2-5μM) treatment 12-16 hours before the experiment. Cells were washed with HBSS and incubated for 30-40 minute with the respective compounds and vehicle followed by 2μM of Tg treatment for 5 min. Cells were fixed with ice cold methanol (100%) for 15 min at -20°C. Cells were then washed twice with PBS and treated with DAPI (1:1000 in PBS) for 5 minutes followed by washing in PBS for 10 min.

Confocal images were acquired using a Leica SP5 microscope equipped with a Plan Apochromat 63x/NA1.4 oil immersion objective. The excitation wavelengths (ex) and emission filters (em) were as follows: DAPI, ex 364 nm/em 385-470 nm; Orai1-GFP, ex 488 nm/em 500-515 nm; STIM1-mCherry, ex 543 nm/em 610 nm. Acquired images were processed using the ImageJ (National Institutes of Health). Acquired images were processed using the ImageJ (National Institutes of Health). For quantification of STIM1-mCherry and Orai1-GFP puncta formation, the puncta were selected as spots of high fluorescence intensity ranging from approx. 0.5 to 1.0μm in diameter and their number was determined as per previously published method ((Yazbeck et al. 2017).

NFAT translocation assay

HeLa cells stably expressing the NFAT1(1-460)-GFP fusion protein (Gwack et al. 2006) were grown on glass bottom petri-dishes. Cells were then washed with HBSS and incubated for 30-40 minute with the respective compounds and vehicle followed by treatment of 1μM ionomycin and 2μM Tg for 40 min and 10 min respectively. Cells were then washed twice with PBS and treated with DAPI (1:1000 in PBS) for 5 minutes followed by washing in PBS for 10 min. Confocal images were acquired using a Leica SP5 microscope equipped with a Plan Apochromat 63x/NA1.4 oil immersion objective. The excitation wavelengths (ex) and emission filters (em) were as follows: DAPI, ex 364 nm/em 385-470 nm and NFAT1(1-460)-GFP, ex 488 nm/em 500-515 nm. Images captured were processed using imageJ software.

For the quantitative assessment of the ionomycin and Tg induced nuclear translocation of NFAT1(1-460)-GFP in HeLa cells with or without drug/BTP2 pre-treatment, NFAT-GFP fluorescence intensity ratio of nuclear to cytosol was followed.

2.2.4 Cell proliferation assay for lung cancer cells

Lung cancer cell line: LK2, H520, H1792 were seeded at a density of 2500 cells/well in a clear flat bottom 96-well plate (Corning). After 24 hours, cells were exposed to test compounds or vehicle, as indicated, and were incubated for 72 hours. After 72 hours incubation, 5μl of Cell Counting Kit-8 (CCK-8, Sigma, UK) was added to each well and the cells were incubated for an additional 2-3 hours at 37°C in the dark. The absorbance of each well was measured using a Mithras LB940 microplate reader (Berthold Technologies, Germany) with an excitation of 450 nm. The amount of formazan formed is directly proportional to the number of viable cells. Cell survival was calculated as a percentage of cells treated with vehicle alone (Bai et al. 2019).

2.2.5 OPCs isolation using mixed glia culture (MGC) method

OPC cultures were prepared from neonatal (P0-P2) Sprague-Dawley rats as described previously by McCarthy and de Vellis, 1980 (Mccarthy 1980). The overall procedure is briefly described below.

Sprague-Dawley rats aged between postnatal day P(0) and P(2) were used throughout. All research involving animals was approved by the University of Cambridge Ethics Committee and by the Home Office of the United Kingdom under the Animals Scientific Procedures Act, 1986. Rat pups were decapitated after lethal injection of benzodiazepines; forebrains were exposed and then transferred to sterilin plate with dissection Media. Under dissecting microscope, using curved forceps, two hemispheres were severed, and meninges were removed. The hindbrain/midbrain and olfactory bulbs were removed, so only the cortex was left. The cortices were transferred into 5ml universal tube containing 4ml of dissection Media which was kept on ice. Tissues were cut thoroughly with scissors by rotating the vial and chopping with scissors. Filtered dissociation solution (1ml/pup) was added into vial of mince cortices and then incubated for 1 hr at 37°C. After 1 hr, supernatant was gently removed and 1ml of ovomucoid solution was added to stop papain digestion. The final volume for the centrifuge was made up to 8ml with mixed glia culture media to allow the pellet to be clearly visible after centrifugation. Tissue volume was then centrifuged for 8 min at 1000rpm. After aspiration of the supernatant, pellet was resuspended with 1ml of MGM and triturated vigorously. Volume was brought to a final of 1.5 pup cortices/ ml. Resuspended digested cortices were added to each T-75 flask, which was previously coated with Poly-D-Lysine (PDL) (Sigma). Culture media was changed in every 2–3 days for ~10 days. OPCs were ready for mechanical dissociation after 10-12 days. Each pup was usually expected to yield ~ 1 million OPCs.

The caps of the T-75 flasks containing mixed glia were wrapped with parafilm to ensure no gas exchange. The sealed flasks were then placed onto the universal platform of the orbital shaker and shaked for 1 hour at 195 rpm at 37°C. After the hour, the medium was aspirated and replaced with pre-equilibrated mixed glia media and resumed shaking overnight for ~16 hours at the same speed. This shaking allows microglia and OPCs to detach and remain in cell suspension. After the long shaking, cell suspension was transferred to 10 cm sterilin non-treated plastic dishes and incubated for 30 minutes. This process removes microglia as they attach to plastic quickly; OPCs remain in the cell suspension. Media was then removed from dishes and centrifuged for 8 min at 1000 rpm. 1ml of OPC culture medium was added to dilute

cell pellet. 10µl of diluted OPCs was taken to count the OPCs number using haemocytometer. Cells were then resuspended in the appropriate volume and plated on PDL coated plates/coverslips according to **table 2.4**.

2.2.6 OPCs isolation using magnetic activated cell sorting (MACS) method

Neonatal (P5-P7) rats were decapitated after lethal injection of benzodiazepines. Brains were removed shortly after death (including cerebrum and cerebellum) and placed into ice cold HALF isolation medium (Hibernate A Low Fluorescence), supplemented with 2% of B27. Meninges, olfactory bulbs were removed from brain and chopped mechanically into pieces (~1mm) using sterile scalps. The tissue was then spin down in 100g for 2 min in room temperature (RT) and then suspended in dissociation solution for 30 min in 37°C on a shaker set to 55 RPM. Papain digestion was stopped through addition of HBSS (Gibco). The tissue was then centrifuged for 5 min in 250g. Supernatant was aspirated followed by resuspension in trituration solution for 5 min in RT.

To obtain single cell suspension the tissue suspension was triturated 10 times using a 5ml serological pipette followed by further 3 times trituration with fire polished glass pipettes (opening diameter > 0.5mm). After each trituration step the suspension was allowed to sediment (~1-2 min) and the supernatant was transferred into a fresh tube. 2ml of fresh trituration solution were added after each trituration step. Supernatant was then filtered through 70mm cell strainers to remove undigested tissue bits. 90% isotonic percoll (GE Healthcare, 17-0891-01, in 10xPBS pH7.2 (Gibco) was added to the filtered suspension. Final percoll concentration of 22.5% was achieved by adding phenol-red free DMEM/F12 (Gibco). Cell suspension was centrifuged for 20 min in 800g which resultant separation of debris and cells. Cells containing pellet was then exposed to red blood cell (RBC) lysis buffer (Sigma-Aldrich) in order to remove contaminating red blood cells.

After that 10ml of HBSS was added and centrifuged for 5 min in 300g. The cell pellet was resuspended in 0.5ml MWB supplemented with 10ng/ml human recombinant insulin (Gibco). Then 2.5mg of mouse-anti-rat-A2B5-IgM antibody (Millipore) was added for every 10 million cells, incubated for 15 min, kept on a slow rotating shaker at 4°C. The tube was then fill with 7ml of MWB and centrifuged for 5 min at 300g. The pellet as then resuspend in 80ml of MWB supplemented with 20ml of rat-anti-mouse-IgM antibody (Milteny), incubated for 10 min, kept on a slow rotating shaker at 4°C. After that, 7ml MWB was added and centrifuged for 5 min at 300g to wash out secondary antibody residue. The cell pellet was resuspended in 0.5ml and MACS was performed according to the recommendations of the supplier. Briefly, a MS column (Milteny) were inserted into Mini MACS Separator (Miltenyi) and pre-wet with 0.5ml MWB. Resuspended cells were put onto one MS column. Subsequently the column was washed three

times using 500µl MWB for each wash. Finally, A2B5 positive cells were flushed out the column with 1ml pre-warmed, CO_2 and O_2 pre-equilibrated OPC medium.

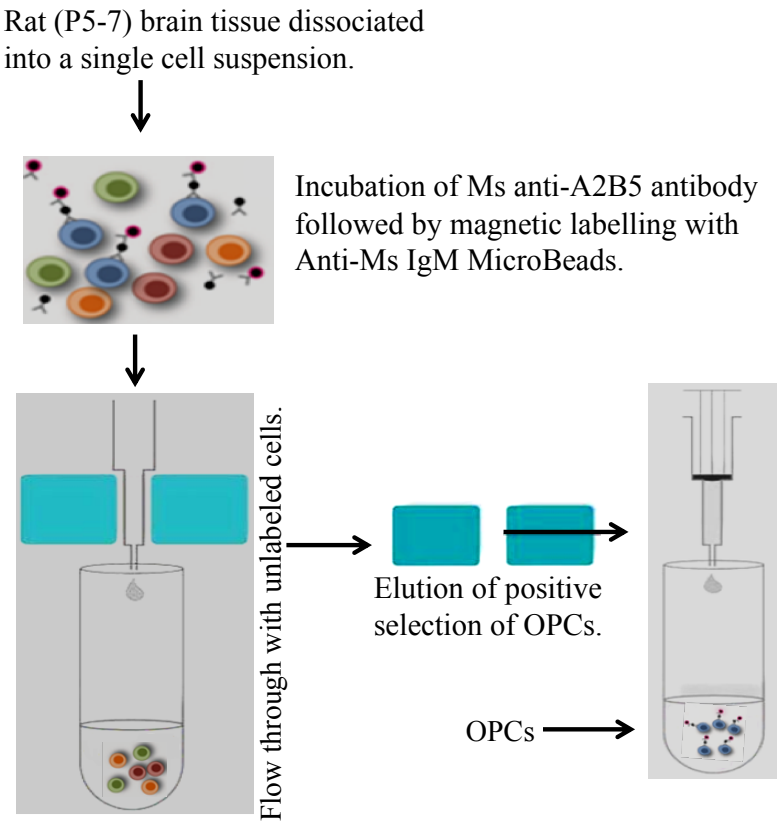

Figure 2.1 Schematic presentation of OPCs isolation procedure using MACS.

2.2.7 Culture of OPCs

A day before the cell dissociation and isolation, cover slips were prepared. 13mm cover slips were first dipped into ethanol to avoid contamination. Each of the cover slips was then placed in a 24 well plate and left resting against the side of the well to dry out. Both coverslips and petri-dishes were coated with PDL for ~1 hour at 37°C, 5 % CO_2 in an incubator followed by washed out with distilled water. After isolation of OPCs, cells were plated on PDL coated plates/coverslips according to **table 2.4.** Approximately 30,000 cells per well in 24 well plate and 100,000 cells per 23mm petri-dish were plated onto the centre of each pre-prepared cover slip and dishes. Isolated OPCs were cultured at 37°C in 5% CO2 in OPCs medium.

The medium was completely exchanged to OPC medium with 10ng/ml bFGF and PDGF-AA after overnight culture to remove any dead cells. A high proportion of OPCs within the cell culture were maintained by daily addition of 10ng/ml PDGF-AA and 10ng/ml bFGF. Oligodendrocytes (OLGs) were generated by growing cells in OPCs in medium supplemented with 40ng/ml T_3 for 4 day in vitro (DIV). During differentiation or proliferation experiments 70% of the medium were replaced every 48h and growth factors, T_3 or other small molecules were added fresh to the culture. The culture medium used was 500ml for cultures in 24 well plate wells and 2ml for cultures in 10mm glass bottom petri-dishes.

Table 2.4 Recommended cell density for different culture plates

Cell number	Culture Plate	Surface area
$1.27x10^6$	T-75	$7500mm^2$
423,729	T-25	2500 mm^2
163,050	6 well	962 mm^2
30,000	24 well	177 mm^2
6,505	96 well	38.4 mm^2
53,220	20mm cover slip	314 mm^2
22,542	13mm cover slip	133 mm^2

2.2.8. Immunocytochemistry

Fixation

OPCs and OLGs from different DIV in culture were considered for immunostaining. Cell media was carefully aspirated from the wells. The cells were fixed with 4 % paraformaldehyde (PFA) and incubated for 10 min at room temperature. PFA was removed and the cells were washed two times for 10 min in PBS.

Blocking

The blocking solution was prepared with 5% normal goat serum in PBS for cell surface antigens and in PBS with 0.1 % triton (PBS-T) for non-surface antigens. Solution (~100µl) was added to each well and incubated for 1h at room temperature in the dark.

Primary antibodies

The cells were incubated overnight in the dark at 4°C with primary antibodies in 5 % NGS in PBS-T solution.

Secondary antibodies

The following day, the cells were washed three times for 10 min in PBS to remove all unlabelled primary antibodies. The cells were then incubated for 1h in the dark at RT with secondary antibodies in 5% NGS in PBS-T solution. After the incubation with secondary antibodies, the cells were washed two times for 10 min in PBS. Cells were then treated with DAPI (1:1000 in PBS) for 5 minutes and washed two times for 10 min in PBS

Mounting

Approximately 10µl of mounting media was added onto a glass slide. The cover slip with cells was then carefully taken from the well and placed onto the mounting media with the cells facing down. Slides were left to dry and stored at 4 °C.

Confocal microscopy

All cell images were captured with Leica SP5 confocal laser scanning microscope system and edited in imageJ software.

2.2.9 Single cell Ca^{2+} imaging

To measure Ca^{2+} signalling, cells were seeded in 10mm glass bottom dishes and used when cells were ~90% confluent. Since human jurkat T cells were non-adherent therefore these cells were seeded on a PDL coated petri-dhishes. OPCs were also grown in PDL coated dish due to their less-adherent characteristics. All other cells like, RBL-1, SHSY-5Y, and lung cancer cells used for Ca^{2+} imaging were adherent therefore no coating required.

Fura-2 acetoxymethyl (AM) was dissolved in 20% Pluronic® F-127 solution in DMSO to 2mM stock concentration. The cells were thoroughly washed several times using pre-warmed HBSS buffer. The pH was maintained at 7.4. Special care was taken while handling the cells, as they could easily detached from the dishes. All the cells were loaded with 1μM fura-2/AM except OPCs that required 4μM, in HBSS++ for 40min at room temperature in the dark chamber. The Fura-2/AM ester is an uncharged ester and as such is spontaneously taken up by the cells. Once within the cell, endogenous non-specific esterase cleaves off the AM group and free fura-2 becomes trapped inside the cell because of being charged. Fura-2 is sensitive to Ca^{2+} due to presence of carboxyl groups. Finally, the cells were washed in fresh pre-warmed buffer to remove the dye from the medium and transferred to fresh supplemented HBSS buffer for 30min to ensure the de-esterification of all the dye inside the cells. All the experiments were carried out at room temperature. The calcium concentration in the buffer was 1.25mM as indicated by the provider, which lies in the physiological range for extracellular calcium. This procedure has been adopted after trying several fura-2/AM concentrations and different loading times at 37°C or at room temperature. It has been reported that 37°C can favour the compartmentalization of the dye in several organelles, removing the de-esterified dye from the cytosol. Inspecting the spatial distribution of the indicator is usually enough to diagnose any uneven loading of the dye.

In this work, several experiments were performed from where $[Ca^{2+}]_i$ response was determined by different stimulus including 100μM Carbachol (CCh), 2μM Tg, 40ng/ml PDGF-AA, 70mM KCl and 100μM OAG. CCh, Tg, and OAG were dissolved in DMSO whereas PDGF-AA and KCl were diluted in deionized water. To quantify store Ca^{2+} depletion and Ca^{2+} entry from stimulus, responses were calculated from calibrated traces using MetaFluor® Fluorescence Ratio Imaging Software (Molecular Devices, USA). Ca^{2+} add-back experiments (Bird et al. 2008) were performed when it was required to measure both intracellular Ca^{2+} release as well as extracellular Ca^{2+} entry. Fura-2 fluorescence was monitored continuously using excitation wavelength of 355nm and 380nm, respectively.

The typical experimental design was as follows: baseline fluorescence was captured for >50s, after which stimulus were added. The calcium response to the applied stimulus was followed for ~15 min, and then a fluorescence calibration was performed *in situ*. 10μM ionomycin (Cayman Chemical, USA) and 1mM MnCl2 were added to the buffer ~5min before finishing the experiment to determine auto-fluorescence.

Image acquisition and analysis

Fluorescence images were captured using a Nikon Eclipse Ti-S Microscope mounted with a QImaging QIClick digital CCD camera and using a 10X (NA 0.25) air objective. Excitation was provided by a Dual OptoLED Power Supply (Cairn), alternating between both 355nm and 380nm wavelength LEDs. Both LEDs have a 10nm spectral bandwidth, i.e., the full width of the emitted spectra at half-maximum intensity. Emission fluorescence of the fura-2 signal was collected at 510nm (470nm–550nm). 12-bit images were acquired every 5 seconds with MetaFluor® (Molecular Devices, USA). The fluorescence at each time-point was extracted for both 355nm and 380nm wavelengths, corrected for autofluorescence and the 355nm/380nm ratios were calculated.

2.2.10 Evaluation of cytotoxicity for OPCs

Cell death was assessed by propidium iodide staining as per the method previously published by Lecoeur 2002. Briefly, OPCs were first chronically treated with drugs, compounds or vehicle. Afterwards, cells were incubated with 10µg/ml propidium iodide for 20 min at 37°C. Cells were then washed with PBS and fixed for 15 min with 100% ice cold methanol at -20°C. Cells within each treatment group were later imaged using confocal microscopy with the 20x objective.

2.2.11 Statistical analysis

Results were expressed as means ± SEM for n independent experiments, with each experiment performed minimally in triplicate. The latter in this study involved Ca^{2+} imaging of drug-treated cells in at least three different days (3 petri-dish of cells per drug per day) done with paired control group (3 petri-dishes of cells per day). Statistical comparisons of mean values were performed using GraphPad Prism 5 (GraphPad software Inc., CA, USA). One-way ANOVA followed by Dunnett's test was used to compare among groups. Data for the two groups were compared using the unpaired two-tailed Student's t-test. The level of significance was also indicated on graphs ($P<0.05$*, $P<0.01$**, $P<0.001$***).

Chapter 3

Results I - FDA approved drugs as SOCE inhibitors

3.1 Results

3.1.1 Ligand-based virtual screening and identification of hits for bioassay

Several well-known SOCE inhibitors were used as 3D baits (**Fig.3.1**) to virtually screen a conformer library of approved drugs namely the eDrug3D database (Pihan et al. 2012) using ROCS (Open Eye Scientific) (Naylor et.al. 2019). Initial ranking of the hits was based on the Tanimoto Combo (TC) score which is a linear sum of the shape tanimoto and colour tanimoto score. First 300 hits obtained this way were then re-ranked on the basis of electrostatics tanimoto combo (ET_combo) score using EON.

After visual inspection of each hit for electrostatic similarity (**Fig. 3.2**) and considering their ranks in ROCS and EON based outputs, total of 10 drugs were purchased for the study. ET_combo score of the chosen drugs are given in **table 3.1**.

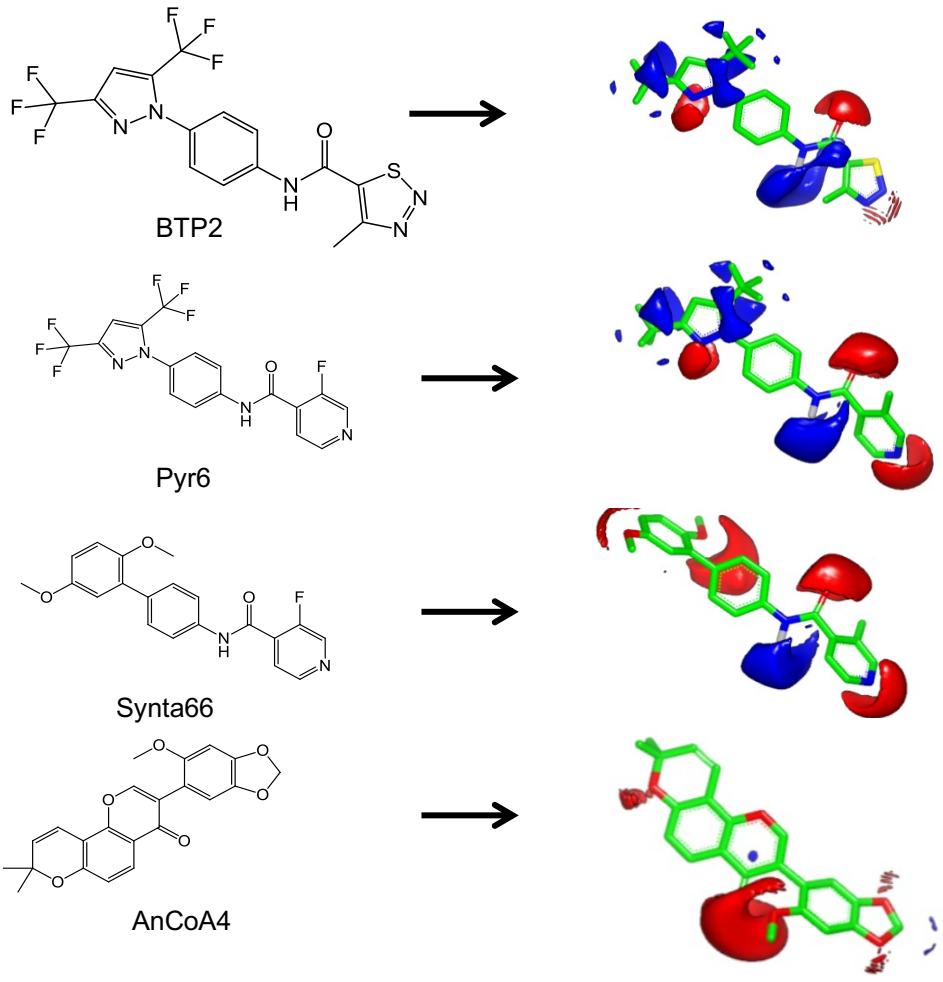

Figure 3.1 2D and 3D representations of the bait molecules.

2D representations of the bait molecules and their corresponding 3D queries used in the ligand-based virtual screening. The 3D queries were generated using EON (version 3.2.1.4, OpenEye Scientific Software, Santa Fe, NM).

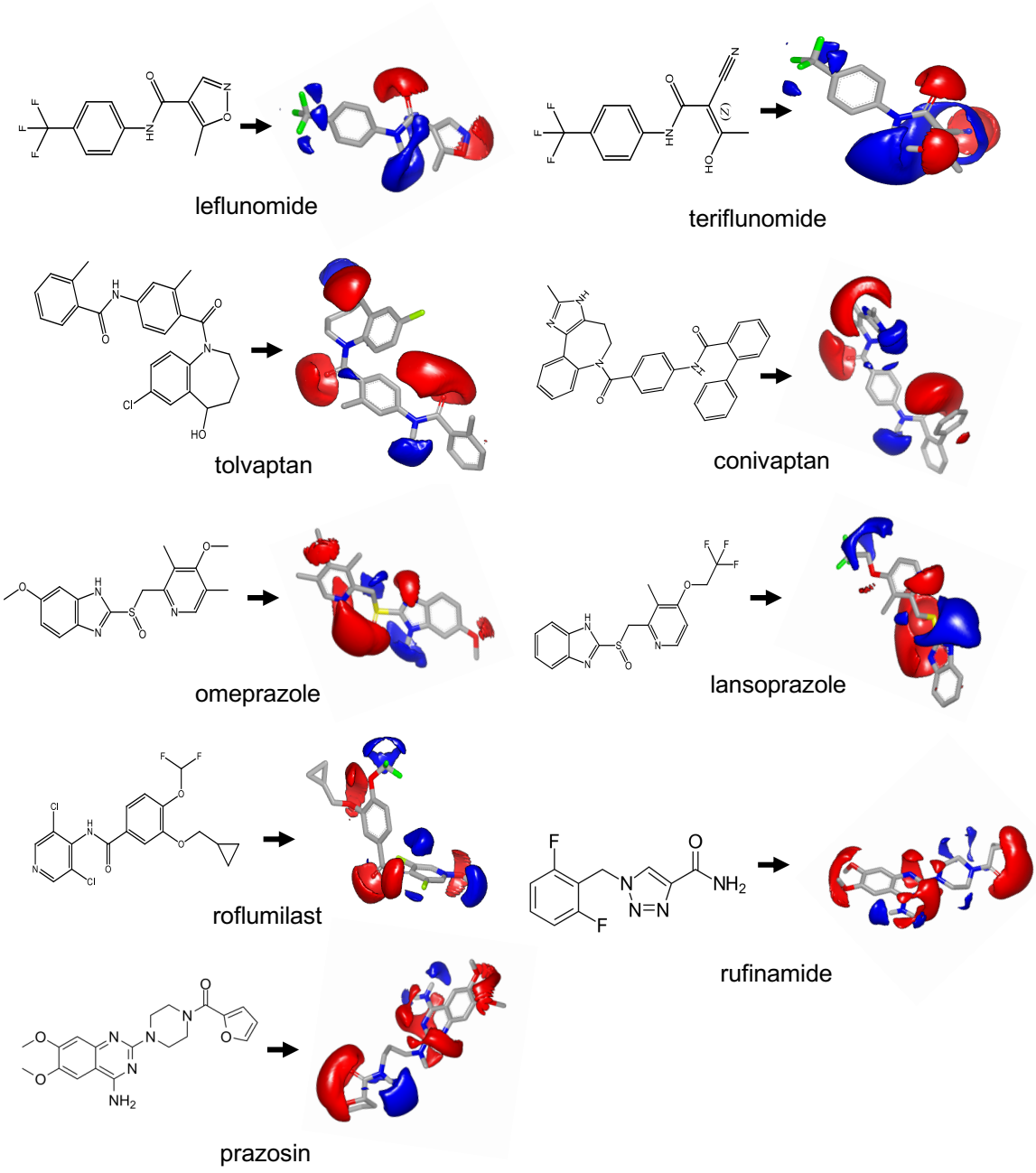

Figure 3.2 2D and 3D representations of drug molecules.

2D representations of the drug molecules and their corresponding 3D queries used in the ligand-based virtual screening. The 3D queries were generated using EON (version 3.2.1.4, OpenEye Scientific Software, Santa Fe, NM).

Table 3.1 Primary list of drugs tested for their ability to inhibit SOCE

	Similarity indices of the tested drugs with the cognate query compounds							
	query: BTP2		**query: Pyr6**		**query: Synta66**		**query: AnCoA4**	
Hit	ROCS rank (TC score)	EON rank (ET combo score)	ROCS rank (TC score)	EON rank (ET combo score)	ROCS rank (TC score)	EON rank (ET combo score)	ROCS rank (TC score)	EON rank (ET combo score)
Leflunomide	1(1.301)	1 (1.239)	1 (1.265)	1(1.1230)	1(1.244)	2 (1.20)	368(0.847)	268 (0.637)
Teriflunomide	48 (0.897)	5 (1.036)	14 (0.973)	10 (1.016)	9(1.003)	7 (1.131)		266 (0.541)
Tolvaptan	10 (0.973)	20 (0.925)	3 (1.063)	6 (1.0600)	2(1.204)	9 (1.129)	431 (0.83)	68 (0.684)
Conivaptan	155 (0.834)	-	65(0.885)	99 (0.7690)	25 (0.963)	16 (1.057)	575 (0.875)	125 (0.564)
Omeprazole	32(0.913)	42 (0.853)	70(0.882)	4 (1.0860)	33 (0.945)	22 (1.002)	2 (1.087)	1 (1.3)
Lansoprazole	50 (0.895)	72 (0.805)	49(0.901)	291(0.667)	358 (0.811)	-	21 (1.01)	7 (1.034)
Rufinamide	318 (0.79)	311 (0.689)	317(0.789)	253 (0.679)	78 (0.901)	19 (1.03)		
Prazosin	40 (0.901)	132 (0.757)	90(0.866)	131 (0.7410)	41 (0.937)	13 (1.073)	19 (1.013)	14 (1.001)
Terazosin	27 (0.915)	7 (1.015)	39(0.918)	7 (1.0420)	10 (1.002)	3 (1.189)	9 (1.041)	13 (1.011)
Roflumilast	2 (1.181)	331 (0.683)	2(1.167)	136 (0.738)	466 (0.793)	194(0.741)	49 (0.973)	54 (0.853)

Table 3.1 summarizes list of drugs those were chosen on the basis of several aspects including visual inspection using VIDA, their similarities in electrostatic isopotential contour surfaces (EON-genrated) with the cognate bait, their TC score and ET_PB score, their rank and frequency of appearing within top 100 hits in ROCS as well as EON based screening.

Of the 10 chosen drugs, leflunomide and its pro-drug teriflunomide are known to inhibit *de novo* pyrimidine biosynthesis by acting on dihydroorotate dehydrogenase (DHODH) (Yara and Bidin 2015). Tolvaptan and conivaptan are effective non-peptide antagonists for the arginine vasopressin (AVP) receptor subtypes (Bhatt et al. 2014). Omeprazole and lansoprazole are

gastric proton pump inhibitors (Shin and Kim 2013) and roflumilast is a selective inhibitor of phosphodiesterase isoform 4 (PDE4) (Rabe 2011).

Prazosin and terazosin are acting as alpha-1 adrenergic receptor blockers (Tsujii 2000). Rufinamide is a novel FDA approved anticonvulsant medication, some evidences showed this drug acts through voltage gated sodium channel modulator (David and Elizabeth 2013).

3.1.2 Investigation of the effects of the selected hits on SOCE

Single cell Ca^{2+} imaging experiments with rat basophilic leukemia-1 (RBL-1) cells and human SHSY-5Y neuroblastoma cells (**Fig. 3.3**) were used (Bird et al. 2008) for evaluating the performance of the purchased drugs as SOCE modulator. This is a widely-used approach for studying SOCE (and other Ca^{2+} entry mechanisms) at cell population level (Putney 2010).

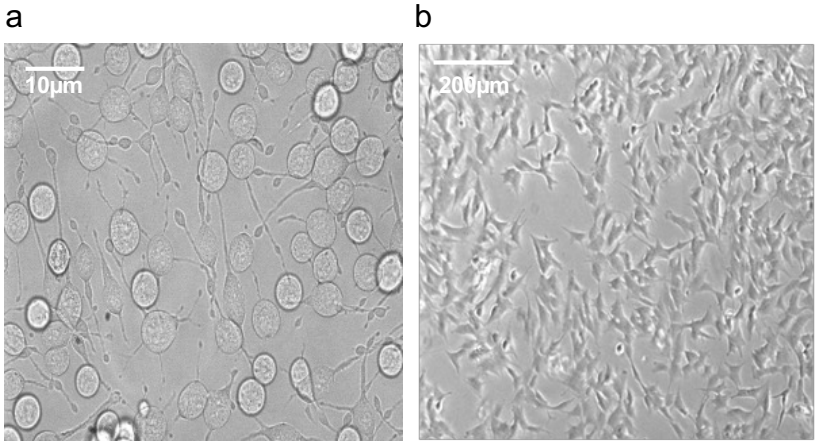

Figure 3.3 Bright field images of cells used for single cell Ca^{2+} imaging.
(a) RBL-1 cells and **(b)** SHSY-5Y cells.

RBL cells were developed in 1973 by inducing leukemia in rats fed with the chemical carcinogen, β-chlorethylamine (Eccleston et al. 1973). RBL-1 cells expressed the high affinity receptor for immunoglobulin E (FcεRI) and displayed mast cell characteristics (Siraganian and Hook 1975). This cell is widely used for the identification of the causative agent of an individual's allergic response (Wilson et al. 1993) as well as for studying SOCE pathway using microscopy and electrophysiology technique (i.e I_{CRAC}) (Bakowski et al.2001; Fasolato et al. 1998; Fierro and Parekh 1999; Huang and Putney 1998; Parekh et al. 1997).

SHSY-5Y neuroblastoma cells were first derived from cells of the neural crest (Goodman et al. 1985). The SK-N-SH neuroblastoma cell line was established in 1970 from a bone marrow aspiration of a 4 year old female with metastatic neuroblastoma (Biedler et al. 1973) . The SK-N-SH cell line is comprised of N- and S-type cells. It has three clone including SH-SY, SH-SY5, and SH-SY5Y. Predominately composed of N-type cells, the SH-SY5Y cell line remains heterogeneous in nature as N-type cells are able to give rise to S-type cells (Ross et al. 1983). This cell line has been extensively utilized for studying neuronal differentiation, as model for neurodegenerative diseases as well as for Ca^{2+} signalling pathways.

The latter can be triggered in these cells by either stimulating G_q coupled receptors (e.g. muscarinic receptors, purinergic P2Ys, vasopressin receptors etc.) using suitable agonists or depolarisation of the plasma membrane using high concentration of salt such as KCl (Vaughan et al. 1995).

3.1.2.1 Evaluation of the effects of chosen drugs on SOCE in RBL-1 cells

Extracellular Ca^{2+} entry inhibition by the higher dose of drug was observed in RBL-1 cells loaded with 2μM fura-2/AM, stimulated by 2μM thapsigargin (Tg). Tg irreversibly inhibits the sarco-endoplasmic reticulum Ca^{2+} ATPase dependent pumps (SERCAs) (Lytton et al. 1991) which then allows passive depletion of the ER Ca^{2+} store leading to the triggering of SOCE (Pozzan et al. 1994; Putney 2009). Cells were pre-incubated 100μM of each drug for ~15min. Control cells were pre-incubated with 0.01% DMSO. With the application of 2μM Tg in absence of any extracellular Ca^{2+}, $[Ca^{2+}]_i$ increased substantially and typically peaked within 100s of application and then slowly declined towards the baseline within 400-500s. At that point addition of 2mM $CaCl_2$ extracellularly triggered the entry of extracellular Ca^{2+} into the cytosol (**Fig. 3.4**). The drugs were first screened at 100μM and at this concentration most of the purchased drugs showed substantial (by ≥60%) suppression of SOCE. When compared to the control group, 7 out of 10 drugs at 100μM caused substantial and statistically significant ($P<0.001$) decrease in the fluorescence ratio corresponding to the Ca^{2+} entry phase (**Fig. 3.4**). Among all, tolvaptan and teriflunomide appeared to manifest the maximum suppression of the Ca^{2+} entry. Only prazosin, terazosin and rufinamide had no effect on SOCE at this high concentration and therefore discarded for further investigation.

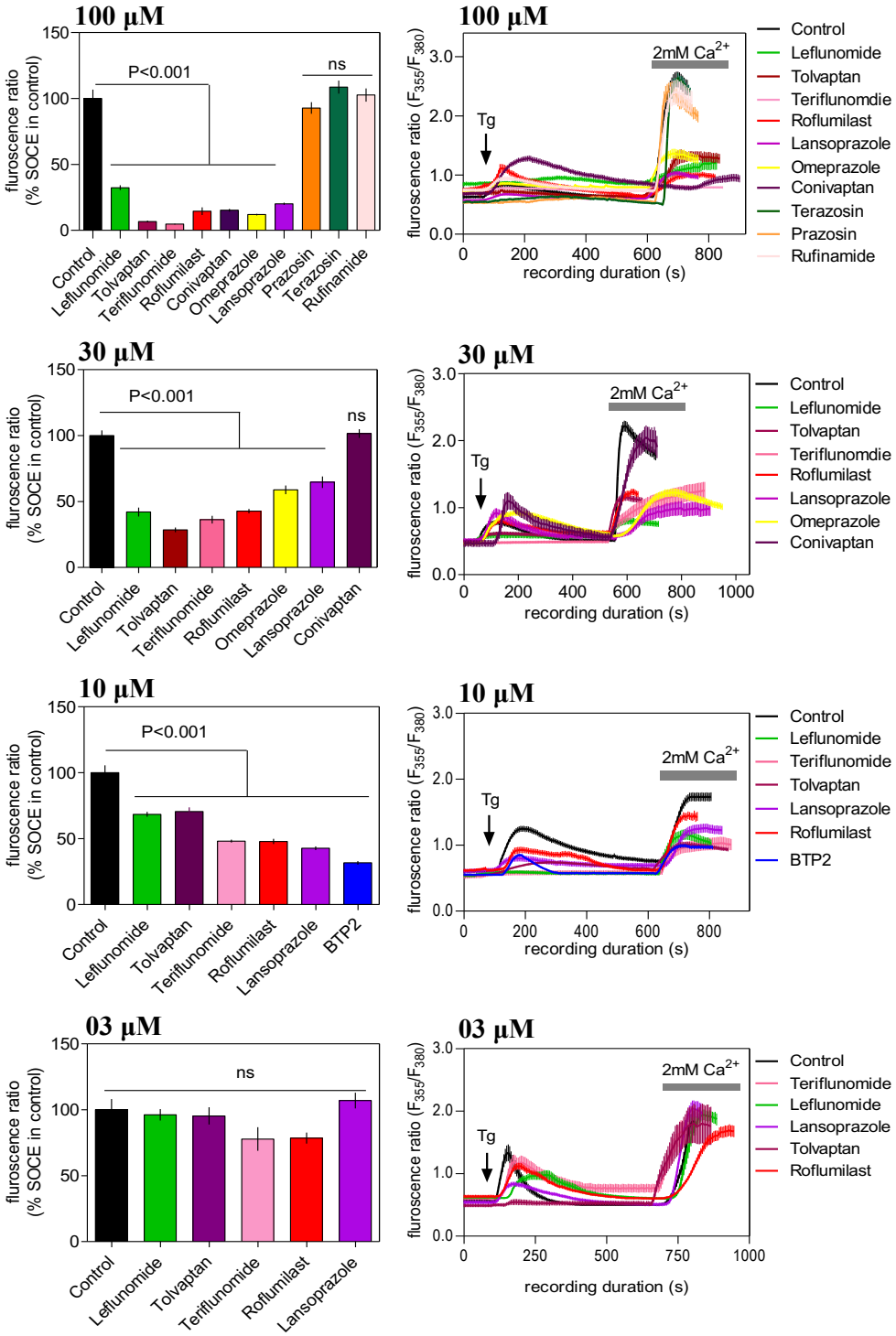

Figure 3.4 Effects of chosen drugs on the SOCE in RBL-1. Histograms **(left column)** showing the highest peak SOCE levels triggered by Tg (2µM) in control cells and cells pre-treated with each drug at different doses (µM). Sample traces **(right column)** representing Ca^{2+} signals (indicated by fura-2 fluorescence ratio) triggered by adding Tg to cells with or without pre-treatment of the chosen drugs (shown in various coloured lines). Each value (mean ± SEM) was derived from 3-5 independent experiments done in different days with 30-80 cells. One-way ANOVA followed by Dunnett's test was used for statistical comparison.

Subsequently the remaining drugs were tested at progressively lower doses; the lowest concentration at which all seven drugs except omeprazole and conivaptan, retained their ability to inhibit SOCE significantly was 10μM (**Fig. 3.4**).

3.1.2.2 Concentration-response studies to determine IC_{50} for selected drugs

For those 5 drugs which significantly suppressed SOCE at 10μM, complete concentration-response studies were carried out with a view to evaluating the concentration-dependence of their action as well as determining the half-maximal inhibitory concentration (IC_{50}) for each drug. As can be seen in **Fig. 3.5**, all 5 drugs as well as the positive control, BTP2 showed dose-dependent suppression of SOCE over the concentration range of 300μM to 3μM. At concentration below 3μM, none of the drugs under the standard experimental protocol (~20 min pre-incubation before the Ca^{2+} add back) manifested any significant SOCE-inhibitory property.

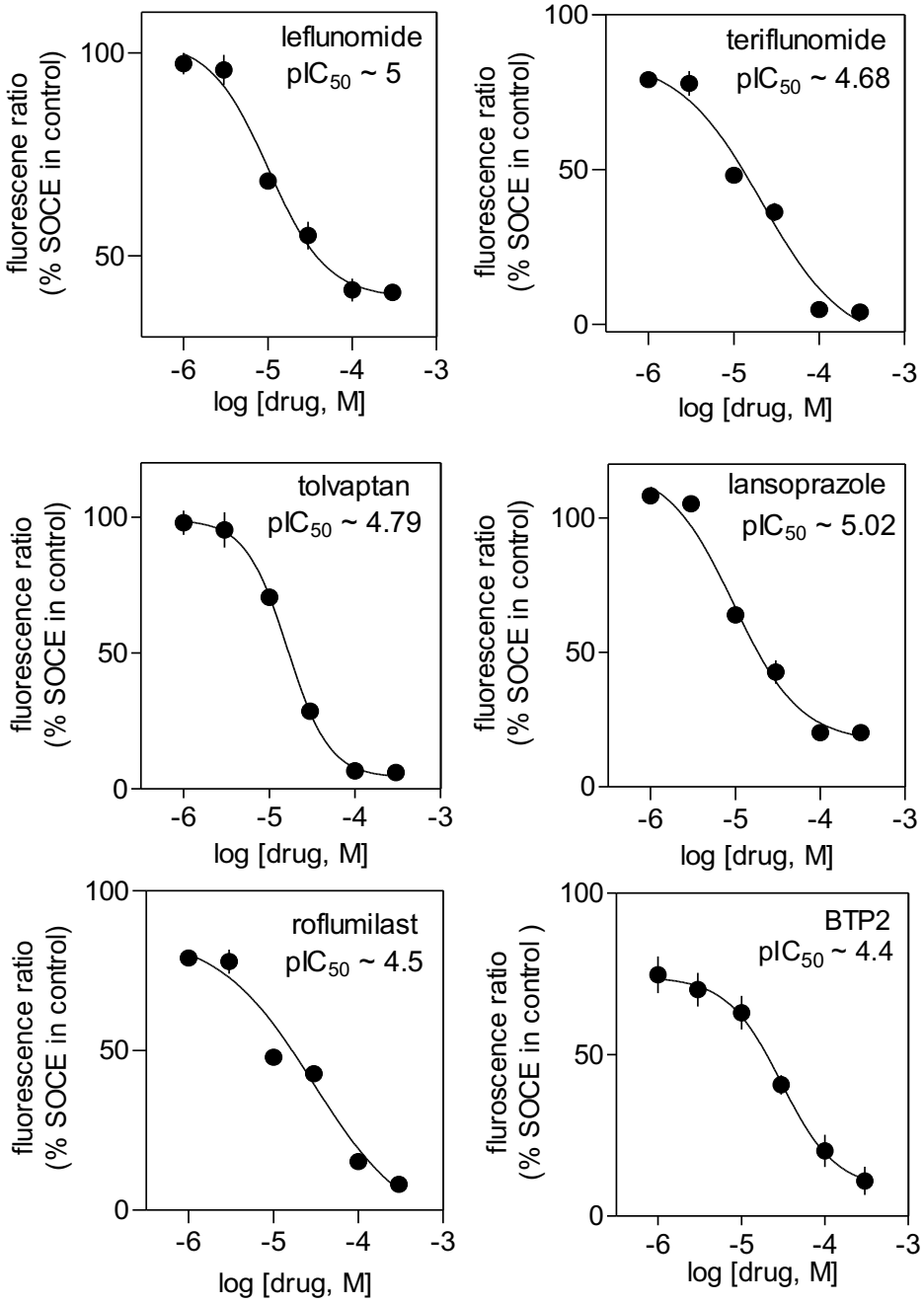

Figure 3.5 Dose response curves (DRCs) for selected drugs.

DRCs demonstrating the dose-dependence of inhibitory effect of indicated drugs and BTP2 at μM dose on the SOCE in RBL-1 cells triggered by Tg. Each value (mean ± SEM) was derived from 3-5 individual experiments and a total of 60-100 cells.

3.1.2.3 Evaluating the drugs in SHSY-5Y neuroblastoma cells

In order to know whether the observed effect of the five drugs on SOCE was cell-type specific or not, those 5 drugs then screened at 10µM dose against SOCE also in SHSY-5Y cells (a human neuroblastoma cell line) using the same protocol that used for the RBL-1 cells. As can be seen in **Fig. 3.6**, all those drugs retained their ability to suppress SOCE significantly in SHSY-5Y cells as well.

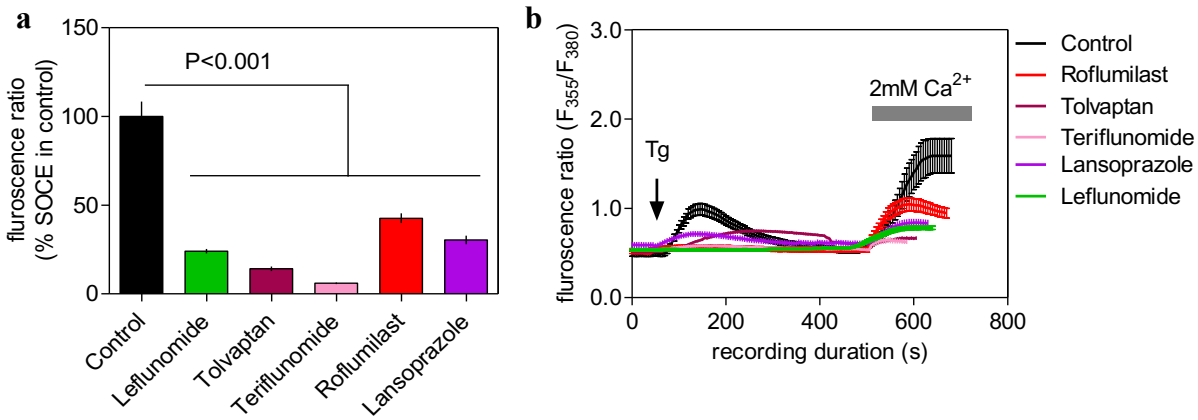

Figure 3.6 Best performing drugs on the SOCE in SHSY-5Y cells.

(a) Histograms showing the highest peak SOCE levels triggered by Tg in control cells and cells pre-treated with each drug at 10µM. **(b)** Sample traces representing Ca^{2+} in cells with or without pre-treatment of the chosen drugs. Each value (mean ± SEM) was derived from 3-5 independent experiments done in different days with 30-60 cells. One-way ANOVA followed by Dunnett's test was used for statistical comparison.

3.1.2.4 SOCE inhibitory properties of the drugs after prolonged treatment

To evaluate whether longer incubation of the cells with these drugs could improve their potency for SOCE suppression, RBL-1H cells were pre-treated with 1μM of the selected drugs and SOCE was recorded after 48 hours. As can be seen in **Fig. 3.7**, significantly inhibition of SOCE was observed only for cells treated with leflunomide, teriflunomide and BTP2.

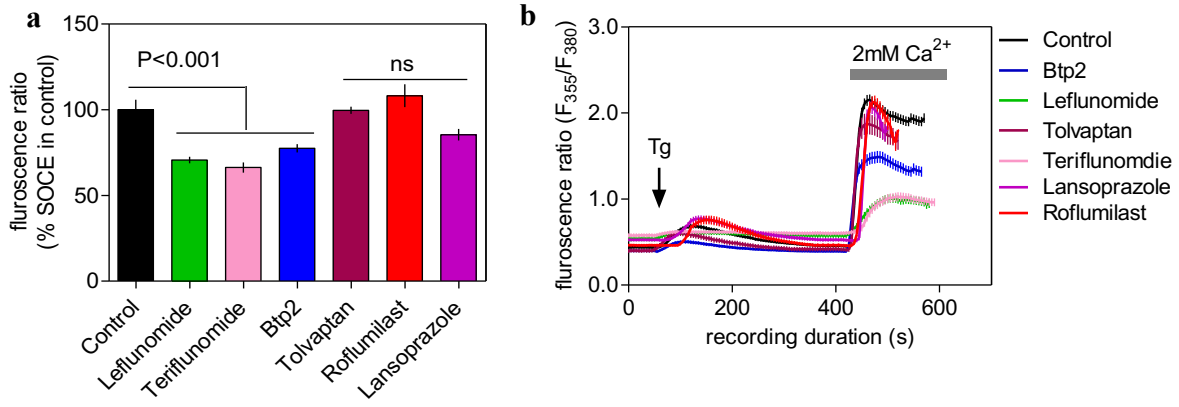

Figure 3.7 The chosen drugs on SOCE of RBL-1 cells following prolonged treatment. **(a)** Histograms showing the peak SOCE levels triggered by Tg in control cells and cells pre-treated with each drug at 1μM dose for 48 hrs. **(b)** Sample traces representing Ca^{2+} in cells with or without pre-treatment of the chosen drugs. Each value (mean ± SEM) was derived from 3-5 independent experiments done in different days with 50-70 cells. One-way ANOVA followed by Dunnett's test was used for statistical comparison.

3.1.2.5 Instantaneous effect of the drugs on SOCE inhibition in RBL-1 cells

In most of the single cell Ca^{2+} imaging experiments mentioned above, cells were exposed to drugs for ~15 minutes which was a sort of semi-acute challenge. In order to evaluate whether the drugs could affect SOCE if added in a more acute way, these drugs were added at a final concentration of 50μM to the bath solution (containing no Ca^{2+}) to just 5-10s prior to the Ca^{2+} addition. It turned out that 3 drugs namely leflunomide, teriflunomide and tolvaptan, could significantly suppress SOCE when added in this acute fashion (**Fig. 3.8**).

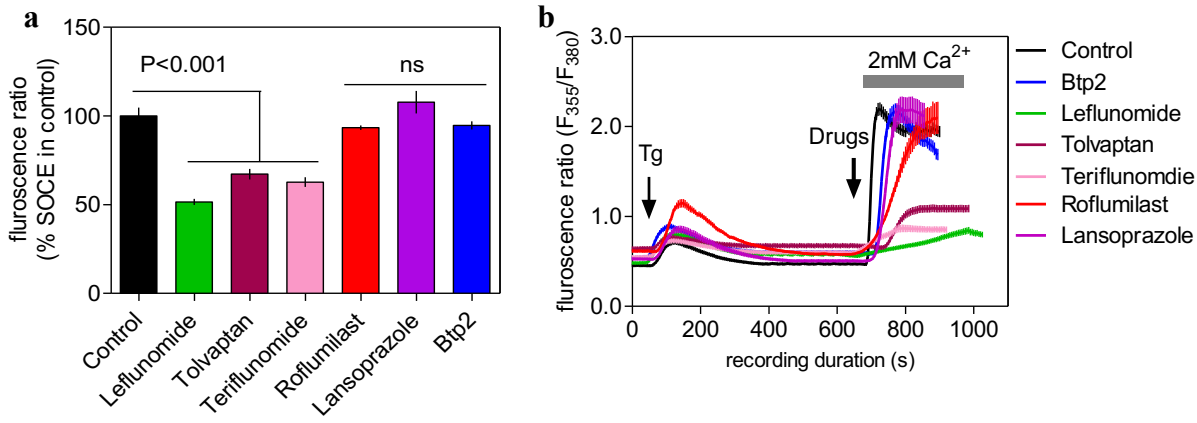

Figure 3.8 Instantaneous effect of the chosen drugs on SOCE in RBL-1 cells.

(a) Histograms showing the peak SOCE levels triggered by Tg in control cells and cells super-acutely exposed to each drug at 50μM dose. **(b)** Sample traces representing Ca^{2+} in cells with or without super-acute treatment of the chosen drugs. Each value (mean ± SEM) was derived from 3-5 independent experiments done in different days with 50-80 cells. One-way ANOVA followed by Dunnett's test was used for statistical comparison.

3.1.2.6 Drugs on transient receptor potential channel C (TRPC) mediated Ca^{2+} entry

Next, it was investigated whether the drugs that suppressed SOCE, could affect Ca^{2+} entry in RBL-1 cells in response addition of 1-oleoyl-2-acetyl-sn-glycerol (OAG). The latter is a membrane permeable, synthetic analogue of diacylglycerol (DAG) and is well known to activate members of the TRPC family of ion channels including TRPC3, TRPC6 and TRPC7 (Hofmann et al. 1999). As can been seen in **Fig. 3.9**, OAG at 150µM did trigger Ca^{2+} signal only in presence of extracellular Ca^{2+} in RBL-1 cells. Among the tested drugs at 10µM dose, only leflunomide and teriflunomide showed significant inhibition of the OAG-evoked Ca^{2+} entry in RBL-1 cells.

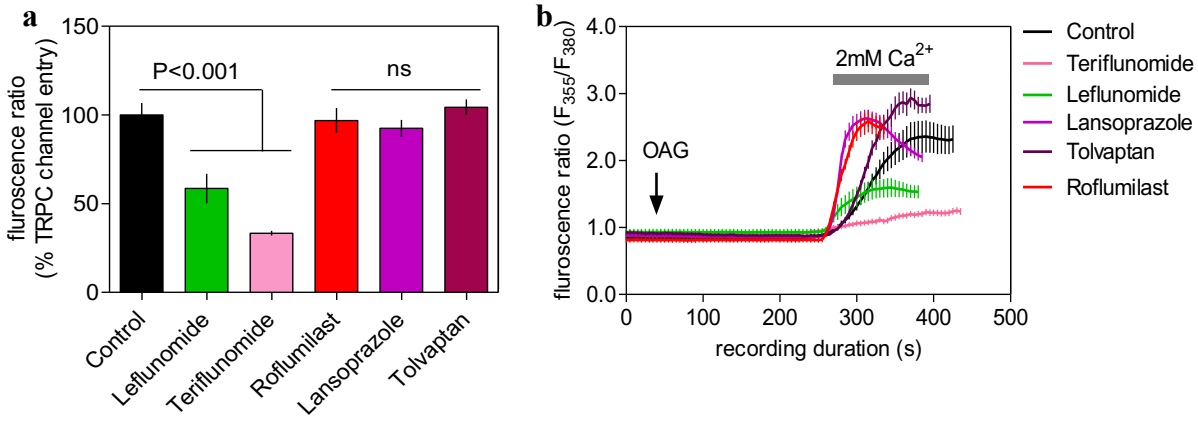

Figure 3.9 Effect of the drugs on TRPC channel mediated Ca^{2+} entry in RBL-1 cells.

(a) Histograms showing the peak OAG-activated Ca^{2+} entry in control cells and cells treated with 10µM of each drug. **(b)** Sample traces representing Ca^{2+} signals triggered by adding 150µM of OAG to RBL-1 cells with or without pre-treatment of the chosen drugs. Each value (mean ± SEM) was derived from 3-5 independent experiments done in different days with 30-80 cells. One-way ANOVA followed by Dunnett's test was used for statistical comparison.

3.1.2.7 Effects of selected drugs on nuclear translocation of NFAT

To determine whether the chosen drugs could affect SOCE-dependent cell signalling and relevant biological responses in intact cells, their effect was evaluated on the nuclear translocation of the nuclear factor of activated T cells (NFAT). HeLa cells stably expressing NFAT1 (1-460)-GFP (Gwack et al. 2006) was used for this. As can be observed in **Fig. 3.10**, ionomycin treatment (1μM for 40 min) significantly increased the nuclear translocation of NFAT1 (1-460)-GFP in the control group but such increase was not observed for cells treated with BTP2 and all the chosen drugs except leflunomide

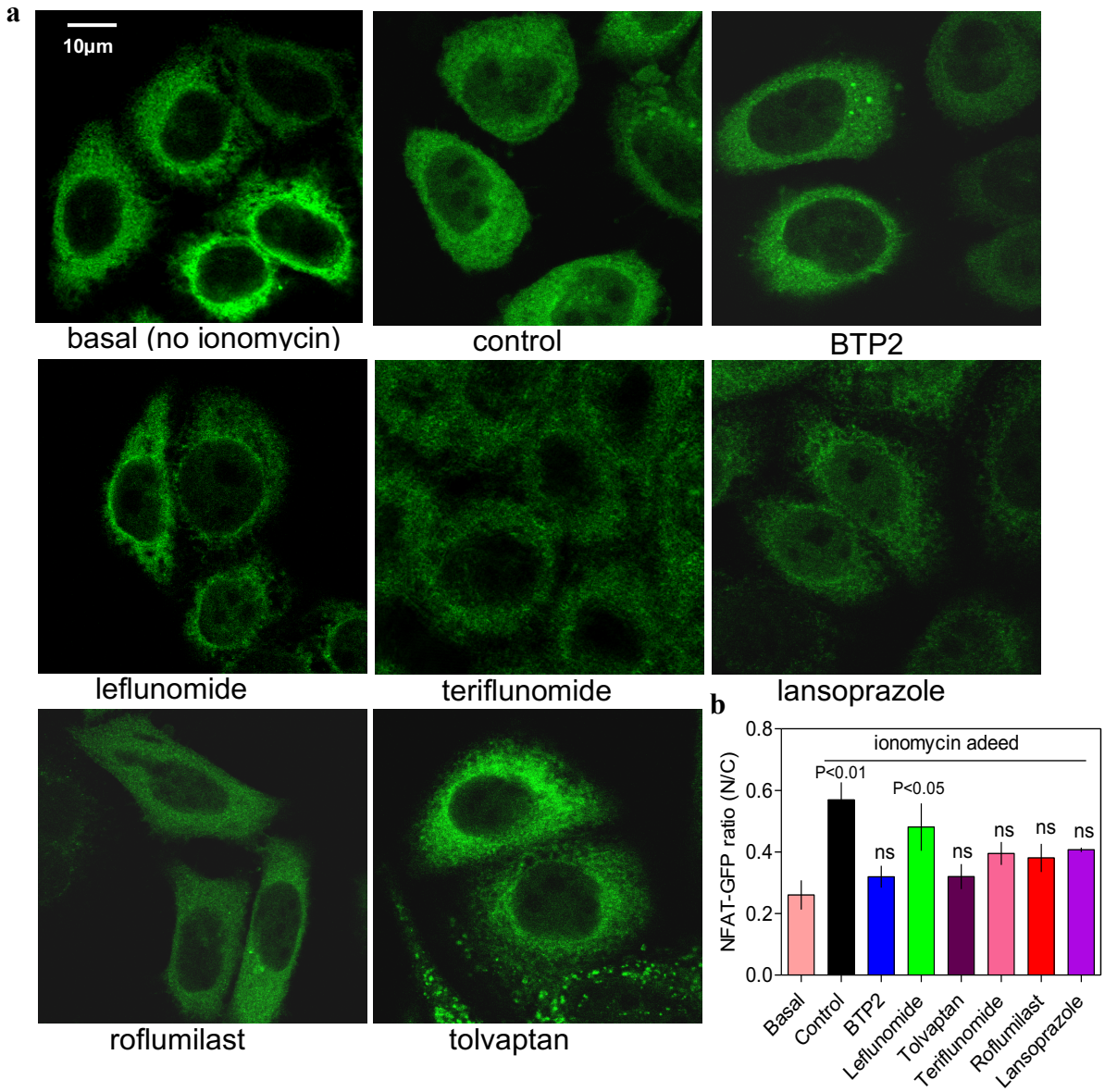

Figure 3.10 Effects of the drugs on nuclear translocation of NFAT.

(**a**) Representative confocal images of HeLa cells showing subcellular localisation of NFAT (1–460)-GFP following application of ionomycin (1µM for 40 min) preceded by pre-treatment with the chosen drugs (20µM) and BTP2 (10µM) for 30 min. The basal and control groups received only DMSO pre-treatment and no ionomycin was added to the basal group subsequently. (**b**) Bar graphs showing the nucleus to cytoplasm ratio (mean ± SEM, n= 3 independent days, 12-15 cells for each condition) for the NFAT (1-460)-GFP under various conditions. One-way ANOVA followed by Dunnett's test was used for statistical comparison.

3.1.2.8 Effects of chosen drugs on the oligomerisation of STIM1 and Orai1

With a view to gaining some insight into the possible mechanism underlying the SOCE-inhibitor property of those 5 drugs, the effects of the drugs were then evaluated on the clustering of STIM1 and also of Orai1, using confocal microscopy with a HEK293 cell line with an inducible mCherry-STIM1-T2A-Orai1-eGFP (Sadaghiani et al. 2014). Qualitative and quantitative assessment showed there was no significant change in the punctuate distribution of mCherry-STIM1 or Orai1-eGFP in presence and absence of any of the 5 drugs and BTP2, after cells were treated with 2μM Tg (**Fig. 3.11** and **Fig. 3.11a**).

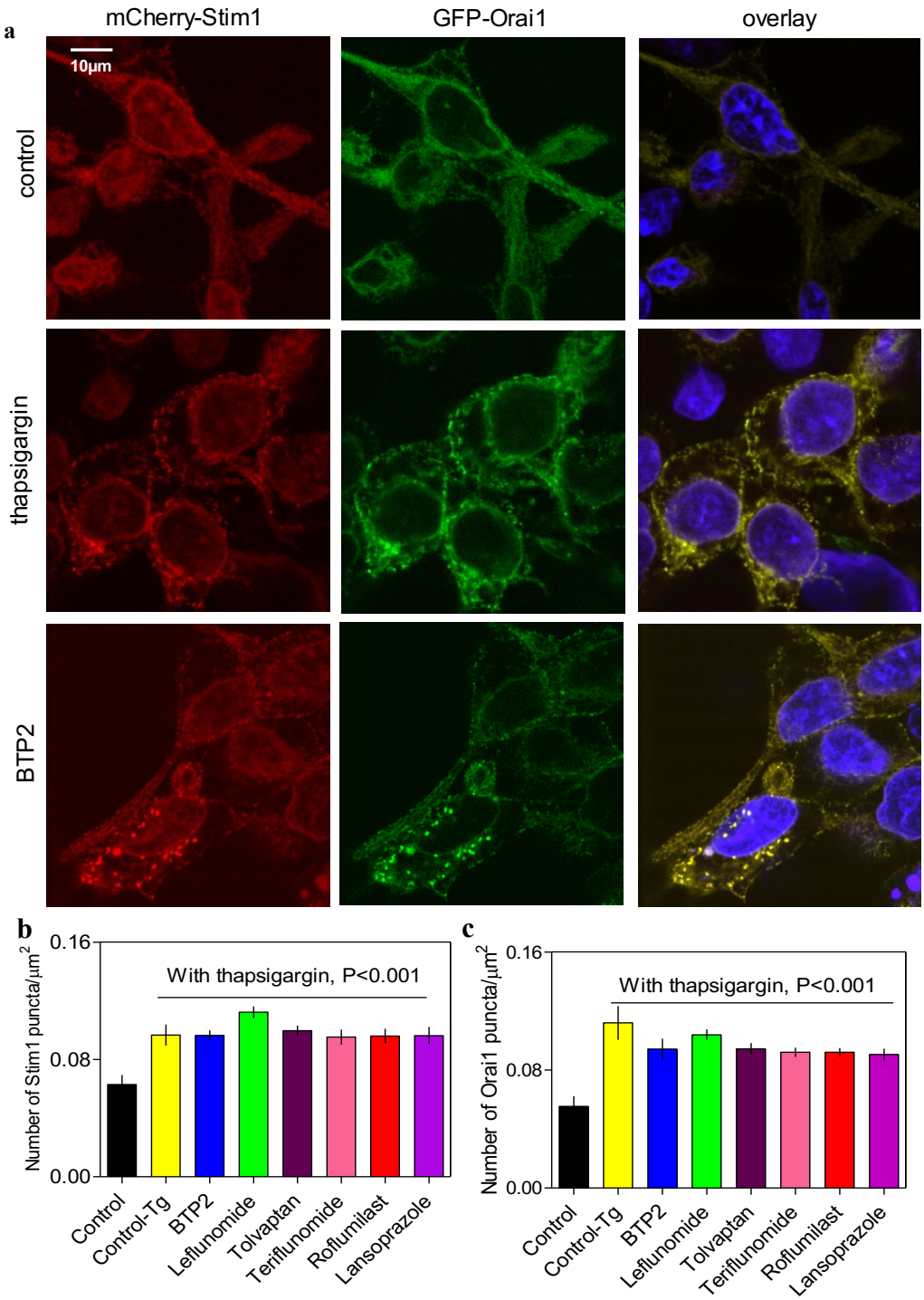

Figure 3.11 Effects of the drugs on clustering of STIM-1 and Orai-1 protein.

(**a**) Representative images of HEK293 cells co-expressing mCherry-STIM1 (red) and Orai1-eGFP (green) showing translocation and colocalization of both proteins in characteristic puncta after treatment with Tg, no Tg and drugs (images shown in next page). Quantification of mCherry-Stim1 **(b)** and GFP-Orai1 **(c)** puncta formation. The number of puncta were determined using ImageJ software and were expressed as mean/µm2 of area ± SEM. Each bar represents data from 15-18 cells from 3 different experiments. One-way ANOVA followed by Dunnett's test was used for statistical comparison.

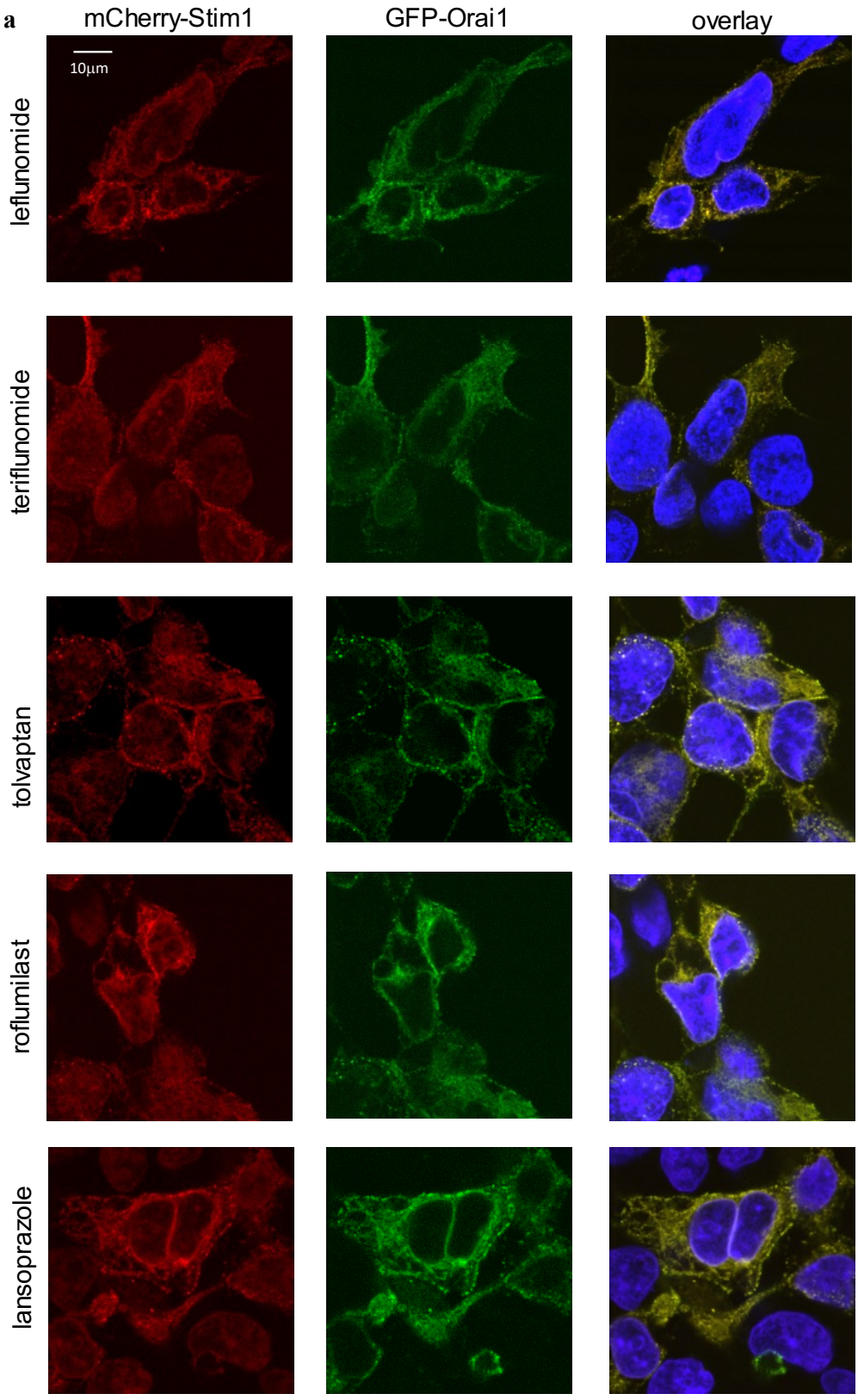

Figure 3.11a Effects of the drugs on clustering of STIM1 and Orai1 protein.

(a) Representative images of HEK293 cells co-expressing mCherry-STIM1 (red) and Orai1-eGFP (green) showing translocation and colocalization of both proteins in characteristic puncta after treatment with drugs

3.2 Discussion

There are quite a few small molecule inhibitors of SOCE available. 2-APB, BTP2 (also known as YM-58483 or Pyr2), Pyr6, Synta 66 and AnCoA4 are the most potential SOCE inhibitors (Sweeney et al. 2009; Anant B. Parekh 2010; Jairaman and Prakriya 2013; Tian et al. 2016).

Structures of some widely-used SOCE inhibitors namely BTP2, Pyr6, Synta66 and AnCoA4 were exploited as baits and sought out to find whether members of the existing drugs share any significant similarity in 3D shape and surface electrostatics with these baits and if so, whether those drugs could phenocopy the known SOCE inhibitors in suppressing SOCE. The overall underlying principle stems from the notion that ligands with similar 3D shape and electrostatic properties are likely to bind to the similar binding pocket on target proteins and thus are likely to manifest similar pharmacological properties (Naylor et al. 2009, and Vasudevan et. a. 2012). Following completion of ligand-based virtual screening, 10 drug molecules were shortlisted.

Following ~15min pre-incubation, of the 10 drug molecules and compounds purchased, 07 drugs and compound caused significant suppression of SOCE when used at 100μM (**Fig. 3.4**) in RBL-1 cells. Drugs pre-incubated at progressively lower doses (30μM, 10μM, and 3μM respectively), only three of these drugs namely leflunomide, teriflunomide and tolvaptan retained their ability for SOCE inhibition in RBL-1 cell lines but none of these drugs had any effect on SOCE at 3μM (**Fig. 3.4**). Complete concentration-response studies for the 5 drugs as well as the positive control, BTP2 were carried out in RBl-1 cells to evaluate the concentration-dependence of their action as well as determining the IC_{50} for each drug. Of these 5 drugs, roflumilast was the most potent SOCE inhibitor drug with lowest IC_{50} dose (~4.5μM) (**Fig. 3.5)**. BTP2 blocked SOCE in RBL-1 cell with IC_{50} of ~4.4μM which is way higher than previously reported IC_{50} dose (0.1-0.3μM) in HEK293 cells, DT40 B cells, and A7r5 smooth muscle cells (He et al. 2005). This indicated IC50 dose might vary depending on cell types. Drugs also retained their ability to inhibit SOCE in SHSY-5Y cells, indicating that the observed effect was not cell type specific (**Fig. 3.6**). Chronic incubation (~24hrs) at lesser dose (1μM), leflunomide and teriflunomide exhibited SOCE inhibition (**Fig. 3.7**).

Study showed SOCE channels not only form heteromeric complex with Orai proteins but also with TRPCs (Liao et al. 2008), therefore checking any effect of these drugs on TRPCC mediated Ca^{2+} entry was also considered. Of these drugs, only leflunomide and teriflunomide could significantly inhibit Ca^{2+} signals mediated by TRPC channels (**Fig. 3.9**), although other 3 drugs did not supress such entry, the former can be justified as 2-APB, another known SOCE inhibitor, is widely known to block TRPC and therefore, ROCE (Lievremont et al. 2005).

It is interesting to note that the concentrations used in the present study were perhaps achievable physiologically, given what is known about the pharmacokinetics of these drugs (**table 3.2**).

SOCE mediated Ca^{2+} signals are critical for the calmodulin-dependent activation of the phosphatase calcineurin in lymphocyte and relevant cell lines including RBL-1 cells. Calcineurin in these cells then dephosphorylates and thus promotes the nuclear translocation of NFAT isoforms. NFAT translocation into nucleus can be disrupted by inhibition of SOCE, which usually happens due to either structural defect in the underlying proteins (for e.g. R91W mutation in CRAC channel pore) or presence of SOCE blockers. Identification of SOCE modulators or evaluation of the consequences of attenuated SOCE in intact cells can be studied using fluorescence-tagged NFAT (Prakriya and Lewis 2015).

Given the observed SOCE-inhibitory property of the chosen drugs, it was satisfying to see their complementary ability to retard nuclear translocation of NFAT1(1-460)-GFP in HeLa cells (**Fig. 3.10**). Although leflunomide was qualitatively looking similar to other drugs however, upon quantitative assessment, was proven to be not affecting the nucleus to cytoplasm ratio of NFAT1(1-460)-GFP, significantly (**Fig. 3.10**). Whether this was a genuine property of leflunomide or a contribution from a contradictory off-target effect, requires further investigation.

Cells were incubated with drugs acutely (~20min) prior to the Ca^{2+} imaging experiment. This was probably enough time for the drugs action against STIM1 oligomerisation and/or STIM1-Orai1 coupling that are critical for SOCE activation. Drugs were applied super acutely (~10 sec before Ca^{2+} add-back) during imaging to know whether the drugs could affect SOCE upon more acute challenge which could at least indicate whether they could inhibit SOCE when Orai1 was already activated, presumably through interaction with aggregated STIM1 proteins.

Leflunomide, teriflunomide and tolvaptan retained their ability to inhibit SOCE in super acute experiment (**Fig 3.8**). Surprisingly BTP2, known SOCE inhibitor, and two other drugs, roflumilast and lansoprazole, did not affect SOCE under such experimental setup. This could

be due to lower degree of lipid solubility of the drugs and compound which may delay the diffusion (Cerpnjak et al. 2013).

Previous studies reported SOCE inhibition by BTP2 depends on cell types and duration of treatment (Ishikawa et al. 2003; Zitt et al. 2004; He et al. 2005). For example, Ishikawa et al. indicated BTP2 was equally effective on SOCE inhibition in Jurkat T cells regardless of acute or chronic treatment. Although in another study led by Zitt et al. have shown, BTP2 only affected SOCE substantially in Jurkat T cells when the cells were preincubated with the compound at least for 2 hrs or more. On the other hand, according to He et al. 2005, BTP2 potentially inhibited SOCE in HEK-293 cells, DT40 cells and A7r5 cells within 10 min of incubation. So, variability in BTP2 mediated SOCE inhibition and related molecules appeared to be credible depending on cell types and/or treatment duration. However, the reasons for such variation remain obscure.

The matter of fact that leflunomide, teriflunomide and tolvaptan could block SOCE entry even at acute application which was intriguing. This implied that these drugs could act either on Orai1 channels that were already activated due Tg triggered ER store depletion via interaction with aggregated STIM1 proteins or these drugs may block SOCE extracellularly. Immediate cell permeability of these drugs may also be another possible mode of action mechanism in case if they worked intracellularly. Although in acute challenge, roflumilast and lansoprazole did not inhibit SOCE, it was difficult to be definitive about their lack of effect on STIM1 oligomerisation and/or coupling of STIM1-Orai1. This can be said because the known SOCE blocker, BTP2, had no effect on STIM1 puncta formation either and also wasn't effective in acute challenge experiment. Therefore, experiments were executed to see the effects of the drugs on the clustering of STIM1 and also of Orai1, using confocal microscopy with a HEK293 cell line with an inducible mCherry-STIM1-T2A-Orai1-eGFP. None of the drugs along with BTP2 showed any efficiency on either STIM1 puncta formation or Orai1 puncta formation (**Fig 3.11**). Studies already have shown that BTP2 neither affected STIM1 puncta formation nor STIM1-Orai1 coupling (Jairaman and Prakriya 2013) and thus its SOCE-inhibitory properties were attributed to its possible extracellular action, for example, acting as pore blocker. This may be true because it was also found that SOCE channel inhibition mediated by BTP2 was affected by the external Ca^{2+} concentration; higher external Ca^{2+} concentrations were correlated with reduced inhibitory effect on the SOCE channel (Zitt et al. 2004). Another presumable BTP2 action site on SOCE inhibition could be the drebin, an actin reorganizing protein, that was identified as a potential binding site of BTP2 (Zanto et al. 2011). Drebrin may

play a role in regulating SOCE by affecting the actin cytoskeleton, although its already been reported that actin cytoskeleton has not any significant role to play in SOCE (Ribeiro, Reece, and Putney 1997).

Given the significant similarities of the drugs with the baits, particularly, BTP2, used in this study and the observation that they did not interfere neither with STIM1 puncta nor with STIM1-Orai1 complex formation (**Fig 3.11**), it can be hypothesized that these agents inhibited SOCE probably via pore blocking at extracellular site or other extracellular binding sites, for instance, on dbrein protein. This requires direct experimental validation in future.

Out of the best performing drugs, leflunomide and its active metabolite, teriflunomide were ranked the top in both ROCS and EON-based ranks of the hits obtained from screening with the known SOCE blockers, those were considered as baits in this study. Leflunomide is a pro-drug and ~70% of the orally-administered leflunomide rapidly undergoes opening of the isoxazole ring to produce the active malononitrilamide metabolite teriflunomide (Yara and Bidin 2015). Both these drugs have been clinically used as orally-active, disease-modifying immunosuppressive drugs for treating autoimmune type-inflammatory diseases like rheumatic arthritis (RA), and multiple sclerosis (MS).

Leflunomide (Arava) was first approved and licensed for the treatment of RA in 1998. Later on, teriflunomide (Aubagio) was synthesised, approved and licensed for the treatment of MS in 2012. The only known mechanism of action of these drugs involve the inhibition of de novo pyrimidine biosynthesis by acting on the mitochondrial enzyme dihydroorotate dehydrogenase (DHODH)- an enzyme expressed at high levels in proliferating lymphocytes. This results in blockade of de novo pyrimidine biosynthesis and reduction of activated lymphocytes proliferation, therefore it has also been used as an immunosuppressive drug (Yara and Bidin 2015). However, teriflunomide intake might cause other cellular effects which can be independent of DHODH inhibition mechanism. These cellular effects include lowering the cytokine production, cell surface molecules expression as well as cellular migration (Korn et al. 2004). Therefore, it can be said that alongside the ability to inhibit lymphocyte proliferation by inhibiting pyrimidine synthesis, teriflunomide has other immunological effects.

Table 3.2 Drugs with their doses and maximum plasma concentrations (C_{max})

Drug name	Daily oral dose	maximum plasma concentrations (C_{max})	Reference
Roflumilast	250-500mg	~1-nM	(Rabe 2011)
Lansoprazole	10-30mg	~3.5μM	(Shin and Kim 2013)
Tolvaptan	30mg	~0.9-1μM	(Shoaf et al. 2014)
Teriflunomide	7-14mg	~72-168μM	(Oh and O'Connor 2014)

Table 3.2 demonstrates that the concentrations used in the present study were perhaps achievable physiologically, given what is known about the pharmacokinetics of these drugs.

Hitherto it is known that high doses of leflunomide as well as teriflunomide, can inhibit other targets including protein tyrosine kinases, cyclooxygenase-2, PDK1, NFκB, integrins etc (Yara and Bidin 2015). The average steady-state maximum plasma concentrations (C_{max}) of teriflunomide achieved with doses used in clinical trials are 72 μM (7 mg) and 168 μM (14 mg) (Oh and O'Connor 2013).

Based on the current study, it can be expected that teriflunomide and its prodrug leflunomide should inhibit SOCE at clinically relevant dose. Such effect (SOCE inhibition at clinical dose) might contribute significantly to the observed biological effects and therapeutic benefits of these immunosuppressive drugs. Given the biological effect of teriflunomide and/or leflunomide, SOCE inhibition can be a potential target to down regulate the chemokines production, migration, and lymphocytes proliferation. Few recent studies have shown that SOCE inhibition can be an attractive strategy in treating such autoimmune diseases, this can be true as present study clearly demonstrated that these two drugs, which are being currently used as immunosuppressant, inhibit SOCE.

Tolvaptan and conivaptan are orally and intravenously effective nonpeptide antagonists for the arginine vasopressin (AVP) receptor subtypes. These drugs promote water excretion without creating electrolytic imbalance, therefore these have been using for the treatment of hyponatremia (Aditya and Aditya 2012; Bhatt et al. 2014).

In this study tolvaptan ranked within the top 20 of the hits on the basis of ROCS and EON-based ranking. Conivaptan also ranked within top100 hits from Pyr6 and Synta66 based screening. Visually there were some similarities between the vaptans and the three individual baits (**Fig. 3.1** and **Fig. 3.2**). Tolvaptan could inhibit SOCE significantly at 10μM dose whilst

conivaptan was active only at 100μM dose (**Fig. 3.4**). However, tolvaptan is unlikely to affect SOCE at therapeutic doses as the C_{max} of this drug goes down at sub-micromolar level though a single 60 mg oral dose is subjected to human with normal kidney function (Shoaf et al. 2014).

Omeprazole and lansoprazole are gastric proton pump inhibitors and as such are widely used in treating peptic ulcer as well as few other gastroesophageal diseases including Helicobacter pylori infection (Shin and Kim 2013). Both these drugs ranked within top 10 hits from AncoA4 based screening (**table 3.1**), although omeprazole was within the top 50 hits on EON based ranking from screening with BTP2, Pyr6, and Synta66 (**table 3.1**). Apparently these two agents seemed to share some similarities with the baits (**Fig. 3.1** and **Fig. 3.2**). Qualitatively, these two drugs seemed to share some similarities in surface electrostatics with the baits (**Fig. 3.2**). Although omeprazole looked better in computational analysis (**table 3.1**), but, lansoprazole was more potent in inhibiting SOCE (**Fig. 3.4**). However, the C_{max} of lansoprazole and omeprazole at clinically relevant oral doses (15–30 mg) is likely to be ≤ 3.5μM (Shin and Kim 2013), therefore very little effect of this drug on SOCE could be seen during clinical uses.

Roflumilast is an orally administered drug, selective inhibitor of phosphodiesterase isoform 4 (PDE4). This drug is known to treat inflammatory disease conditions in the lungs such as chronic obstructive pulmonary disease (COPD). Most of its pharmacological effects on PDE4 inhibition (possibly up to 90%) can be attributed to its active metabolite roflumilast N-oxide (Rabe 2011). This drug was included in the tested drugs list due to its top rank in both BTP2 and Pyr6 based screening using ROCS. At therapeutic doses (usually 500μg once a day), the C_{max} of roflumilast N-oxide remains within low nanomolar range (Rabe 2011), and therefore little effect on SOCE is anticipated

Chapter 4

Results II - Extended investigation of some SOCE inhibitory class

4.1 Introduction

In chapter 1, out of 10 potential hits, 5 drugs, namely, leflunomide, teriflunomide, tolvaptan, lansoprazole and roflumilast, have found to supress SOCE significantly at ≤10μM dose. Apart from newly discovered SOCE inhibitory properties, these drugs have their own action mechanism which were already known.

Leflunomide and its active metabolite teriflunomide are known to inhibit dihydroorotate dehydrogenase (DHODH) enzyme. The enzyme, DHODH is involved in the *de novo* pyrimidine nucleotides biosynthetic pathway through conversion of L-dihydroorotate (DHO) to orotate. This pathway is crucial for cell proliferation, therefore inhibition of the *de novo* nucleotide biosynthetic pathways offers therapeutic benefits for the treatment of autoimmune diseases, such as rheumatoid arthritis, multiple sclerosis and cancer (Vyas et al. 2014). In addition to leflunomide and its active metabolite teriflunomide, more DHODH inhibitors available in the market which are based on completely different chemo-types, while sharing the same clinical benefits. Brequinar, initially studied for anti-cancer properties (Joshi et al. 1997) as well as vidofludimus and their analogues are few examples of well-known DHODH inhibitors (Leban et al. 2005).

Not only drug or drug-like DHODH inhibitors were developed but also a handful number of non-drugs based DHODH inhibitors are now available. Efficient virtual screening strategy has facilitated identification of a wide range of chemo-diverse DHODH inhibitors. Some of these possessed novel scaffolds and showed distinct binding features with improved properties, such as better bioavailability, selectivity and potency. Thiazole, pyrazole, hydroxyazole and their analogues are some perfect examples of recently developed non-drug like DHODH inhibitors(Li et al. 2015).

One of the best performing SOCE inhibitors in this study was Roflumilast, a selective inhibitor of phosphodiesterase isoform 4 (PDE4). PDE4 is one of the subclass of Phosphodiesterase (PDE) super family. PDE is a ubiquitous enzyme that enable to inactivate cyclic 3,5 adenosine monophosphate (cAMP) and 3,5 cyclic guanosine monophosphate (cGMP) through hydrolysis. This enzyme could be activated by magnesium ions (Earl and Rall 1958).

PDE inhibitors have various pharmacological characteristics including anti-inflammatory, anti-oxidant, vasodilator, cardiotonic and anti-cancer. Therefore these can be used as therapeutic agents for many diseases such as asthma, erectile dysfunction, depression, dementia, chronic obstructive pulmonary disease (Shafiee et al. 2017).

Table 4.1 PDE families and their inhibitors (Victoria et al. 2006; Shafiee et al. 2017).

Family	**Substrate**	**Examples of inhibitors**
PDE1	cAMP/ cGMP	nimodipine, vinpocetine, IC224, phenothiazines, and SCH51866
PDE2	cAMP/ cGMP	EHNA, BAY 60-7550, PDP, and IC933
PDE3	cAMP/ cGMP	Cilostamide, cilostazol, anagrelide, amrinone, milrinone, vesnarinone, motapizone, trequinsin
PDE4	cAMP	apremilast, crisaborole, ibudilast, luteolin, mesembrine, rolipram, piclamilast, roflumilast, tetomilast
PDE5	cGMP	Sildenafil, vardenafil, avanafil, mirodenafil, icariin, dasantafil, tadalafil
PDE6	cGMP	dipyridamole, vardenafil, tadalafil, zaprinast
PDE7	cAMP	ASB16165, IR- 202, US8637528, IR-284, BRL-50481
PDE8	cAMP	PF-04957325,
PDE9	cGMP	PF-04447943, BAY 73-6691 zaprinast
PDE10	cAMP/ cGMP	Papaverine, Azetidine
PDE11	cAMP/ cGMP	Dipyridamole, zaprinast**,** tadalafil

Table 4.1 summarizes different PDE families and commercially available inhibitors of these families.

Lansoprazole was another SOCE inhibitors found in this study which belongs to proton pump inhibitors (PPIs) family. PPIs inhibits the gastric H^+, K^+-ATPase by covalent bonding at cysteines near the ion pathway. Their acid influx inhibition ability is due to the covalent bond, for this the inhibition lasts longer (Shin et al. 2006).

PPIs have been used by care provider vastly as well as by modern gastroenterologist. For many people drug based PPIs represent the first choice for treatment of esophagitis, nonerosive reflux disease (NERD), peptic ulcer disease (PUD), prevention of nonsteroidal anti-inflammatory drugs (NSAID) associated ulcers, Zollinger-Ellison syndrome (ZES), and functional dyspepsia. Combined with antibiotics, PPIs act as an important part of eradication therapy for *Helicobacter pylori* (Strand et al. 2017). Since the discovery of first PPI, Omeprazole, till now more drugs include lansoprazole, pantoprazole, rabeprazole, esomeprazole and dexlansoprazole have been inaugurated. Recently, tenatoprazole, another novel PPI has undergone preliminary preclinical and clinical evaluation. Albeit these drugs have different substitution on their chemical ring which is different from each other, generally speaking they are almost similar in their pharmacological properties (Strand et al. 2017).

Tolvaptan, a vaptan family drug, also found to be another potential SOCE inhibitor drug. The vaptans are non-peptide arginine-vasopressin-receptor (AVR) antagonists, that are orally and intravenously active. Arginine-vasopressin hormone is known to regulate osmolality by controlling urinary volume and composition (Bhatt et al. 2014). Peptide based AVR antagonists have been developed long ago. However, these antagonists have some crucial drawbacks when these apply to *in vivo* system. Peptide antagonists lost their antagonist effect, reversely showed an agonistic effect when taken chronically (Thibonnier et al. 2001). Non-peptide based AVR antagonists are being used for the treatment of euvolaemic or hypervolaemic hyponatraemia. These are also being taken for specific disorders such as cirrhosis and congestive heart failure (Decaux et al. 2008).

Table 4.2 AVR families, mechanism, and inhibitors (Decaux et al. 2008).

AVR subtypes	Action mechanism	Clinical development	non-peptide antagonist
V1a	activates phosphatidylinositol and 1,2,-diacylglycerol signalling pathways	CTH-independent macronodular adrenal hyperplasia,	Relcovaptan, OPC-21268
V1b	activates phosphatidylinositol and 1,2,-diacylglycerol signalling pathways	Depressive disorders	SSR-149415
V2	activates the adenylyl cyclase signalling pathway through the stimulatory G protein	Hyponatraemia (SIADH, cirrhosis, CHF), polycystic kidney disease	Mozavaptan (V1/V2) Conivaptan (V1/V2) Satavaptan Tolvaptan Lixivaptan

Table 4.2 summarizes different AVR families, their action mechanism and inhibitors.

4.1.1 Aim of the project

Using *In silco* based virtual screening followed by biological screening, five potential drugs were identified as SOCE inhibitors. Its mentioned earlier that these drugs are known to inhibit three distinct cellular paths; hence they were categorized as AVR antagonist, PPIs, and DHODH inhibitors class respectively. Although inhibitors from each class share the same clinical benefits but the potency, plasma concentration or selectivity varies due to their differences in structure and mode of action. Therefore, few more drugs, drug-like compounds and chemical scaffold from each class were further investigated aiming to get better SOCE inhibitor and also intriguing to know whether any SOCE inhibitory property, if there, is shared by all other members within the same class of inhibitors and also wanted to assess whether the observed SOCE-inhibitory property was due to the same pharmacophore used by these drugs for their canonical role.

4.2 Results

4.2.1 Selected arginine-vasopressin receptor (AVR) antagonists on SOCE

To explore the effect of non-peptide AVR antagonists on SOCE, more 4 vaptans namely, mozavaptan, lixivaptan, OPC21268, SR49059 were purchased. SOCE inhibition was evaluated using fura-2/AM based Ca^{2+} imaging protocol described in chapter one. RBL-1 cells were loaded with 2µM fura-2/AM, stimulated by Tg to observe SOCE inhibition. Cells were pre-incubated with each vaptan for ~15 min at 10µM dose. DMSO (0.01%) was pre-incubated in the cells as control group. When compared with control group, none of the vaptan caused any significant SOCE inhibition at 10µMdose (**Fig 4.1**), therefore, no further investigation was proceeded with these group.

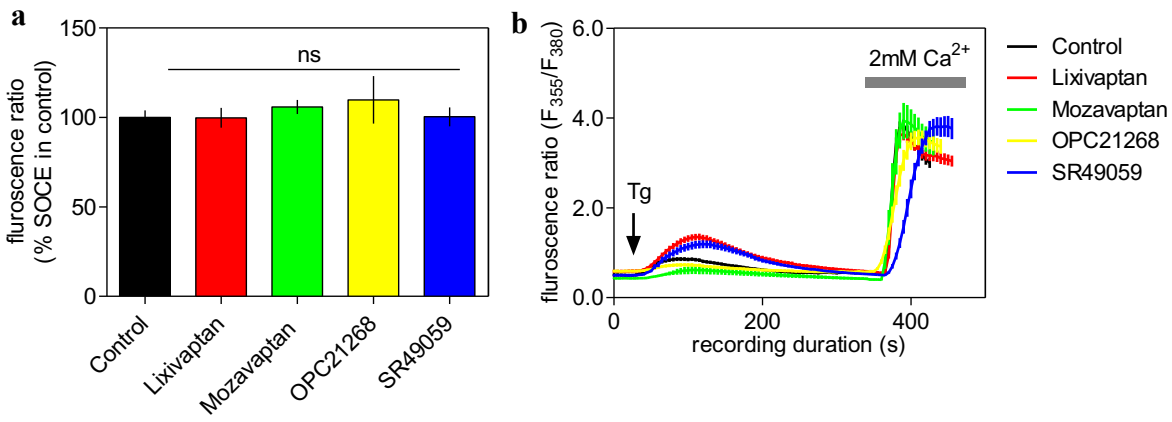

Figure 4.1 Evaluation of AVR antagonists on the SOCE in RBl-1 cells.

(a) Histograms showing the highest peak SOCE levels triggered by Tg in control cells and cells pre-treated with each VR antagonist at 10µM. **(b)** Sample traces representing Ca^{2+} triggered by adding Tg to cells with or without pre-treatment of the chosen drugs/compounds. Each value (mean ± SEM) was derived from 3-5 independent experiments done in different days with 50-60 cells. One-way ANOVA followed by Dunnett's test was used for statistical comparison.

4.2.2 Evaluation of selected proton pump inhibitors (PPIs) on SOCE

To get more PPI based SOCE inhibitors, additional 3 prazole and 2 non-prazole PPIs were further investigated. RBL-1 cells were incubated with each of the PPIs at 10μM dose for ~15 min before doing single cell Ca^{2+} imaging. Data showing no PPI was capable to inhibit SOCE at 10μM dose when compared with control group (**Fig 4.2**).

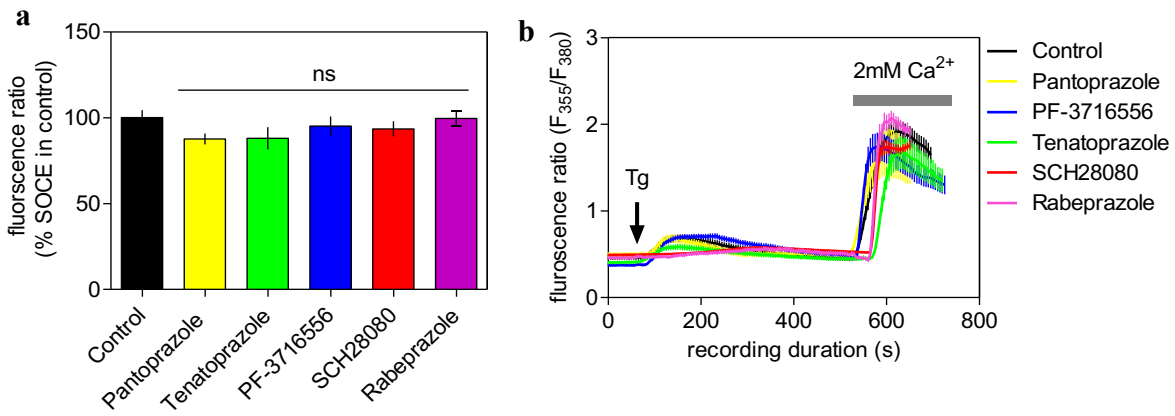

Figure 4.2 Evaluation of PPI on the SOCE in RBl-1 cells.

(a) Histograms showing the highest peak SOCE levels triggered by Tg in control cells and cells pre-treated with each PPI at 10μM. **(b)** Sample traces representing Ca^{2+} triggered by adding Tg to cells with or without pre-treatment of the chosen compounds. Each value (mean ± SEM) was derived from 3-5 independent experiments done in different days with 50-60 cells. One-way ANOVA followed by Dunnett's test was used for statistical comparison.

4.2.3 Evaluation of some phosphodiesterase (PDE) inhibitor family on SOCE

4.2.3.1 Selected phosphodiesterase type 4 (PDE4) inhibitor family on SOCE

Additional 4 PDE4 inhibitors namely roflumilast N-oxide, apremilast, piclamilast, and 3,4-Bis roflumilast were evaluated with a view to finding whether any other member(s) within the PDE4 inhibitor class offer better potency towards SOCE inhibition. RBL-1 cells were pre-incubated with each drug for ~15min before starting single Ca^{2+} imaging. DMSO (0.01%) and BTP2 (2μM) were included as negative and positive control respectively. Screening of the compounds was started with 10μM and at this dose only roflumilast N-oxide supressed SOCE. The very same molecule retained its SOCE inhibition ability at 3μM but failed to supress at 1μM (**Fig. 4.3**).

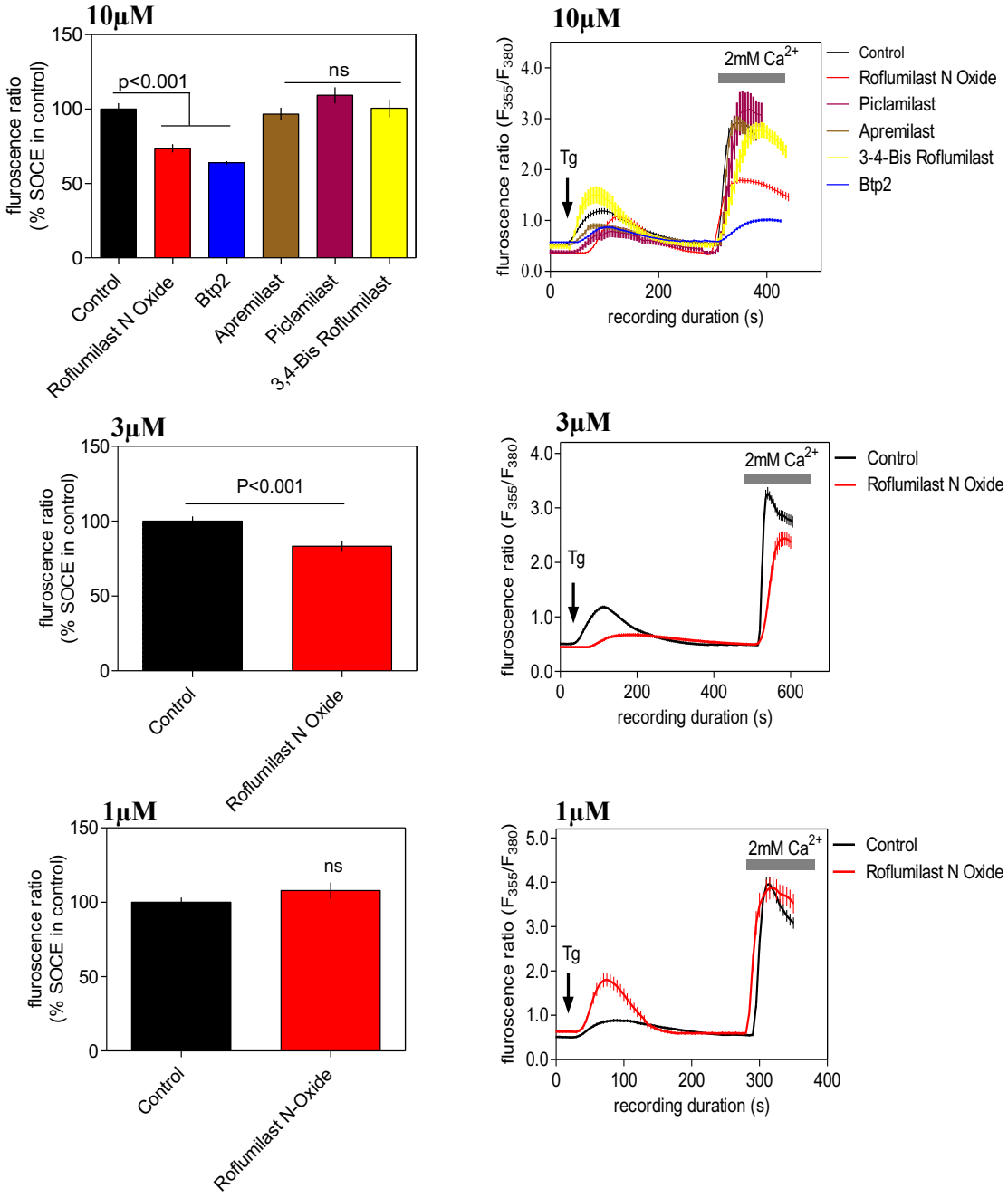

Figure 4.3 Evaluation of the effects of PDE4 inhibitors on the SOCE in RBL-1. Histograms (**left column**) showing the highest peak SOCE levels triggered by Tg in control cells and cells pre-treated with each PDE4inhibitor at different doses (µM). Sample traces (**right column**) representing Ca^{2+} signals triggered by adding Tg to cells with or without pre-treatment of the chosen PDE4 inhibitors. Each value (mean ± SEM) was derived from 3-5 independent experiments done in different days with 40-90 cells. One-way ANOVA followed by Dunnett's test was used for statistical comparison among groups and two-tailed unpaired t-test was used to compare data between groups.

4.2.3.2 More inhibitors from other PDE inhibitors family

To find more potential SOCE inhibitors, selected inhibitors from different PDE inhibitor family were further investigated. For this, 7 drug-like compounds and small molecule, namely, trequinsin, Bay736691, BR1138, cilostamide, milirinone, rolipram, and BRL 50481 were purchased. Drugs treated for ~15 min in RBL-1 cells to start with single cell Ca^{2+} imaging. As mentioned earlier, fura-2/AM, a Ca^{2+} sensitive dye was loaded for ~40 min to prepare the cells to be imaged. DMSO and BTP2 were again included as negative and positive control respectively. At 10μM dose, of the seven agents only trequinsin and bay736691 have shown efficiency to inhibit SOCE. Trequinsin retained its ability to restrict SOCE entry at 3μM while other agent lost such ability (**Fig 4.4**).

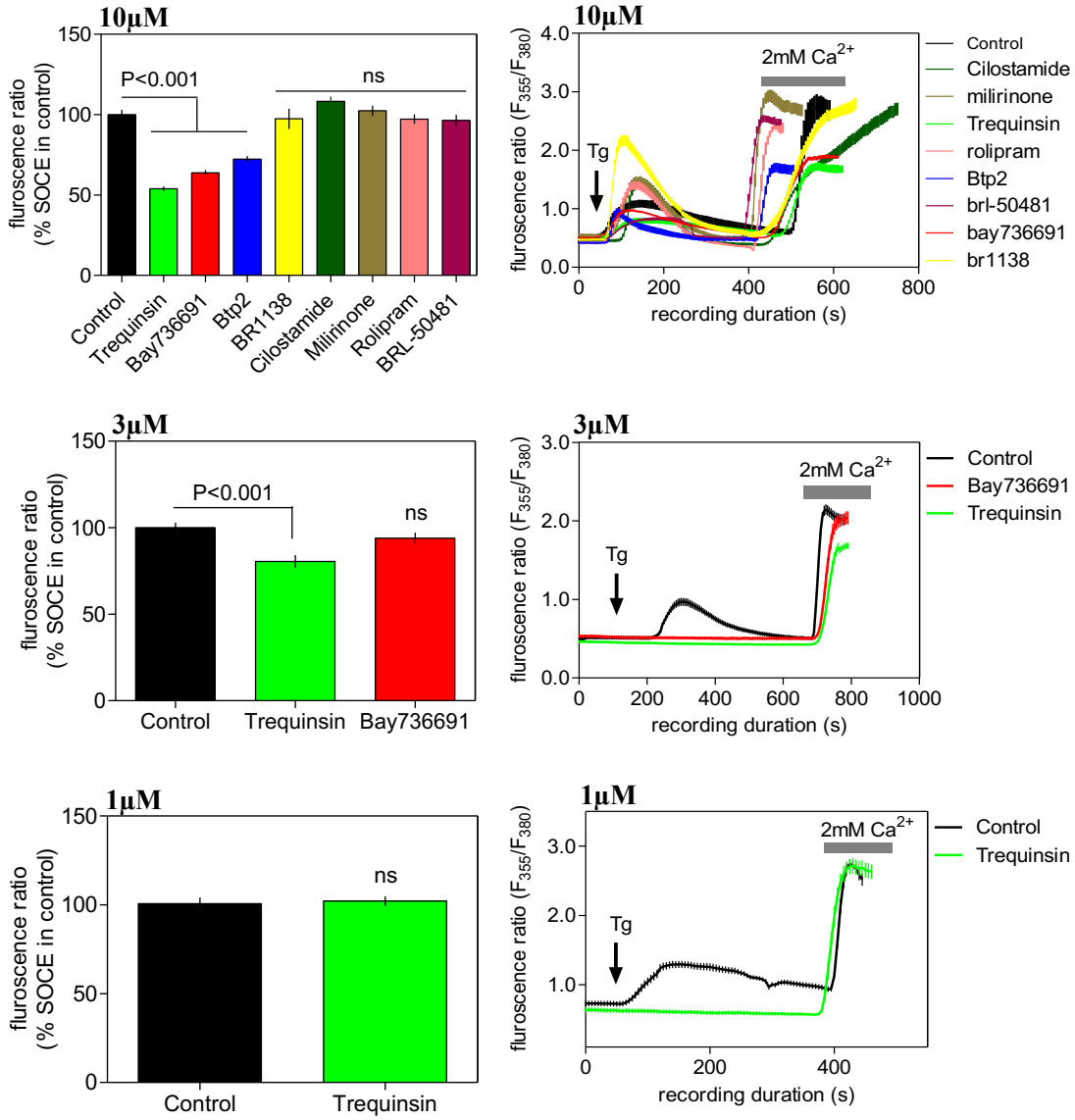

Figure 4.4 Evaluation of inhibitors from different PDE inhibitor family in RBL-1. Histograms (**left column**) showing the highest peak SOCE levels triggered by Tg in control cells and cells pre-treated with each PDE inhibitor at different doses (μM). Sample traces (**right column**) representing Ca^{2+} signals triggered by adding Tg to cells with or without pre-treatment of the chosen PDE inhibitors. Each value (mean ± SEM) was derived from 3-5 independent experiments done in different days with 40-80 cells. One-way ANOVA followed by Dunnett's test was used for statistical comparison among groups and two-tailed unpaired t-test was used to compare data between groups.

4.2.3.3 Best performing PDE inhibitors in SHSY-5Y neuroblastoma cells

Since trequinisn and roflumilast N-oxide were found to be the best performing PDE inhibitor to supress SOCE therefore these 2 compounds were taken into consideration to check whether the observed effect of these drugs on SOCE was cell-type specific or not. The drugs were tested against SHSY-5Y cells using the same protocol used for RBL-1 cells. Only trequinsin retained its ability to inhibit SOCE in SHSY-5Y cells at 10µM (**Fig. 4.5**).

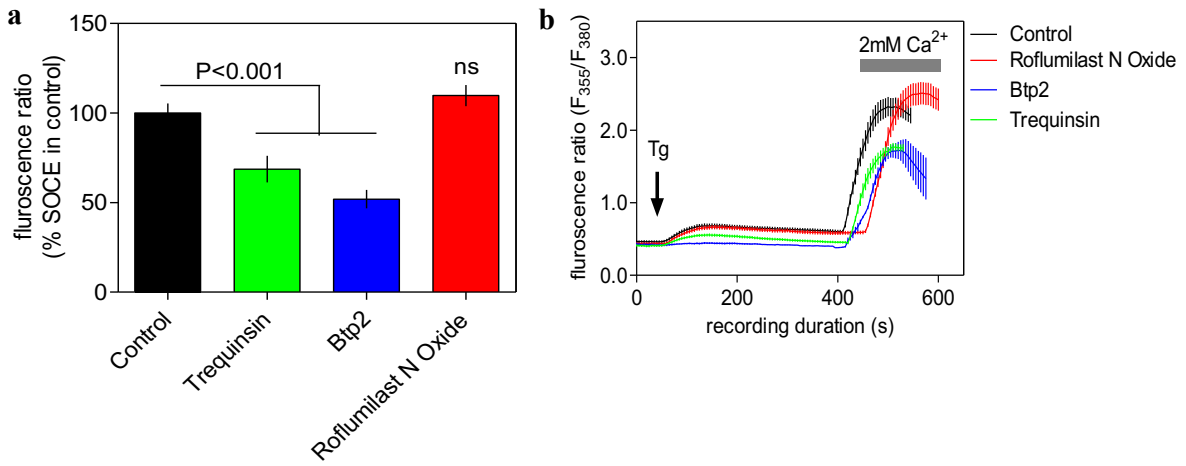

Figure 4.5 Best performing PDE inhibitors on the SOCE in SHSY5Y cells.

(a) Histograms showing the highest peak SOCE levels triggered by Tg in control cells and cells pre-treated with each PDE inhibitor at 10µM. **(b)** Sample traces representing Ca^{2+} triggered by adding Tg to cells with or without pre-treatment of the chosen PDE inhibitors. Each value (mean ± SEM) was derived from 3-5 independent experiments done in different days with 35-60 cells. One-way ANOVA followed by Dunnett's test was used for statistical comparison.

4.2.3.4 Best performing PDE inhibitors on TRPC-mediated Ca^{2+} entry

Next experiment was executed to investigate to know whether these drugs could affect TRPC mediated Ca^{2+} entry which is triggered through addition of 1-oleoyl-2-acetyl-sn-glycerol (OAG). As can be seen in **Fig. 4.6**, none of the compounds at 10µM inhibited TRPC mediated Ca^{2+} entry triggered by 100µM OAG in RBL-1 cells. As excepted, known TRPC channel blocker, SKF9635, significantly supressed relevant Ca^{2+} signal (**Fig. 4.6**).

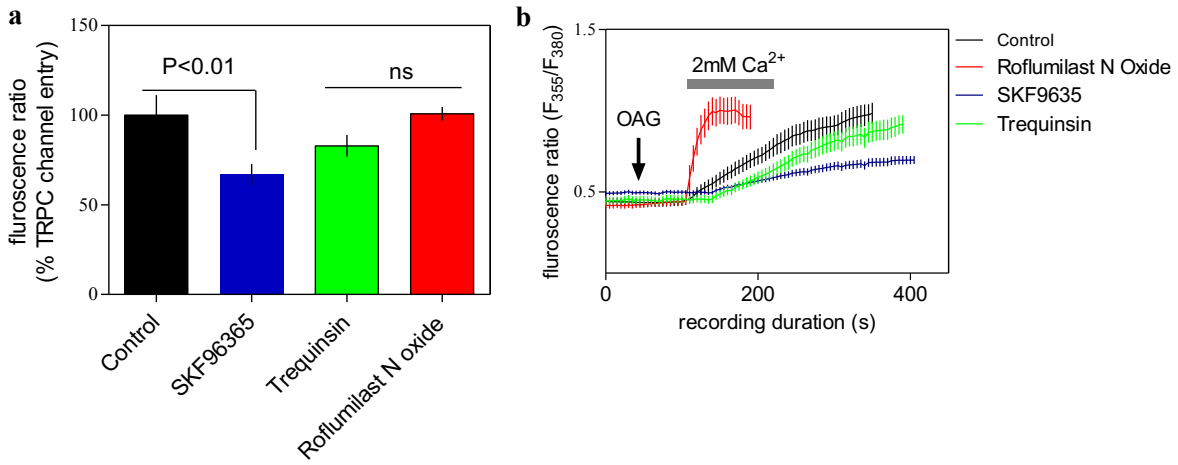

Figure 4.6 PDE inhibitors on OAG-evoked Ca^{2+} entry in RBL-1 cells.

(a) Histograms showing the peak OAG-activated Ca^{2+} entry in control cells and cells treated with 10µM of each PDE inhibitors. **(b)** Sample traces representing Ca^{2+} signals triggered by adding 100µM of OAG to RBL-1 cells with or without pre-treatment of the chosen PDE inhibitors. Each value (mean ± SEM) was derived from 3-5 independent experiments done in different days with of 30-70 cells. One-way ANOVA followed by Dunnett's test was used for statistical comparison.

4.2.3.5 Effects of selected PDE inhibitors on nuclear translocation of NFAT

To see impact of the selected PDE inhibitors on SOCE-mediated Ca^{2+} dependent cellular signalling, further experimentation was executed. For this, effect of the agents on nuclear translocation of NFAT was tested in stably expressed NFAT1(1-460)-GFP HeLa cells. During experiment, cells were treated with the inhibitors and BTP2 for ~40 min followed by addition of Tg for 5 min. Qualitative and quantitative analysis of confocal images showing increased NFAT level in nuclear region for the control cells, but such augmentation was not observed for cells treated with BTP2 and the selected PDE inhibitors (**Fig 4.7)**

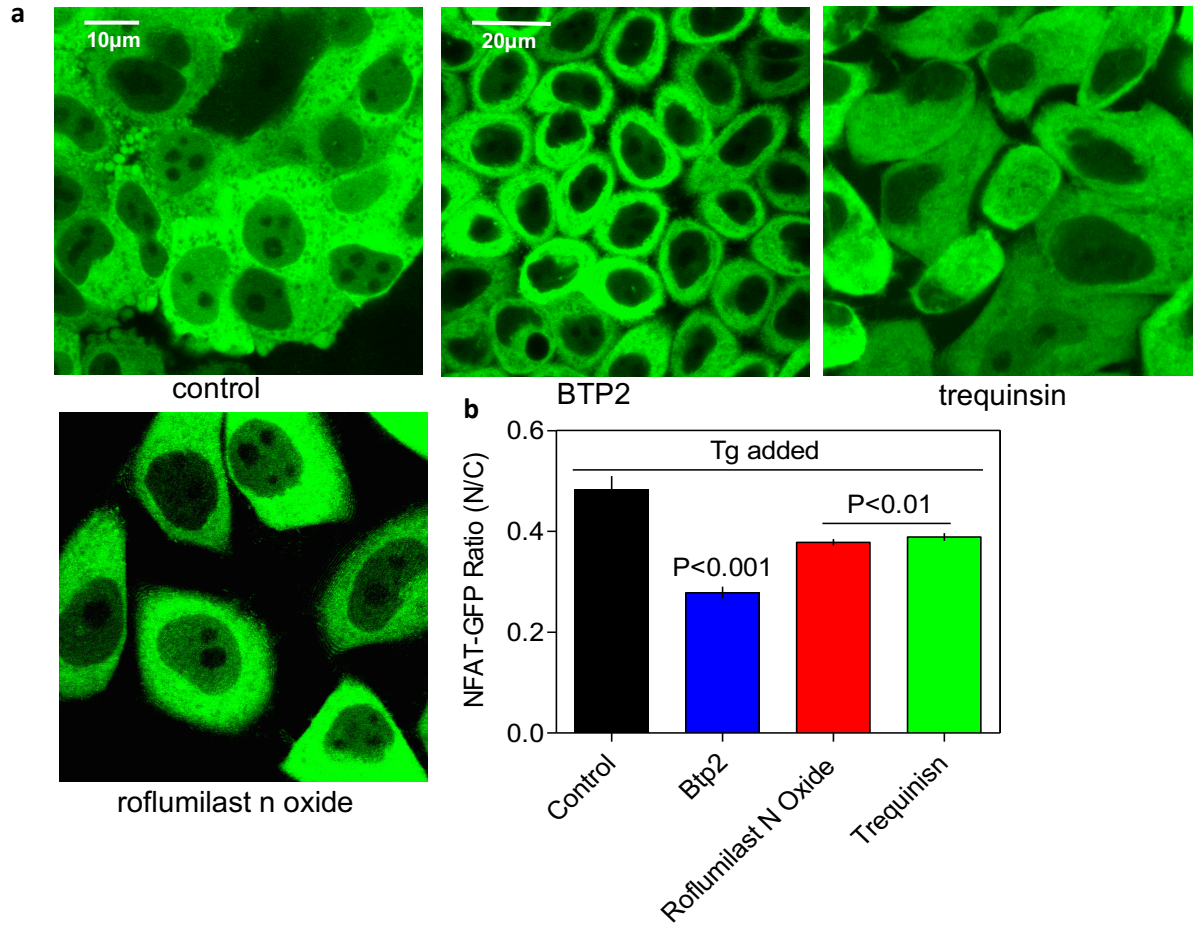

Figure 4.7 Selected PDE inhibitors on nuclear translocation of NFAT.

(a) Representative confocal images of HeLa cells showing subcellular localisation of NFAT (1–460)-GFP following application of Tg (2µM for 40 min) preceded by pre-treatment with the chosen drugs (10µM) and BTP2 (2µM) for 30 min. **(b)** Bar graphs showing the nucleus to cytoplasm ratio (mean ± SEM, n= 3 independent days, 12-15 cells for each condition) for the NFAT (1-460)-GFP under various conditions. One-way ANOVA followed by Dunnett's test was used for statistical comparison.

4.2.3.6 Selected PDE inhibitors on the oligomerisation of STIM1 and Orai1

Having found some more drugs and drug-like molecules with SOCE inhibitory property, next the underlying mechanism for such action was investigated. For this, a HEK293 cell line with an inducible mCherry-STIM1-T2A-Orai1-eGFP was used to evaluate effects of the agents on the clustering of STIM1 and also of Orai1. Before taking images using confocal microscopy, cells were treated with the inhibitors for an hour followed by addition of 2μM Tg. Qualitative and quantitively assessment showed there was no observed change in the punctate distribution of of mCherry-STIM1 or Orai1-eGFP in presence and absence of any of the PDE inhibitors and BTP2, after cells were treated with Tg (**Fig. 4.8**).

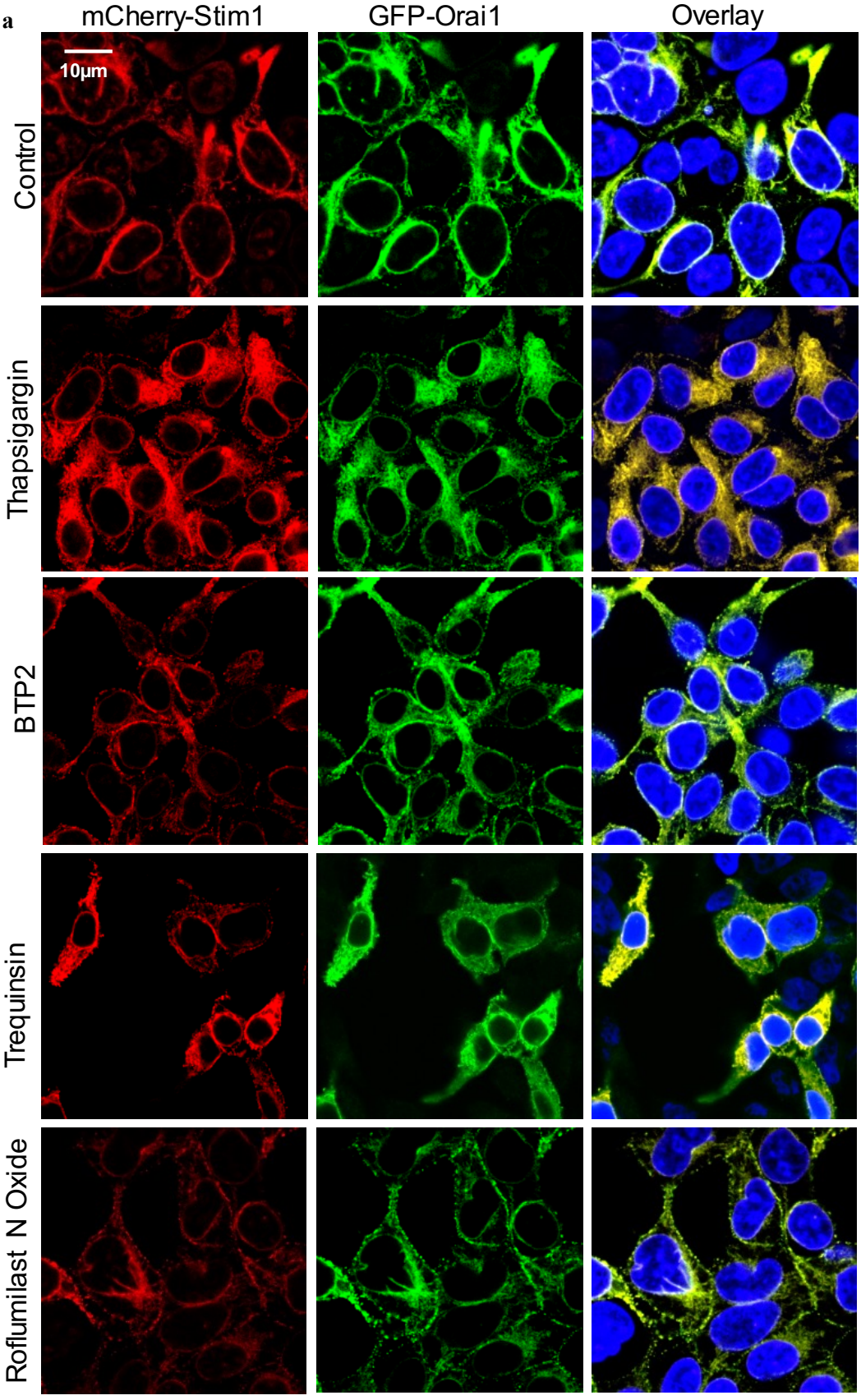
a
mCherry-Stim1
GFP-Orai1
Overlay
10µm
Control
Thapsigargin
BTP2
Trequinsin
Roflumilast N Oxide

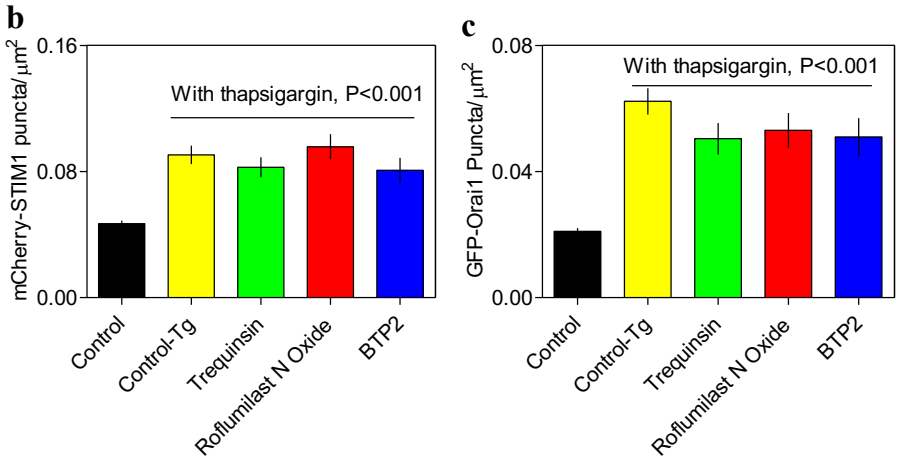

Figure 4.8 Selected PDE inhibitors on clustering of STIM-1 and Orai-1 protein.

(**a**) Representative images of HEK293 cells co-expressing mCherry-STIM1 (red) and Orai1-eGFP (green) showing translocation and colocalization of both proteins in characteristic puncta after treatment with Tg, no Tg and drugs. Quantification of mCherry-Stim1 **(b)** and GFP-Orai1 **(c)** puncta formation in response to Tg treatment and the effect of pre-treatment with drugs. The number of puncta formed in cells belonging to the control (no Tg) and the Tg-treated groups were expressed as mean/μm^2 of area ± SEM. Each bar represents data from 15-20 cells from 3 different experiments. One-way ANOVA followed by Dunnett's test was used for statistical comparison.

4.2.4 Evaluation of some DHODH inhibitors on SOCE

Two (2) defferent DHODH inhibitors were purchased to discover more potential SOCE inhibitors. Eight (8) drug-like and 3 chemical scaffolds of DHODH inhibitors namely, vidofludimus, brequinar sodium, atovaquone, ML390, 9090672,9099120 and STK485210 were tested against SOCE channel in RBL-1 cells. Protocol already described before, briefly, cells were loaded with fura-2/AM dye for ~40 min and then washed with HBSS for twice followed by treatment of each compound for 15 min. DMSO and BTP2 were included as negative and positive control respectively.

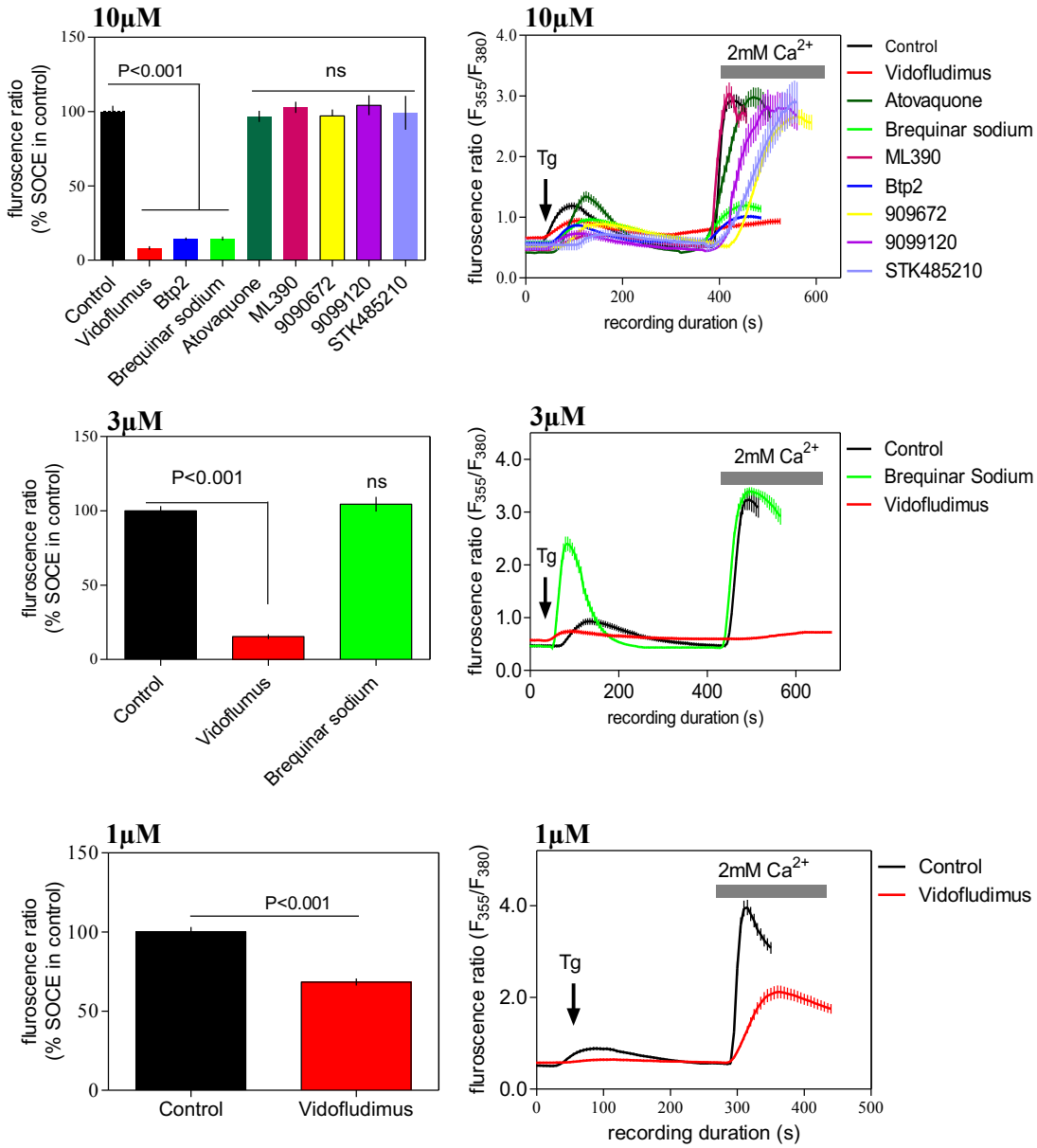

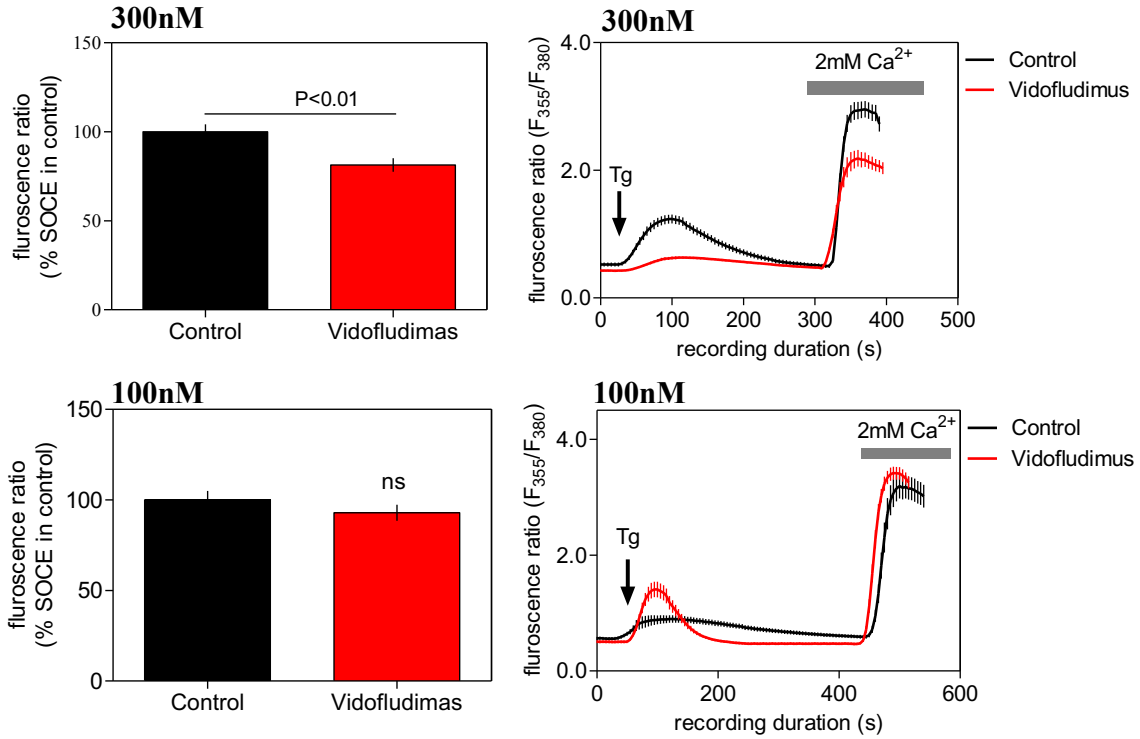

Figure 4.9 Effects of chosen drugs on the SOCE in RBL-1.

Histograms (**left column**) showing the highest peak SOCE levels triggered by Tg (2μM) in control cells and cells pre-treated with each compound at different doses. Sample traces (**right column**) representing Ca^{2+} signals (indicated by fura-2/AM fluorescence ratio) triggered by adding Tg to cells with or without pre-treatment of the chosen compounds. Each value (mean ± SEM) was derived from 3-5 independent experiments done in different days with 35-70 cells. One-way ANOVA followed by Dunnett's test was used for statistical comparison among groups and two-tailed unpaired t-test was used to compare data between groups.

Data generated from single cell Ca^{2+} imaging showing, at 10μM dose, among all, vidofludimus and brequinar appeared to manifest the maximum suppression of the Ca^{2+} entry in RBL-1 cells. At 3μM, vidofludiumus retained its ability to restrict SOCE by ~80% whereas brequinar lost SOCE inhibitory efficiency at same dose. Vidofludimus kept continue its SOCE inhibitory features until reach at dose of 100nM (**Fig 4.9**).

4.2.4.1 Determination of IC_{50} for vidofludimus

As vidofludimus significantly suppressed SOCE at 300nM (**Fig. 4.9**), therefore, complete concentration-response studies were carried out to determine the half-maximal inhibitory concentration (IC_{50}) for this compound.

As can be seen in **Fig. 4.10**, the compound showed dose-dependent suppression of SOCE over the concentration range of 30μM to 100nM. It would require ~1.4μM vidofludimus to curb SOCE by 50% in RBL-1 cells.

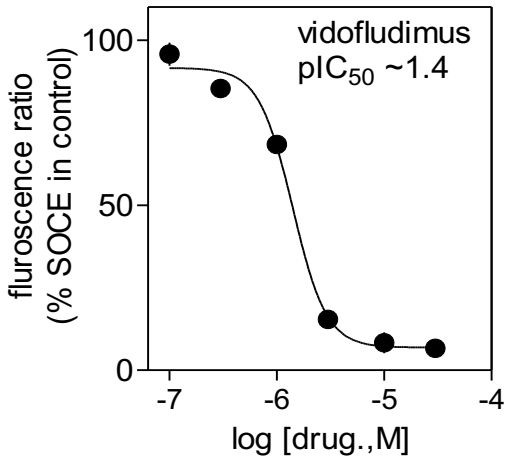

Figure 4.10 Dose response curves (DRCs) for vidofludimus.

Concentration-response curves demonstrating the dose-dependence of inhibitory effect of vidofludimus at μM dose on the SOCE in RBL-1 cells triggered by Tg. Each value (mean ± SEM) was derived from 3-5 independent experiments done in different days with 60-80 cells.

4.2.4.2 Vidofludimus on SOCE in SHSY-5Y neuroblastoma cells

Since vidofludimus was found to be the best performing DHODH inhibitor to suppress SOCE therefore this compound was taken into consideration to check whether the observed effect of these drugs on SOCE was cell-type specific or not. The small molecule was tested against SHSY-5Y cells using the same protocol used for previous SHSY-5Y related experiment. Vidofludimus retained its ability to inhibit SOCE in SHSY-5 cells at 10µM (**Fig. 4.11**).

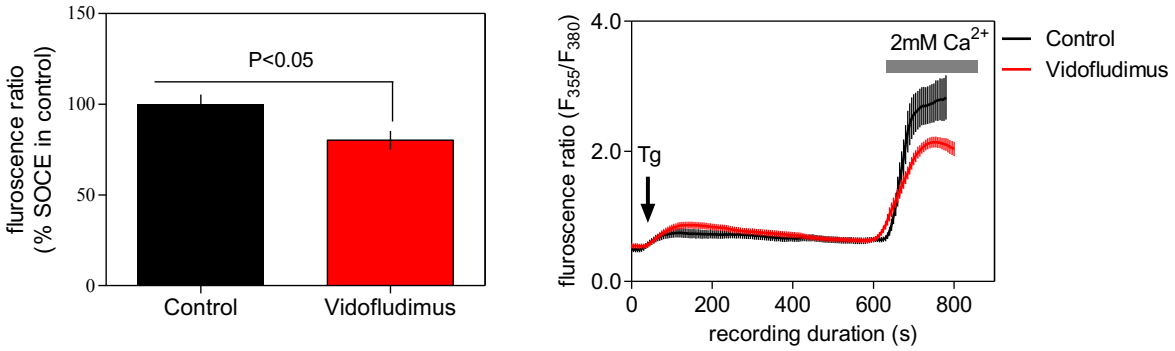

Figure 4.11 Vidofludimus on the SOCE in SHSY5Y cells.

(a) Histograms showing the highest peak SOCE levels triggered by Tg in control cells and cells pre-treated with each compound at 10µM. **(b)** Sample traces representing Ca^{2+} triggered by adding Tg to cells with or without pre-treatment of the chosen compound. Each value (mean ± SEM) was derived from 3-5 independent experiments done in different days with 30-65 cells. Two-tailed unpaired t-test was used to compare data between groups.

4.2.4.3 SOCE inhibition in RBL-1 cells after prolonged incubation

To evaluate whether longer incubation of vidofludimus could improve its potency for SOCE suppression, RBL-1 cells were pre-treated with the compound at 100nM for 48 hours. However, no SOCE inhibition was observed upon longer incubation of the compound (**Fig. 4.12**).

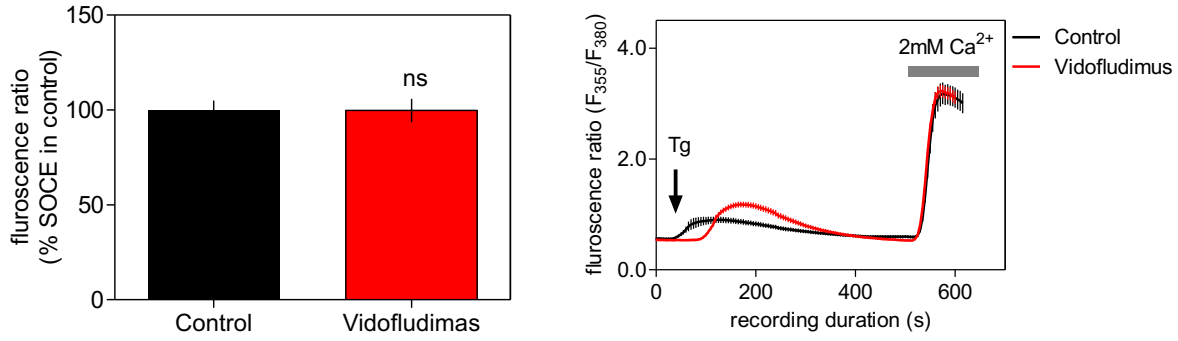

Figure 4.12 Vidofludimus on SOCE of RBL-1 cells following prolonged pre-treatment. **(a)** Histograms showing the peak SOCE levels triggered by Tg in control cells and cells pre-treated with vidofludimus at 100nM for 48 hrs. **(b)** Sample traces of changes in Ca^{2+} signals following Tg (2μM) addition as well as Ca^{2+} add back under indicated conditions of pre-treatment. Each value (mean ± SEM) was derived from 3-5 independent experiments done in different days with 70-80 cells. Two-tailed unpaired t-test was used to compare data between groups.

4.2.4.3 Vidofludimus on TRPC channel mediated Ca^{2+} entry

Next experiment was executed to investigate whether vidofludimus could affect or not TRPC mediated Ca^{2+} entry, which is triggered through addition of OAG. Data showed, vidofludimus at 10µM had no effect on TRPC mediated Ca^{2+} entry triggered by 100µM OAG in RBL-1 cells (**Fig. 4.13**).

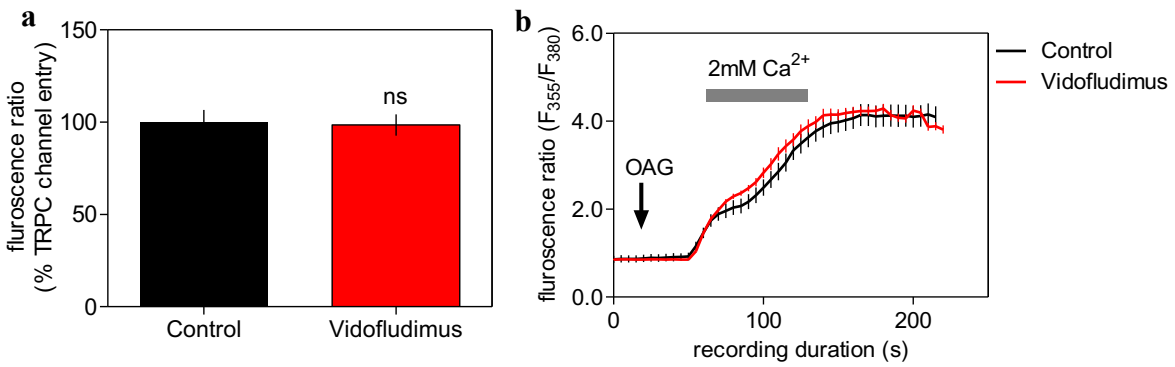

Figure 4.13 Vidofludimus on OAG-evoked Ca^{2+} entry in RBL-1 cells.

(a) Histograms showing the peak OAG-activated Ca^{2+} entry in control cells and cells treated with 10µM vidofludimus. **(b)** Sample traces representing Ca^{2+} signals triggered by adding 100µM of OAG to RBL-1 cells with or without pre-treatment of the compound. Each value (mean ± SEM) was derived from 3-5 independent experiments done in different days with 40-70 cells. Two-tailed unpaired t-test was used to compare data between groups.

4.2.4.4 Testing vidofludimus on SOCE in Human Jurkat T cells

Of the seven DHODH inhibitors, vidofludimus has shown highest potency on SOCE inhibition in various cell types therefore further testing this compound on human immune cell type was considered to check whether the observed effect was apposite to human physiology or not. To serve this aim, the compound was tested against human jurkat T-cells using the same protocol used for other Ca^{2+} imaging experiments. As can be seen in **Fig 4.14**, vidofludimus showed potency to supress SOCE in human jurkat T-cells not only at 10μM but also at 3μM dose. However, no significant SOCE suppression was noticed at 1μM dose.

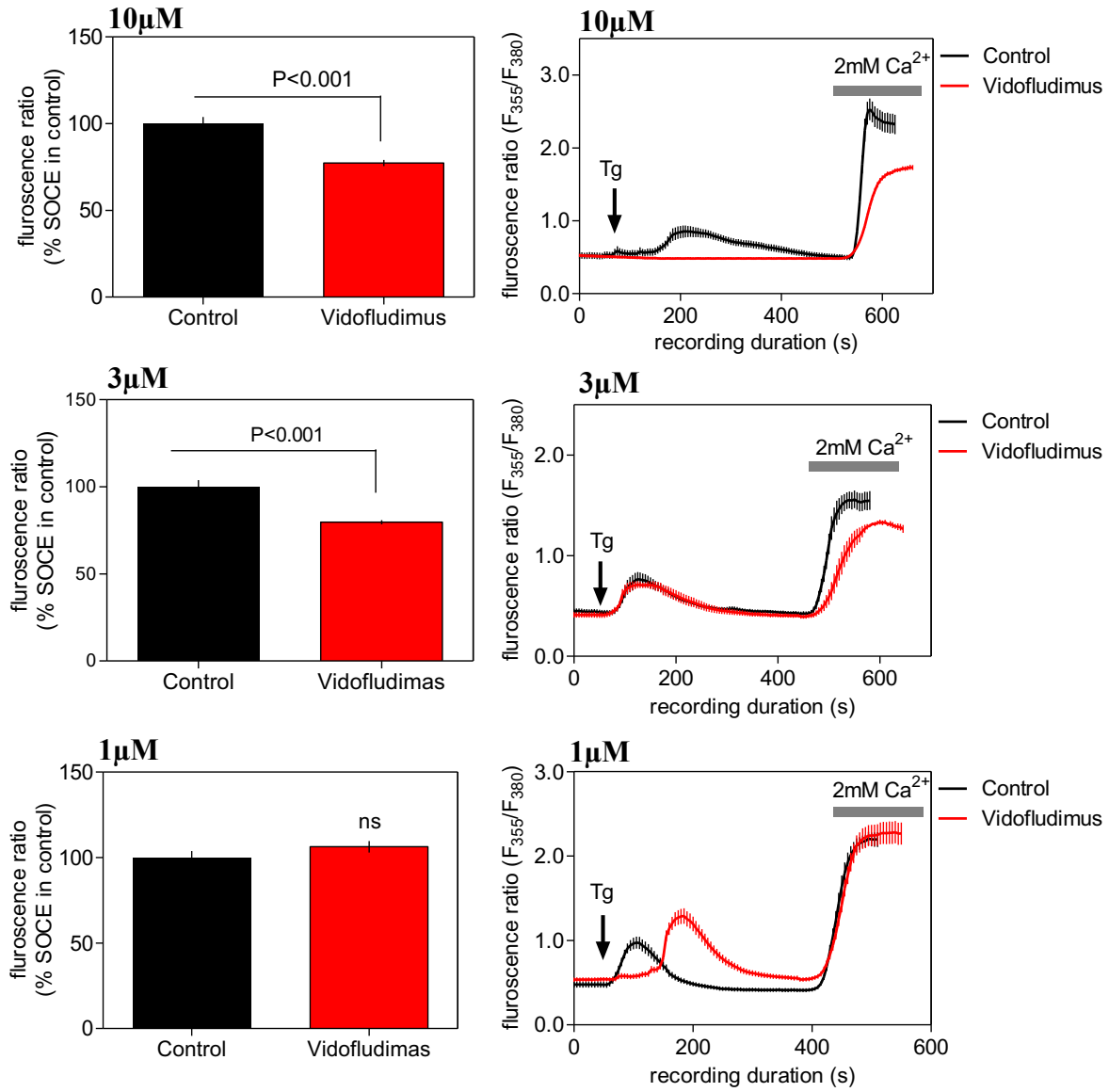

Figure 4.14 Vidofludimus on the SOCE in human jurkat T cells.

Histograms (**left column**) showing the highest peak SOCE levels triggered by 2µM Tg in control cells and cells pre-treated with vidofludimus at different doses. Sample traces (**right column**) representing Tg triggered-Ca^{2+} signals to cells with or without pre-treatment of the drug. Each value (mean ± SEM) was derived from 3-5 independent experiments done in different days with 35-50 cells. Two-tailed unpaired t-test was used to compare data between groups.

4.2.4.5 Effects of vidofludimus on nuclear translocation of NFAT

To observe the impact of vidofludimus on SOCE-mediated Ca^{2+} dependent cellular signalling, further investigation was performed. For this, effect of the compound on nuclear translocation of NFAT was tested in stably expressed NFAT1(1-460)-GFP HeLa cells. During experiment, cells were treated with the drug and known SOCE blocker, BTP2 for ~40 min followed by addition of Tg for 5 min. Qualitative and quantitative analysis of confocal images showing increased NFAT level in nuclear region for the control cells, but such augmentation was not observed for cells treated with BTP2 and the drug (**Fig. 4.15**).

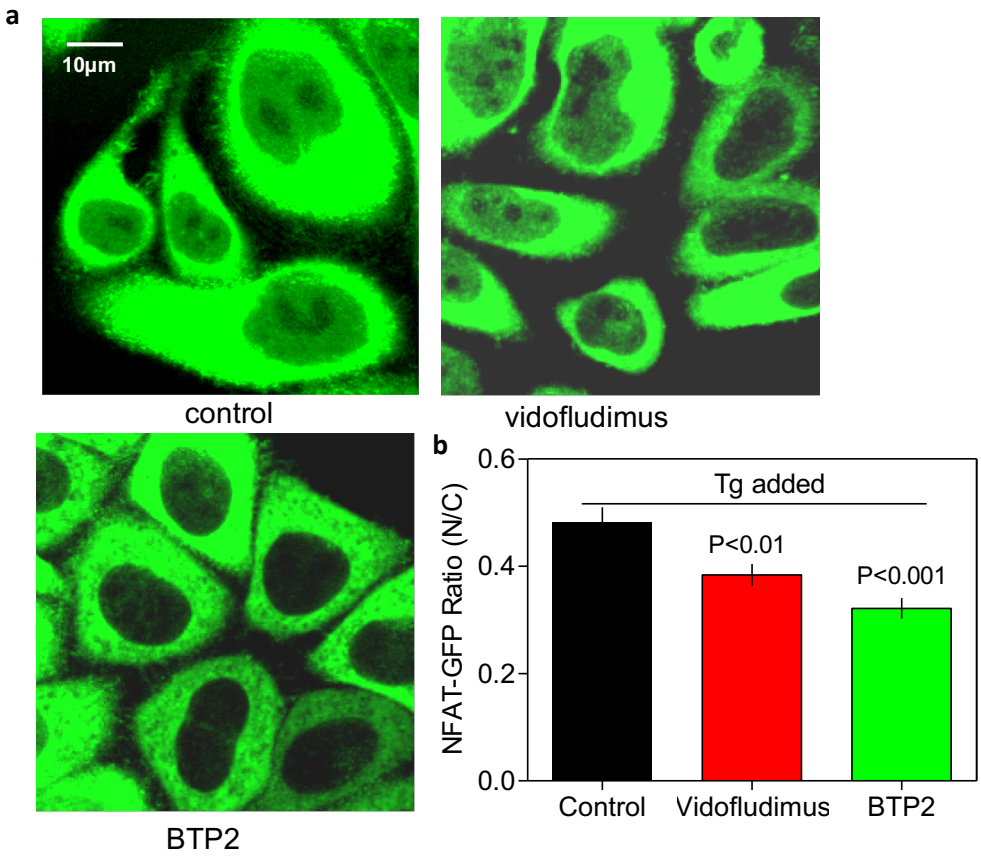

Figure 4.15 Vidofludimus on nuclear transolcation of NFAT.

(a) Representative confocal images of HeLa cells showing subcellular localisation of NFAT (1-460)-GFP following application of Tg (2µM for 40 min) preceded by pre-treatment with the drug (10µM) and BTP2 (2µM) for 30 min. **(b)** Bar graphs showing the nucleus to cytoplasm ratio (mean ± SEM, n= 3 independent days, 12-15 cells for each condition) for the NFAT (1-460)-GFP under various conditions.

4.2.4.5 Effects of vidofludimus on the oligomerisation of STIM1 and Orai1

With a view to inquire possible mechanism underlying SOCE inhibitory properties of the drug further investigation was carried out. HEK293 cell line with an inducible mCherry-STIM1-T2A-Orai1-eGFP was used to evaluate effect of the compound on the clustering of STIM1 and also of Orai1. Cells were treated with vidofludimus and known SOCE inhibitor, BTP2 for an hour followed by addition of 2μM Tg for 5 min. After that cells were imaged using confocal microscope. Qualitative and quantitative assessment showed, no change was observed in the punctate distribution of mCherry-STIM1 or Orai1-eGFP in presence and absence of the compound and BTP2, after cells were treated with Tg (**Fig. 4.16**).

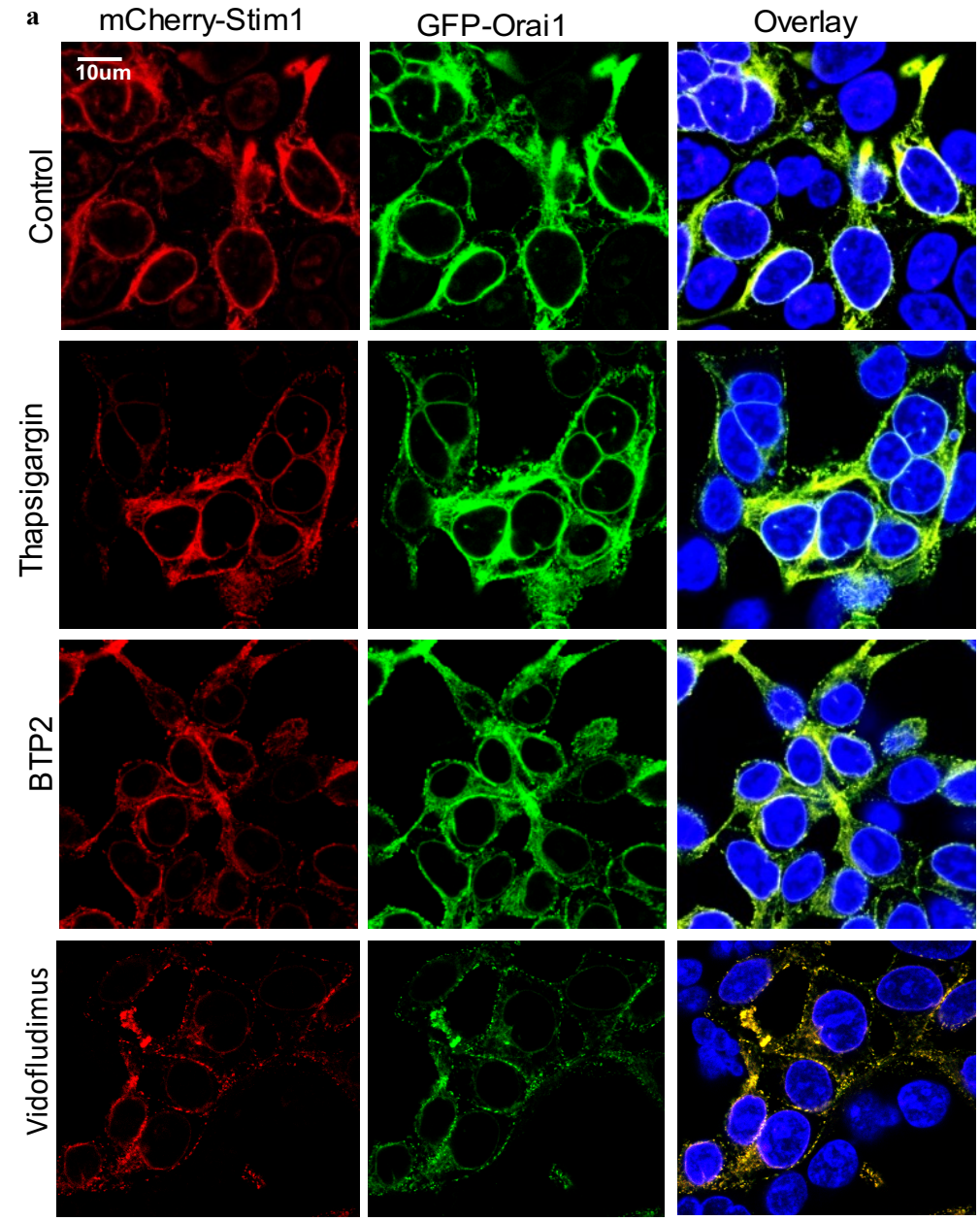
a
mCherry-Stim1
GFP-Orai1
Overlay
10um
Control
Thapsigargin
BTP2
Vidofludimus

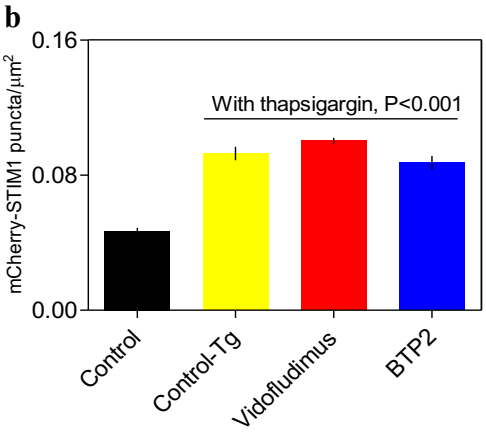
b
mCherry-STIM1 puncta/μm2
0.16
0.08
0.00
With thapsigargin, P<0.001
Control
Control-Tg
Vidofludimus
BTP2

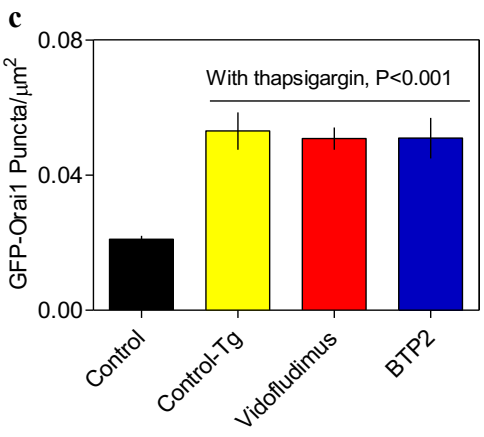
c
GFP-Orai1 Puncta/μm2
0.08
0.04
0.00
With thapsigargin, P<0.001
Control
Control-Tg
Vidofludimus
BTP2

Figure 4.16 Vidofludimus on clustering of STIM-1 and Orai-1 protein.

(a) Representative images of HEK293 cells co-expressing mCherry-STIM1 (red) and Orai1-eGFP (green) showing translocation and colocalization of both proteins in characteristic puncta after treatment with Tg, no Tg and compounds. Quantification of mCherry-Stim1 **(b)** and GFP-Orai1 **(c)** puncta formation in response to Tg treatment and pre-treatment with compounds. Each bar represents data from 10-15 cells from 3 different experiments. One-way ANOVA followed by Dunnett's test was used for statistical comparison.

4.3 Discussion

In chapter 3, it was demonstrated that using virtual screening methodology followed by biological experimental procedure out of 10 chosen drugs, 5 drugs, namely, leflunomide, teriflunomide, tolvaptan, lansoprazole and roflumilast, have been found to supress SOCE significantly at ≤10 μM dose (**Fig. 3.4**). Besides SOCE inhibitory properties, these 5 SOCE inhibitory drugs have their own distinct known action mechanism. Currently, more analogues, drugs or drug-like compounds are available for each of the SOCE inhibitor class, therefore extended investigation was executed aiming to get more potent SOCE inhibitors from respective inhibitory class.

To hunt more SOCE inhibitor with better potency, 4 non-peptides arginine-vasopressin receptor (AVR) antagonists, 5 proton pump inhibitors (PPIs); of them 3 prazole and 2 non-prazole PPI inhibitors; 4 phosphodiesterase4 (PDE4) inhibitors, 7 other PDE family inhibitors and 7 dihydroorotate dehydrogenase (DHODH) inhibitors were purchased.

Since the best performing drugs inhibited SOCE at ~10μM dose in chapter 3, therefore, goal of the present study was to find out any drug or compound that potentially would inhibit SOCE at lower than this concentration. For this reason, 10μM was the maximal dose used for any single cell Ca^{2+} imaging experiment in this study.

AVR antagonists and PPIs were preincubated for ~15 min at 10μM dose, none of them showed any SOCE suppression (**Fig. 4.1** and **Fig 4.2**) in single cell Ca^{2+} imaging experiment, therefore, no further studies were performed with these two classes inhibitors.

From the PDE4 inhibitors, only roflumilast n oxide showed SOCE inhibition potency below 10μM, eventually reached at 3μM (**Fig. 4.3**), the latter dose was lower than the minimal SOCE inhibitory dose of its pro-drug, roflumilast (**Fig. 3.4**). This means roflumilast N-oxide was better potent than its prodrug. After getting a better SOCE inhibitory compound from PDE4 inhibitor family, other PDE inhibitor classes were included and tested them against SOCE in RBL-1 cells. Out of seven different PDE inhibitors, two of them, namely trequinsin, and Bay73966 inhibited SOCE at 10μM. Trequinsin retained its ability to supress SOCE at 3μM (**Fig 4.4**) which was egalitarian to PDE4 inhibitor, roflumilast n oxide. Due to vast number of inhibitors in the market, it was not possible to test all the PDE inhibitor classes against SOCE.

At this point, trequinsin and roflumilast N-oxide, out of the eleven different PDE inhibitors, were found to be the best potent compounds against SOCE. It was worth to mention that both of these compounds have shown better efficiency than their homologous drug, roflumilast (**Fig 3.4**) and their efficiency remain unchanged when tested in a different cell line such as SHSY5Y cells (**Fig. 4.5**).

SOCE inhibition mediated by best performing PDE inhibitors was observed upon acute incubation of the compounds however, any potential effect of chronic incubation (~24hrs) of these compounds on SOCE was not investigated due the fact that their homologous drug, roflumilast previously failed to inhibit SOCE inhibition after longer treatment at lesser dose (1μM) (**Fig. 3.7**).

In many cells including neurons, it has been found that store-depletion allows STIM proteins to activate some TRPC channels as well and Ca^{2+} via these channels then contribute to the SOCE observed (Liao et al. 2008). Best performing PDE inhibitors were tested against TRPC channel, however, no effect on TRPC was noticed (**Fig. 4.6**). This indicated their SOCE inhibition might be specific to Orai- mediated Ca^{2+} entry. Such proposition was set due to the fact hitherto molecular make-up of SOCE channel is largely unknown. One hypothesis proposed SOCE channels to be formed solely by Orai proteins whereas other one proposed, SOCE channels to be composed of both Orai and TRPC proteins(Zagranichnaya, Wu, and Villereal 2005; Hogan and Rao 2007; Liao et al. 2008).

The next step was to see whether these two PDE inhibitors could affect nuclear translocation of NFAT or not. The later, already described, is widely known to be activated via SOCE mediated Ca^{2+} signals therefore NFAT translocation into nucleus can be disrupted by inhibition of SOCE, for instances in presence of SOCE blockers (Ishikawa et al. 2003). The effect of SOCE interruption on NFAT translocation can be studied using fluorescence-tagged NFAT (Prakriya and Lewis 2015). Given the observed SOCE-inhibitory property of the compounds, it was satisfying to see their complementary ability to retard nuclear translocation of NFAT1(1–460)-GFP in HeLa cells (**Fig. 4.7**).

The possible mechanism action of SOCE inhibition by these compounds was something important to unravel. They might act intracellularly or could affect the clustering of STIM1 and Orai1 when supressed $Ca2^{+}$ entry. The former might not be the case because molecules were exposed for short period of time (~15min) which was possibly not enough to modify any intracellular mechanism.

Therefore, experiments were performed to chase the queries, in case if the agents could act either on Orai1 channels that are already activated due to Tg triggered ER store depletion via interaction with aggregated STIM1 proteins or these drugs may block SOCE extracellularly. Using confocal microscopy with a HEK293 cell line with an inducible mCherry-STIM1-T2A-Orai1-eGFP, none of the drugs along with BTP2 showed any efficiency on either STIM1 puncta formation or Orai1 puncta formation (**Fig. 4.8**). Hence SOCE inhibitory properties of these drugs could be attributed to their possible extracellular action, like acting as pore blocker. This presumption might be true and supported by previous study where researchers have shown that higher external Ca^{2+} concentrations are correlated with reduced BTP2 mediated SOCE inhibition (Zitt et al. 2004). Additionally. it can be proposed that these drugs might have unknown extracellular binding sites, however, this definitely requires direct experimental validation. This could be done by blocking the series of plasma membrane receptors through either pharmacological inhibitors or knocking down specific gene for the respective receptor.

Since teriflunomide, a DHODH inhibitor exhibited better potency than other candidates in the earlier studies (**Fig. 3.1**) therefore a handful number of additional DHODH inhibitors were chased against SOCE in RBL-1 cells. Data from single cell Ca^{2+} imaging showing upon acute incubation, of the seven DHODH inhibitors, vidofludimus and brequinar sodium supressed SOCE at 10μM although latter compound did not show any inhibition at 3μM while the former appeared to inhibit SOCE at progressively lower doses unit it reached at 100nM (**Fig. 4.9**).

Vidofludimus was the only candidate from 40 different drugs and compounds showed SOCE inhibition at nanomolar concertation in RBL-1 cells. Complete concentration-response study was carried out in RBl-1 cells to determine the IC_{50} for this drug and it appeared to display IC_{50} of 1.4μM (**Fig. 4.10**) which was eventually the lowest IC_{50} dose in comparison to other potent SOCE inhibitors found in this study. Even this compound has shown more potency than known SOCE inhibitor, BTP2 that blocked SOCE in RBL-1 cell with IC_{50} of ~4.4μM (**Fig. 3.5**).

It was interesting to see vidofludimus showed better potency to inhibit SOCE in comparison to similar class inhibitor, brequinar sodium. The latter case was discovered to be one of the strongest known inhibitor of human DHODH, with an IC_{50} of 1.8nM (Sainas et al. 2017) whereas vidofludimus was found to inhibit DHODH, with an IC_{50} of 134nM (Kulkarni et al. 2010). This indicated SOCE inhibitory properties of these compounds as well as other DHODH inhibitors, were independent of their ability to inhibit DHODH. Hence it can be said that these compounds ensue a different way to supress SOCE other than their known action mechanism.

Like other SOCE inhibitors, vidofludimus also was not cell type specific to inhibit SOCE (**Fig. 4.10**). Although this molecule inhibited least significant SOCE at 300nM upon acute incubation but failed to retain this property during chronic treatment (~24hrs) of 100nM dose (**Fig. 4.12**). This was surprising as leflunomide and its metabolite teriflunomide though showed least significant SOCE inhibition at 10μM but effectual to supress SOCE at very lesser dose (01μM) upon chronic treatment (**Fig. 3.7**). This again pointed out that SOCE inhibitory property is possibly associated with incubation time and structural distinction of the compounds. Since TRPC proteins are conceivably part SOCE (Liao et al. 2008) therefore vidofludimus was examined against TRPC channel and this channel was found to be non-affected by the compound (**Fig 4.13**). Hence presumably like other molecules, vidofludimus also may be specific to Orai-mediated SOCE inhibition.

Vidofludimus, the most potent SOCE inhibitor found in this study, is known to inhibit interleukin 17 (IL-17) production in activated lymphocytes (Fitzpatrick et al. 2010), therefore any effect of this agent on SOCE in human immune cell type was an interesting observant. Human jurkat T cells was considered to serve this purpose. As expected this compound showed its potency to supress SOCE in jurkat T cells at relatively lower dose (3μM) (**Fig. 4.14**).

The suggested mechanism of IL-17 inhibition by the compound was independent of DHODH inhibition (Fitzpatrick et al. 2010) rather due to hitherto known mechanism; attenuation of STAT3 and NF-κB-signalling pathways (Fitzpatrick et al. 2011), hence, SOCE inhibition in jurkat T cells indicated this compound might have a significant role in IL-17 production as well as other interleukins secretion. However, this definitely requires further experimental validation.

Vidofludimus significantly restricted NFAT translocation in nucleus (**Fig. 4.15**) as well as didn't affect either STIM1 puncta formation or Orai1 puncta formation (**Fig. 4.16**). Probably this molecule also shared the similar mechanism of action on NFAT translocation and STIM1-Orai1 puncta formation demonstrated by other inhibitors, therefore any attributes and propositions already suggested for such-like mechanisms also could be implicated to this compound.

Chapter 5

Results III - Selected inhibitors on other Ca^{2+} channels

5.1 Introduction

In calcium signalling cells secure the 'extra' Ca^{2+} as release from the internal stores, e.g., endoplasmic reticulum (ER) as well as entry from the extracellular space. The foremost Ca^{2+} entry mechanism in excitable cells occurs through voltage gated Ca^{2+} channels (VGCC) and through a distinct Ca^{2+} influx mechanism widely known as the store operated Ca^{2+} entry (SOCE) pathway in non-excitable cells (Berridge 1995; Berridge et al., 2000).

Ca^{2+}release via inositol 1,4,5-trisphosphate (IP_3) signalling pathway

In response to many stimuli (such as neurotransmitters, hormones and growth factors) G-protein-coupled receptors located at the plasma membrane (PM) facilitate activation of phospholipase C (PLC). PLC catalyses the hydrolysis of phosphatidylinositol 4,5-bisphosphate (PIP_2), a membrane bound phospholipid, to form both inositol 1,4,5-trisphosphate (IP_3) and diacylglycerol (DAG). DAG remains in the PM and activates protein kinase C (PKC). IP_3 diffuses through the cytosol and binds to and activates IP_3 receptors located on the ER membrane. Opening of these channels allows Ca^{2+} to move down its concentration gradient from the ER (~500μM) into the cytosol (~100nM) and deplete ER stores through IP_3Rs (Berridge 1993; Bootman et al. 2001). This bifurcating messenger system (IP_3 and DAG) operates throughout the life of a typical cell, beginning with gametogenesis, fertilization, cell proliferation and early development and continuing through differentiation to perform very precise control functions in a whole variety of specialized cells in both animals and plants (Berridge 1993).

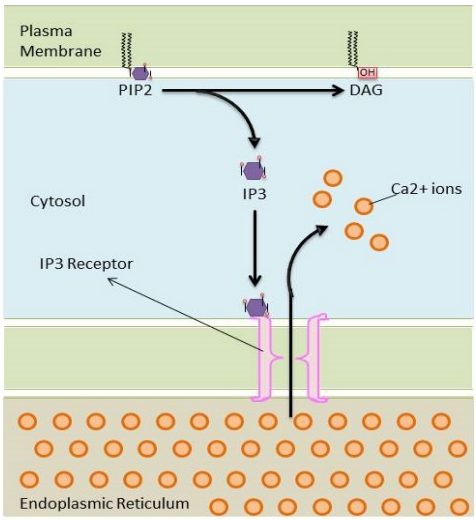

Figure 5.1 IP_3 pathway. Binding of agonist to the plasma membrane initiates the signaling cascade that activates PLCγ, which cleaves PIP2, producing IP_3. IP_3 subsequently binds to the Ca^{2+} channel IP_3 receptor in the endoplasmic reticulum (ER) membrane, triggering a release of Ca^{2+} from the ER stores into the cytoplasm.

Ca^{2+}entry via voltage gated calcium channel (VGCC) pathway

Voltage gated Ca^{2+} channels in many different cell types activates on membrane depolarization and mediate Ca^{2+} influx in response to action potentials and sub-threshold depolarizing signals. There are 10 members of the voltage-gated Ca^{2+} channel family in mammals, and they serve distinct roles in cellular signal transduction.

Ca^{2+} entering the cell through voltage-gated Ca^{2+} channels serves as the second messenger of electrical signalling, initiating many different cellular events including contraction, secretion, synaptic transmission, enzyme regulation, protein phosphorylation/dephosphorylation, and gene transcription (Catterall 2011).

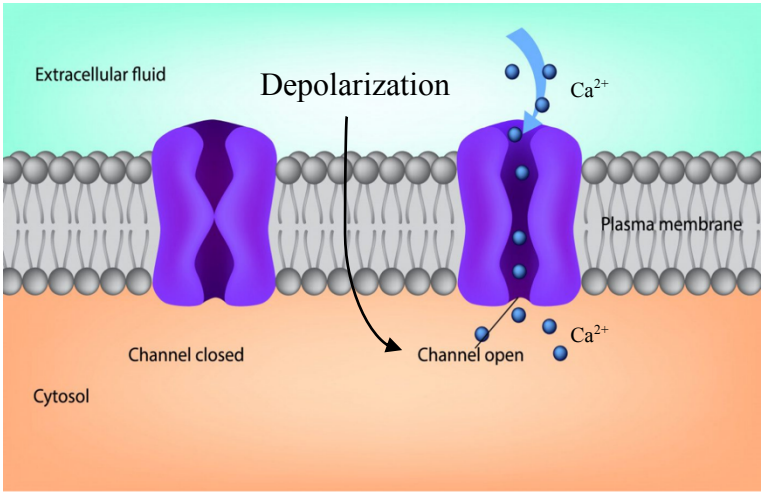

Figure 5.2 Voltage gated calcium channel pathway. In response to depolarizing changes in membrane potential, voltage-gated calcium channels rapidly open (within 1ms), raising intracellular calcium to affect membrane electrical properties such as bursting and firing patterns.

5.1.1 Aim of the project

Since Ca^{2+} release from ER via IP_3 and entry from extracellular environment via VGCC are foremost parts of Ca^{2+} signalling, therefore any possible effect of SOCE inhibitors found in this study on both release and entry pathway were an undeniable step to investigate.

The specific aims of this project were

(a) investigating role of the selected SOCE inhibitors on ER-Ca^{2+} release via IP_3

(b) exploring effect of the inhibitors on voltage gated Ca^{2+} entry.

5.2 Results

5.2.1 Evaluation of selected SOCE inhibitors on Ca^{2+} release from ER

Effect of selected SOCE inhibitors, vidofludimus, trequinsin and teriflunomide, on Ca^{2+} release from ER was observed in SH-SY5Y neuroblastoma cells. Cells were loaded with 2µM fura-2/AM for ~40 min and prepared for single cell Ca^{2+} imaging. Ca^{2+} release from ER was triggered due to addition of 100µM carbamylcholine (CCh) the latter is a widely used agonist of muscarinic acetylcholine receptors (mAChRs). CCh led to the depletion of ER Ca^{2+} through IP_3-induced Ca^{2+} release.

As can be seen in **Fig. 5.3,** vidofludimus significantly reduced Ca^{2+} release from ER triggered via GPCR stimulation while other two compounds had no effect on such signal.

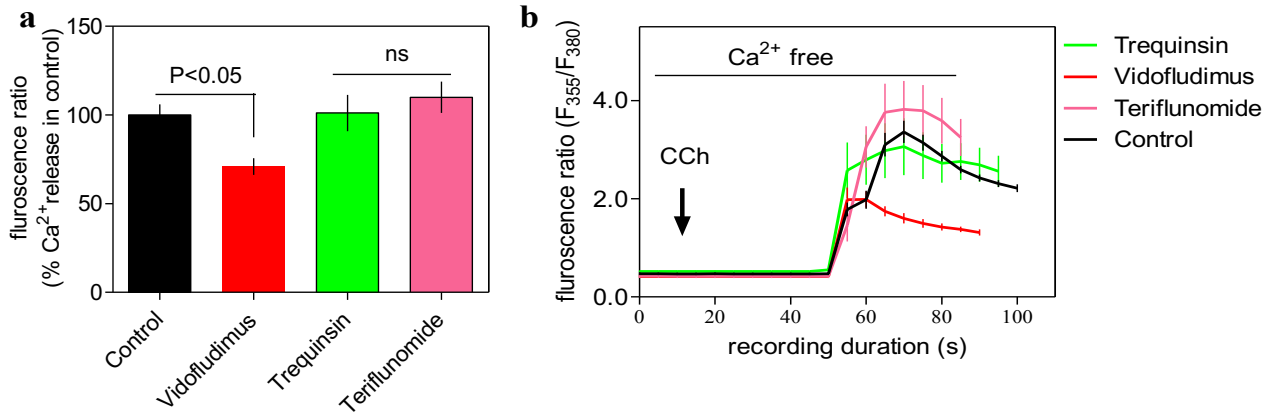

Figure 5.3 Selected SOCE inhibitors on Ca^{2+} release from ER in SHSY5Y cells.

(a) Bar diagram shows fluorescence peak ratio of CCh-evoked-Ca2+ release signals in control cells and cells pre-treated with drugs at 10µM. **(b)** Sample traces representing Ca^{2+} release signal triggered by CCh to cells with or without pre-treatment of the chosen compounds at 10µM. Each value (mean ± SEM) was derived from 3-5 independent experiments done in different days with 60-70 cells. One-way ANOVA followed by Dunnett's test was used for statistical comparison.

5.2.2 Selected SOCE inhibitors on voltage gated channel Ca^{2+} entry

In order to test whether these compounds had any effect on Ca^{2+} entry via voltage gated channel Ca^{2+}, potassium chloride (KCl) evoked depolarization experiment was carried out in SHSY-5Y cells. High concentration of KCl solution (70mM) depolarized the cells which then triggered extra cellular calcium entry into the cells. Data extracted from single cell Ca^{2+} imaging showing none of the selected compounds had any effect on voltage gated channel mediated Ca^{2+} entry (**Fig. 5.4**). As expected known calcium channel blocker, nifedipine, supressed Ca^{2+} entry via VGCC **(Fig. 5.4**).

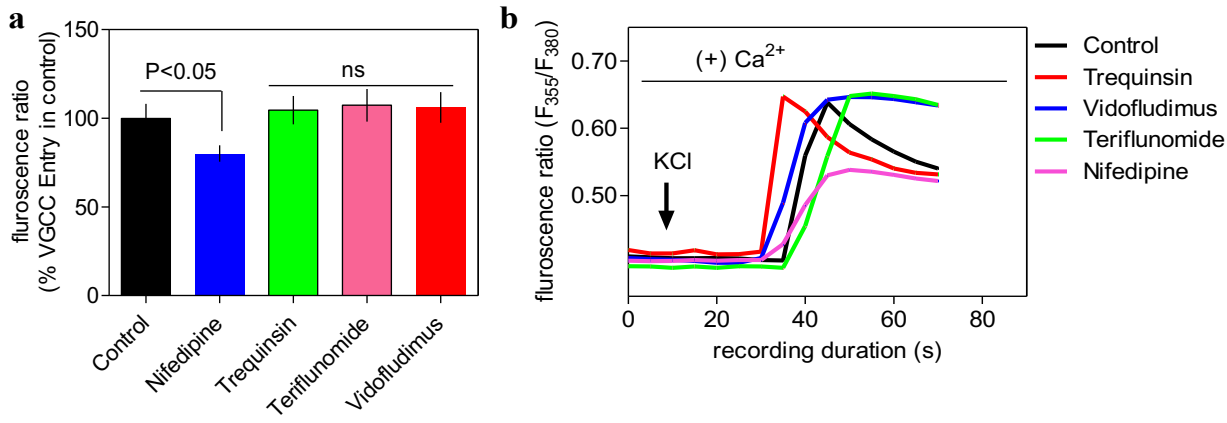

Figure 5.4 Selected SOCE inhibitors on voltage-gated Ca^{2+} entry in SHSY5Y cells.

(a) Bar diagram shows fluorescence peak ratio of voltage-gated Ca^{2+} entry in control cells and cells pre-treated with drugs at 10µM. **(b)** Sample trace representing voltage-gated Ca^{2+} entry triggered via 70mM KCl to cells with or without pre-treatment of the chosen compounds at 10µM. Each value (mean ± SEM) was derived from 3-5 independent experiments done in different days with 450-70 cells. One-way ANOVA followed by Dunnett's test was used for statistical comparison.

5.3 Discussion

SHSY-5Y cells were chosen to study the effect of these compounds on IP_3 and VGCC mediated Ca^{2+} signaling. Previously neuroblastoma and/or neural crest cell lines were used to study both IP_3 evoked ER-Ca^{2+} release (Vaughan et al. 1995) and voltage dependent Ca^{2+} entry (Di Virgilio et al. 1987).

It was interesting to see upon acute incubation (~15min), vidofludimus affected ER-Ca^{2+} release in SHSY-5Y cells (**Fig. 5.3**). This effect could be due to either extracellular occupancy of this compound to the binding site of the receptor in plasma membrane or intracellular blockade of IP_3Rs, either case, could reduce ER-Ca^{2+} release. However, other unknown action mechanism might exist behind this phenomenon though such claim requires experimental evidences to support. None of the compounds found to inhibit VGCC mediated entry upon KCl evoked depolarization (**Fig. 5.4**).

As previously these compounds were not known to have any effect on Ca^{2+} signalling therefore any impact of these agents on Ca^{2+} signalling modification was added-knowledge to the respective research field.

Chapter 6

Results IV - Biological evaluation of selected SOCE inhibitory compounds

6.1 Introduction

SOCE pathway over the years has been implicated in several diseases including severe Combined immunodeficiency (SCID) disorders, inflammatory bowel disease, neurodegenerative diseases, cardiovascular disorders and to various forms of cancers (Parekh 2010; Roberts-Thomson et al. 2010). Ca^{2+} signalling including SOCE plays essential roles in a wide variety of cellular processes, from gene transcription to cell proliferation and differentiation (Berridge et al. 2003).

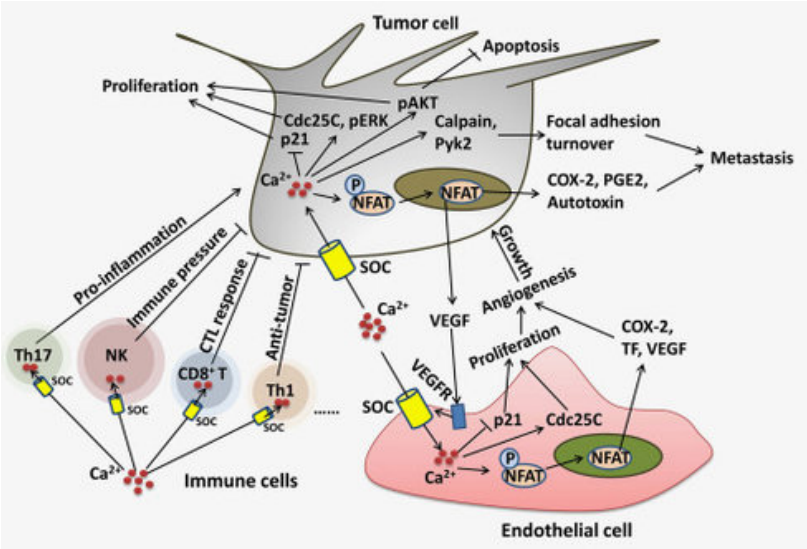

Figure 6.1 Proposed roles of SOCE in cancer. In tumor cells, SOCE promotes cancer cell proliferation via the upregulation of Cdc25C and the downregulation of p21. It also promotes cancer cell metastasis via the modulation of calpain- and Pyk2-mediated focal adhesion turnover or through upregulating the expression of COX-2, PGE2 and autotoxin. SOCE also contributes to drug resistance through an enhancement of AKT activity. In cancer cells, SOCE boosts the secretion of VEGF, which facilitates endothelial cell proliferation, angiogenesis and tumor growth. SOCE-mediated chronic inflammation through activation of Th17 cells is speculated to promote tumor growth. However, in NK, CD81 T and Th1 cells, SOCE is required to inhibit tumor progression. Figure is taken from Xie et al. 2016.

6.1.1 Aim of the project

Best preforming SOCE inhibitors found in this study were tested sought to find any impact on biological processes. The aims of this project were to study the impact of the compounds on

(a) cancer cell proliferation and

(b) neuroblastoma cells differentiation.

6.2 Results

6.2.1 Evaluation of selected inhibitors on lung cancer cell proliferation

To explore any effect of these compounds on cancer cell proliferation, three different lungs cancer cell line, named, H520, H1792, and LK2 were treated with the compounds for 72 hrs. Then adding cell counting kit for few hours followed by absorbance measurement using microplate reader, number of viable cells were detected from counting formazan formation. **Fig. 6.2** showed dose dependence inhibitory effect of the compounds on cell proliferation different lung cancer cell line. pIC_{50} dose for each compound on different lung cancer cell lines was summarised in the **table 4.1**.

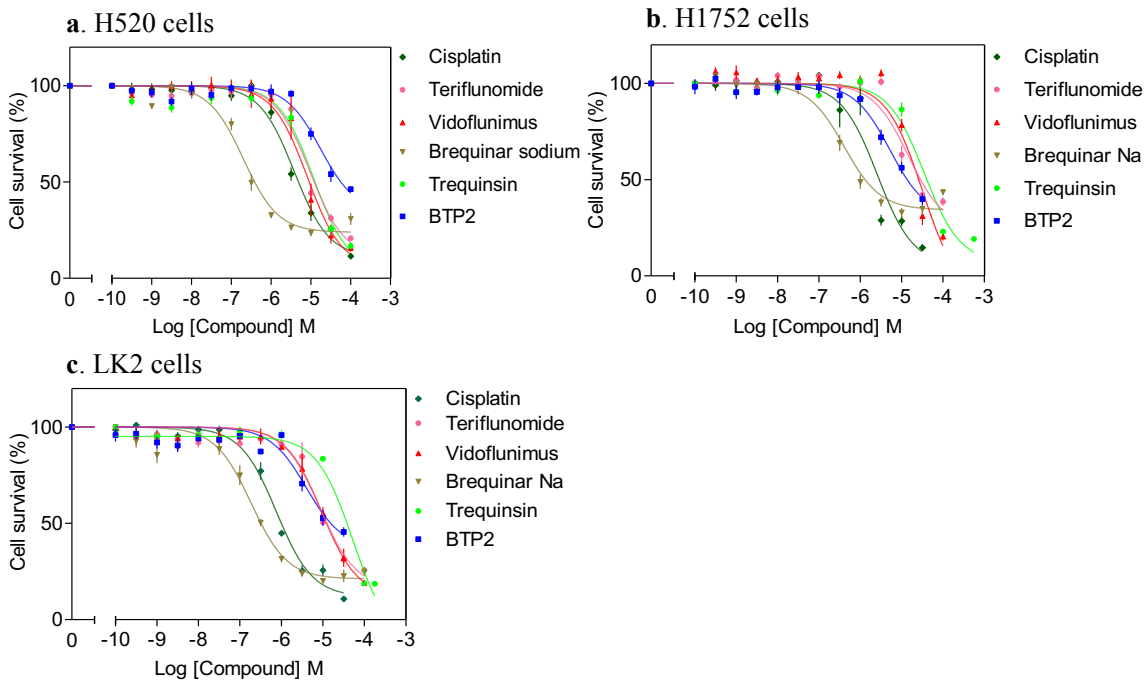

Figure 6.2 Does response curves (DRCs) for selected inhibitors.

Concentration-response curves demonstrating the dose-dependence of inhibitory effect of indicated compounds on cell proliferation in **(a)** H520 cells **(b)** H1752 cells and **(c)** LK2 cells. Each value (mean ± SEM) was derived from 3 individual experiments.

Table 6.1 pIC_{50} of selected compounds for different lung cells

Drug/compound	H520 (pIC_{50}, µM)	H1792 (pIC_{50}, µM)	LK2 (pIC_{50}, µM)
Cisplatin	~3.79	~2.562	~7.62
Teriflunomide	~9.470	~1.475	~8.42
Vidofludimus	~8.096	~3.188	~9.36
Brequinar sodium	~2.018	~4.098	~1.86
Trequinsin	~1.49	~3.51	~4.04
BTP2	~1.14	~5.23	~3.97

Table 6.1 shows half maximal inhibitory concentration (pIC_{50}) of the compounds tested against different lung cells. pIC_{50} of these compounds vary depending on the cell types.

6.2.1.2 SOCE inhibition in lung cancer cell at pIC_{50} dose

To know whether cancer cell proliferation was due to SOCE inhibitory properties of these compounds or not, single cell Ca^{2+} imaging experiments were taken into consideration. Lung cancer cell lines were pre-incubated with the compounds at their respective pIC_{50} dose (**table 6.1**) for ~15 min. Protocol already used in this study was followed for single cell Ca^{2+} imaging experiment. As can be seen in **Fig. 6.3,** each of the compounds supressed SOCE in different cell at their respective dose except compound, trequinsin, didn't show such inhibition in H520 and LK2 cells.

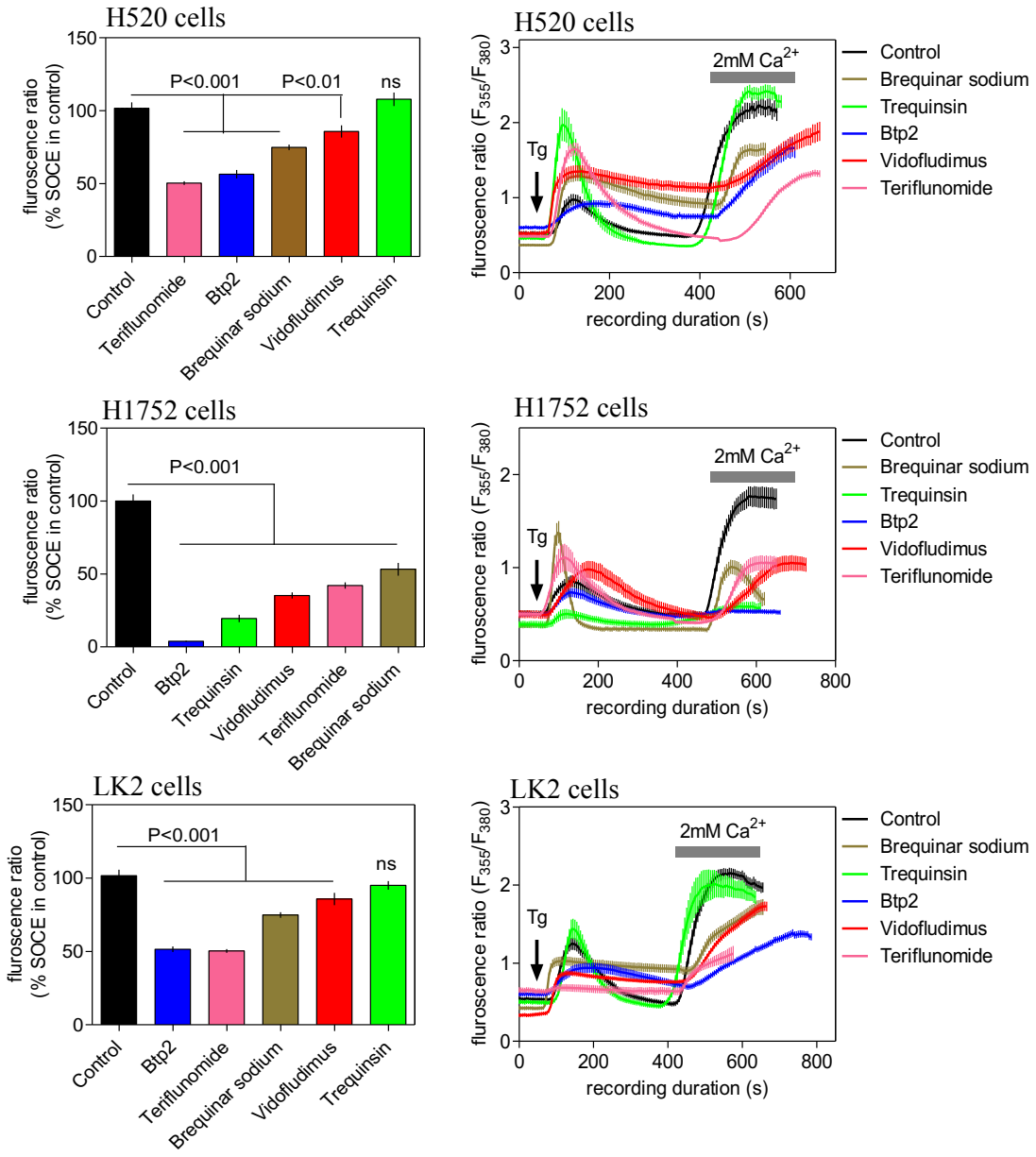

Figure 6.3 Compounds on the SOCE in different lung cancer cells.

Histograms (**left column**) showing the highest peak SOCE levels triggered by Tg in control cells and cells pre-treated with each compound at cell proliferation inhibiting dose. Sample traces (**right column)** representing Ca^{2+} triggered by adding Tg to cells with or without pre-treatment of the chosen compounds. Each value (mean ± SEM) was derived from 3-5 independent experiments done in different days with 40-60 cells. One-way ANOVA followed by Dunnett's test was used for statistical comparison.

6.2.2 Selected SOCE inhibitors on SHSY5Y neuroblastoma cell differentiation

If there any role on differentiation, compounds were tested against SHSY-5Y neuroblastoma cell. Each of compounds and retinoic acid (RA) were treated at 10μM for 10 consecutive days followed by bright filed images captured. Cells with neurite length and cell body ratio of ≥2 were classed as differentiated. Qualitative and quantitative analysis showed none of the compounds including known SOCE inhibitor, BTP2, had any effect on SHSY-5Y cells differentiation although differentiation was noticed in presence of RA as expected (**Fig. 6.4**).

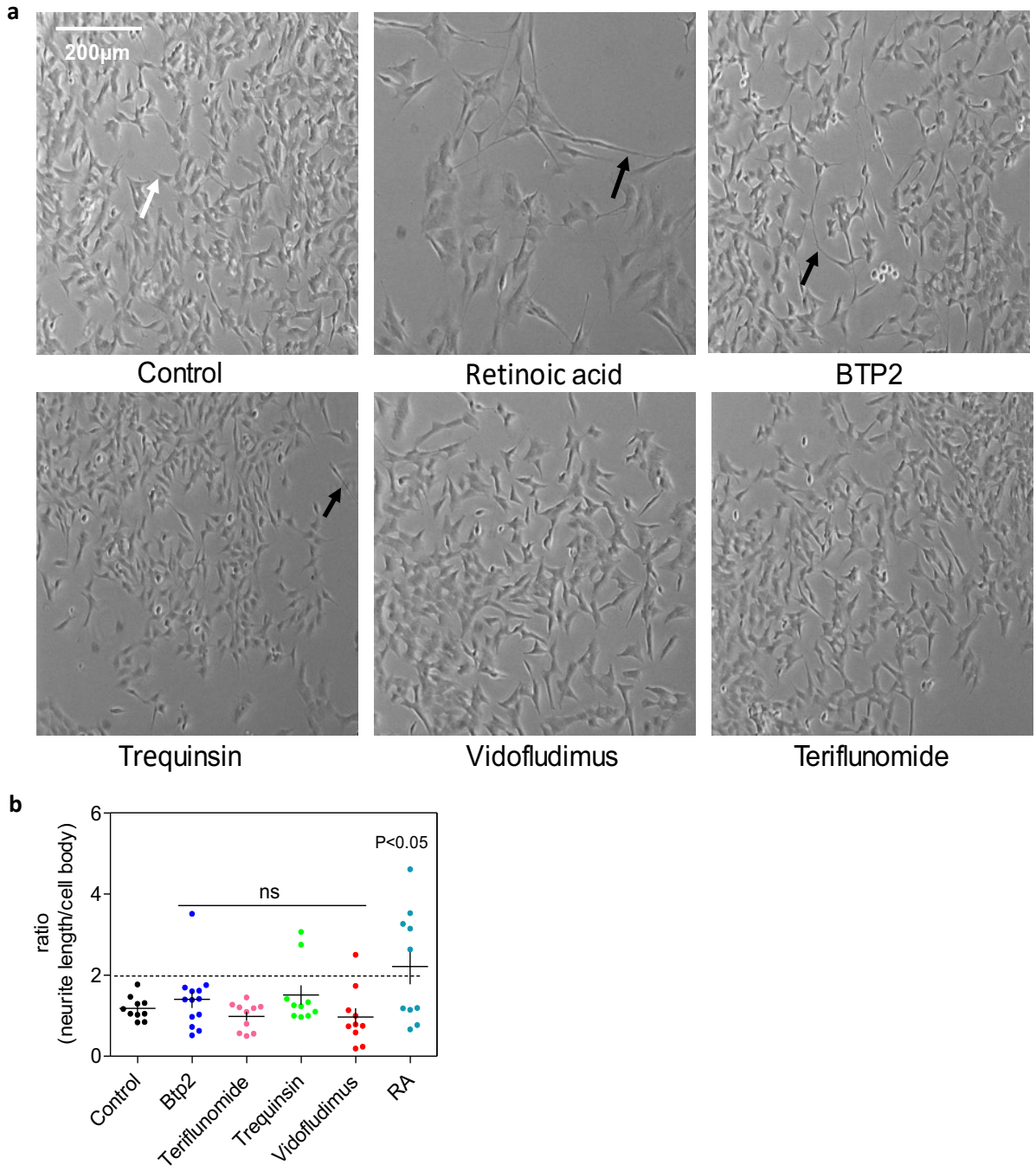

Figure 6.4 SOCE inhibitors on SHSY5Y neuroblastoma cell differentiation.

(a) Images shown after treating cells with vehicle (EtOH), 10µM retinoic acid (RA) and 10µM each of the compound. Short branches (**white arrow**) and extended neurites (**black arrow**) represent non-differentiated and differentiated cells respectively. **(b)** Histograms showing the neurite length and cell body ratio after treating the cells with each compound. Each value (mean ± SEM) was derived from 3-5 independent experiments done in different days with 50-60 cells. One-way ANOVA followed by Dunnett's test was used for statistical comparison.

6.3 Discussion

Since SOCE is involved in many biological processes therefore chasing few of these processes aiming to observe any impact of selected SOCE inhibitors on them was an interesting part of this study.

SOCE inhibitors on lung cancer cell proliferation

SOCE has been recently implicated in various form of oncogenic transformation including malignant transformation, apoptosis, proliferation, angiogenesis, metastasis and antitumor immunity. It has regulatory effect on apoptic cell death, proliferation and metastasis of cancer cells (Xie et al. 2016). Targeting SOCE using pharmacological modulator to control cancer has recently got attention in the cancer research field. Hence the most potent SOCE inhibitors found in this study were tested against different lung cancer cells. Data from cell proliferation assay showed tested compounds had diverse effect on proliferation and such effects were cell type specific (**table 6.1**). Cisplatin, an important chemotherapeutic drug, used in the treatment of advanced cancer, also have shown anti-proliferative effect tested in lung cancer cell (Li et al. 2013). Of the tested compounds, overall brequinar sodium have shown realtibely better anti-proliferative action in every cell line. Trequinsin showed almost similar fashion of inhibition as brequinar did. On the other hand, overall, teriflunomide and vidoflunomide were relatively less potent against proliferation LK2 and H520 cells although both of the compounds were very effective on anti-proliferation when tested against H1752 cell (**table 6.1**).

It was not surprising to observe anti-proliferative properties of these compound in lung cancer cell line. Recently it has been reported that both brequinar and teriflunomide (A771726) inhibited proliferation of various cancer cell lines including human melanoma (A375), human myeloma (H929), and human Burkitt's lymphoma (Ramos) cell lines (Dorasamy et al. 2017). Though not trequinisn but other PDE3 family compounds have been reported previously to have cell cytotoxic characteristics in selected cancer cell lines (De Waal et al. 2016).

To find any relevance between anti-proliferative properties and SOCE, all the compounds were then tested against SOCE at pIC50 dose in the very same lung cancer cell lines. Except trequinsin, which didn't inhibit SOCE in two of the cell lines at pIC50 dose, all other compounds supressed SOCE at such concentration (**Fig. 6.3**). Collectively, it can be said that SOCE inhibition and anti-proliferative activity of these compounds may be mutually inclusive and SOCE inhibitory properties of these compounds might have contribution on inhibition of proliferation. However, they could act through a different path other than SOCE to show anti-proliferative activity which again required experimental validation.

SOCE inhibitors on SHSY-5Y neuroblastoma cell differentiation

SOCE have been recently explored in neurogenesis, neural development, proliferation and differentiation (Hao et al. 2014; Somasundaram et al. 2014; Gopurappilly et al. 2018). SOCE also been reported to have role on differentiation in non-neuronal cells (Darbellay et al. 2009). Therefore, selected SOCE inhibitors were tested sought to find if there is any effect on differentiation of SHSY-5Y neuroblastoma cells.

Compounds, as well as retinoic acid (RA) were treated at 10μM for 10 consecutive days in the experimental procedure. RA is known to induce growth seize and differentiation in human neuroblastoma cells (Sidell N 1982). Therefore, RA as expected, induced differentiation in SHSY-5Y cells while none of the drugs exhibited any differentiation effect on this cell type (**Fig. 6.4**). Although statistically insignificant, visual observation indicated trequinsin was better than other compounds in terms of number of differentiated cells formed (**Fig. 6.4**). However, molecular marker-based analysis would have given more clearer evidence for such claim.

Chapter 7

Results V - SOCE in oligodendrocyte cell biology

7.1 Introduction

Myelin sheaths consist of highly organized lipid-rich membrane stacks surrounding axons, the conductive processes of neurons. The presence of myelin sheaths results in axons with high resistance and low capacitance. This enables efficient and rapid saltatory propagation of nerve impulses (Squire et al. 2003) as well as play an important role in maintaining and protecting axons (Irvine and Blakemore 2008). As myelin sheaths seem to provide trophic support to myelinated axons, therefore one of ways to protect axons in the context of disease therefore is to ensure that myelin sheaths are maintained, or if lost that they are rapidly regenerated.

In central nervous system (CNS), there is a process called remyelination, by which the entire myelin sheath is restored as well as the saltatory conduction and the functional deficits (Franklin and ffrench-Constant 2008). Remyelination or myelin regeneration in the adult CNS is mainly mediated by a multipotent parenchymal CNS stem/progenitor cell population traditionally referred to as oligodendrocyte progenitor cells (OPCs). Following a demyelinating incident, OPCs are rapidly amplified in areas of demyelination where they subsequently give rise to myelinating oligodendrocytes (Franklin 2002; Franklin and ffrench-Constant 2008). Successful remyelination depends mostly on the OPCs recruitment into the demyelinated area and their subsequent engagement of denuded axons and finally their differentiation into mature oligodendrocytes (**Fig. 7.1**).

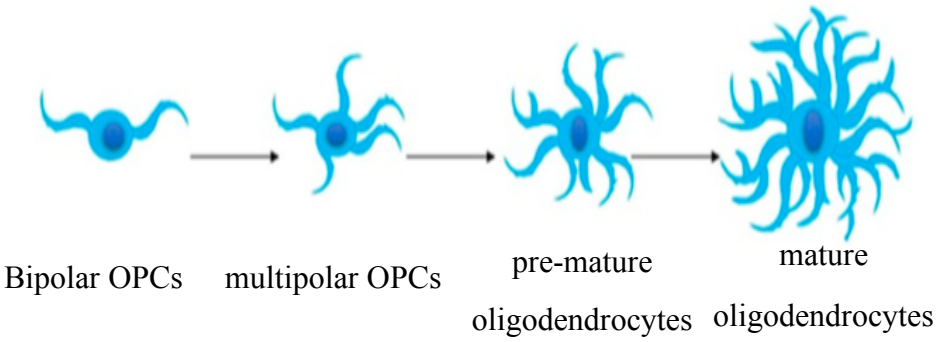

Figure 7.1 OPCs differentiation process.

Differentiation steps of OPCs forming an immature precursor to the mature oligodendrocyte. Figure is taken from Angela et al. 2020.

During normal development, the maturation of the oligodendrocyte lineage cells destined to trigger myelinogenesis takes place according to sequential stages represented by temporal expression of some cell surface markers and morphology. The stages are oligodendrocyte progenitors and precursors, pre-oligodendrocytes, and non-myelinating/immature and myelinating mature oligodendrocytes (Liu et al. 2002).

Proliferation of OPCs

During the early embryonic life, OPCs originate from the neuroepithelium of the ventricular region. OPCs are highly proliferative and motile bipolar cells. Several mechanisms have been suggested to control OPC proliferation. One of the mechanisms was reported to be limited by intrinsic clock through which OPCs passthrough confine number of divisions before differentiated to myelin forming oligodendrocytes (Temple and Raff 1986). However, this mechanism was found to be completely dependent on external environmental factors (Calver et al. 1998).

Neuron-derived growth factors act as effective mitogens for OPCs. Platelet-derived growth factor (PDGF-AA) is thought to be the most potent OPC mitogen which is found to be abundantly expressed in OPCs as well as happen to be down-regulated when the OPCs differentiate into mature oligodendrocyte (Calver et al., 1998). Proteoglycan NG2 (neuron-glia antigen 2) also has influence on OPCs proliferation via acting as co-receptor for PDGFRα (Goretzki et al. 1999). Deletion of NG2 in mice reduced OPCs number which indicates NG2 enhance OPCs proliferation (Kucharova and Stallcup 2010). Fibroblast growth factor (FGF) appeared to enhance OPCs proliferation by regulation of developmental changes of FGF receptor expression, with FGF-3 receptors being abundantly expressed by OPCs and downregulated as OPCs differentiate into myelinating oligodendrocytes (Bansal et al. 1996). Few other growth factors including brain derived neurotrophic factor (BDNF) (Van't Veer et al. 2009), neuregulin (Roy et al. 2007) and neurotrophin-3 (NT-3) (Barres et al. 1994b) also have shown mitogenic activity which enhance OPCs proliferation.

In contrary to those that enhance OPCs proliferation, few messengers have been found to inhibit the process. Especially retinoic acid and thyroid hormone allow OPCs to exit cell cycle and start differentiation (Barres et al. 1994a). The mechanism by which these molecules stop cell cycle and induce differentiation of OPCs is yet to be known precisely.

In addition to growth factors, neurotransmitters may be involved in regulation of OPCs proliferation. It is already well known that OPCs receive synaptic input mediated by

neurotransmitters like glutamate and GABA, which indicated these could also regulate developmental process of OPCs (Karadottir et al. 2008).

Differentiation of OPCs

During developmental processes a large number of proliferated OPCs differentiate into non-myelinating or immature oligodendrocytes which then differentiate into myelin forming oligodendrocytes (Zhu et al. 2008; De Biase et al. 2010; Kukley et al. 2010).

As OPCs differentiate into mature oligodendrocytes, expression of some specific proteins (molecular marker) as well as their morphology undergo significant changes. Although oligodendrocyte lineage expression marker SOX10 and Olig2 do not alter during the entire developmental process but as soon as OPCs start losing lose expression of precursor proteins including NG2 and PDGFRα, immature marker O4 expression begin followed by expression of mature markers including PLP, galactocerebroside and myelin basic protein (MBP) (Nishiyama et al. 2009). Although OPCs are distributed evenly throughout the brain from the birth, however, not all OPCs differentiate into myelinating oligodendrocytes; a significant portion remain non-differentiated oligodendrocytes (Dawson et al. 2003; Rivers et al. 2008; Psachoulia et al. 2009).

Several molecular signalling molecules including growth factors, retinoic acid, glucocorticoid and thyroid hormone and neurotransmitters have been reported to cause OPCs cell cycle arrest and differentiate, however, mechanisms behind the post mitotic switching were largely unknown, although study showed differentiated OPCs express series of microRNAs which probably explain *de novo* level of gene expression (Bartel 2004). Withdrawal of some mitogens from OPCs culture found to induce expression of specific miRNAs (Zhao et al. 2010) and these miRNAs effectively downregulate the responsiveness of OPCs to the signal molecule which resultant a change in expression of some OPC-specific genes that eventually promote differentiation (Dugas et al. 2010; Zhao et al. 2010). This gives a clue to develop molecules that could regulate OPCs development and promote differentiation by changing gene expression.

Not only intrinsic factors like RA and T3 hormone receptors, basic helix-loop-helix (bHLH), Sox-family, zinc finger transcription factors actively promote oligodendrocyte differentiation but other signalling pathways like cAMP-Erk1/2/p38Mapk-Creb1 signalling (Syed et al. 2013) are also important for OPC differentiation. Recent time, a few clinically relevant, FDA

approved compounds also found to OPCs differentiation (Deshmukh et al. 2013; Mei et al. 2014; Najm et al. 2015; Franklin 2015; Neumann et al. 2019).

Myelination

Differentiated oligodendrocytes extent myelin sheaths which then can be wrapped around axonal tracts spirally. But there is no single proposition of wrapping mechanism rather several methods have been suggested till date. Myelin membrane can be wrapped into several layers and wrapping could start from outer part of the myelin sheath, electron microscopy studies showed (Snaierdo et al. 2014).

Not all the axons become myelinated, but only axons with thickness of a certain diameter while thinner axons remain non-myelinated. However, how oligodendrocyte processes recognize axons and vice versa as well as provide trophic support to neurons, are not fully understood yet (Fünfschilling et al. 2012; Simons and Lyons 2013).

7.1.1 Role of SOCE in OPC biology

Ca^{2+} as a ubiquitous and versatile second messenger, is well-known to regulates numerous developmental events in the brain, including neural induction, neurotransmitter specification, growth cone motility, differentiation, growth and proliferation, and neuronal maturation (Nakanishi and Okazawa 2006; Toth et al. 2016).

Several studies have addressed the importance of Ca^{2+} signalling in OLGs differentiation and myelination as well as in process extension and OLGs migration and retraction of membrane sheets and cell death in mature mouse OLGs (reviewed by Walsh et al. 2010).

SOCE and its underlying protein players (STIM, Orai isoforms) are traditionally believed to be important for regulating various aspects of the biology of the non-excitable cells mainly. However, this notion is changing, and evidence amass that SOCE is present and functional in many excitable cells including neurons. Studies implicate SOCE in modulating several neuronal functions, including neurotransmitter release, synaptic plasticity, Ca^{2+} oscillations, and firing of flight motor neurons in Drosophila (Venkiteswaran and Hasan 2009). Moreover, aberrant SOCE has been implicated in hypoxia-mediated neuronal death, epilepsy, and the response to axonal injury. SOCE represents an important mode of Ca^{2+} delivery for the non-excitable cells of CNS. Recently it has been evident that SOCE channels regulate gene expression and proliferation in neural progenitor cells (Somasundaram et al. 2014).

A very few studies have been conducted so far to investigate SOCE in OPCs biology. In the recent past researchers have shown SOCE modulation enhanced OPCs proliferation by the golli products of the myelin basic protein gene in golli-overexpressing and golli-KO mice (Paez et al. 2009; Paez et al. 2011). Nevertheless, the molecular mechanisms of Ca^{2+} signalling tool kits, particularly the SOCE channel during the OPCs development and their physiological functions in proliferation, migration, differentiation and remyelination remain poorly characterized.

7.1.2 Background of the project

In multiple sclerosis (MS), a demyelinating disease, under several circumstances, axons become demyelinated. One of the major causes for primary demyelination in CNS is the inflammation (Franklin and ffrench-Constant 2008). Identification of small molecules, or a signalling pathway that selectively induce differentiation of OPCs at areas of demyelinated lesions and thereby improve remyelination would have a significant impact on the future treatments (MS).

During the initial phase of my PhD work, Teriflunomide and its pro-drug, leflunomide were found to be able to suppress SOCE significantly at doses that are clinically-achievable (**Fig. 3.4**). Teriflunomide has been approved as an oral disease-modifying therapy for treating relapsing or relapsing-remitting multiple sclerosis (RR-MS) (Confavreux et al. 2014). As teriflunomide, a drug for RR-MS, blocked SOCE at clinically-relevant concentration (~10μM) (Claussen and Korn 2012; Mehta et al. 2009), therefore it was hypothesized that SOCE-modulatory properties of this drug may also contribute to the observed clinical benefits in MS. Therefore, I sought out to evaluate SOCE in the context of OPC biology and specifically pursued the following aims:

(a) basic characterisation of SOCE in OPCs

(b) investigation of the role of SOCE on OPCs proliferation and differentiation.

7.2 Results

7.2.1 Isolation of OPCs

Isolation OPCs was the starting point of this project and for this, two different methods were employed. Mixed glia culture (MGC) shaking method proposed by McCarthy and de Vellis, 1980 (see methods section for details) was used to isolate OPCs from neonatal rat brain, aged between P0 to P2, whereas using magnetic activated cell sorting (MACS) method (see methods section for details) OPCs were collected from P5-P7 aged rat brain. Approximate yield of 0.5 x 10^7 cells from each brain were obtained through both methods. After 24 hrs, cells were immunostained to see the OPCs enrichment, cell population obtained via MACS procedure were more enriched in OPCs than MGC shaking method. An estimation of 20-30 percent of microglial and astrocytic contamination were noticed in cell population (**Fig.7.1**). Cells isolated through MACS procedure with purity of ~70% or more were considered for further experiments.

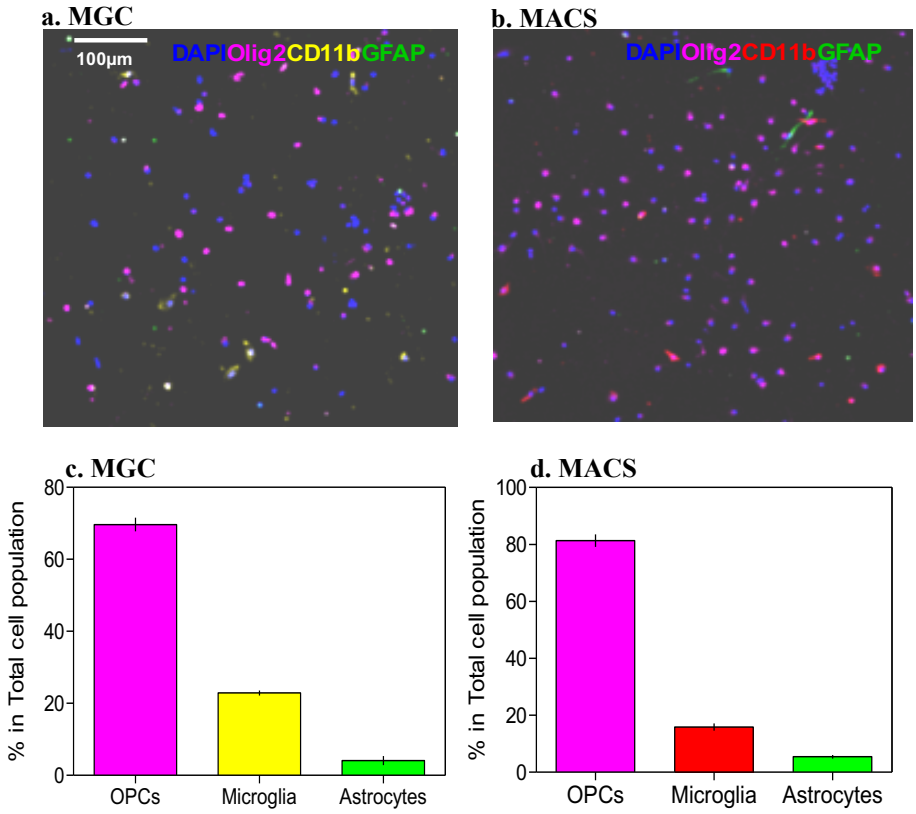

Figure 7.1 Purity level of OPCs population.

Representative images of OPCs isolated from neonatal rat brain using **(a)** MGC and **(b)** MACS procedure. OPCs, microglia and astrocytes were stained with antibodies olig2, CD11b and GFAP respectively. Histograms showing enrichment of OPCs (%) in total cell population achieved through (**c)** MGC and (**d)** MACS procedure.

7.2.2 Maintaining OPCs culture and generating mature oligodendrocytes (OLGs)

Fostering OPCs culture and yielding OLGs were required incessantly for different experimental procedures throughout this project. Hence OPCs were maintained in proliferation medium supplemented with daily addition of 10ng/ml growth factors; PDGF-AA and basic bFGF while OLGs were produced by growing OPCs in differentiation medium supplemented with daily addition of 50ng/ml T_3 (Triiodo-L-Thyronine) hormone. After respective treatment, significant increase of OPCs (**Fig. 7.2**) and OLGs (**Fig. 7.3**) were observed after 4 days *in vitro* (DIV) culture.

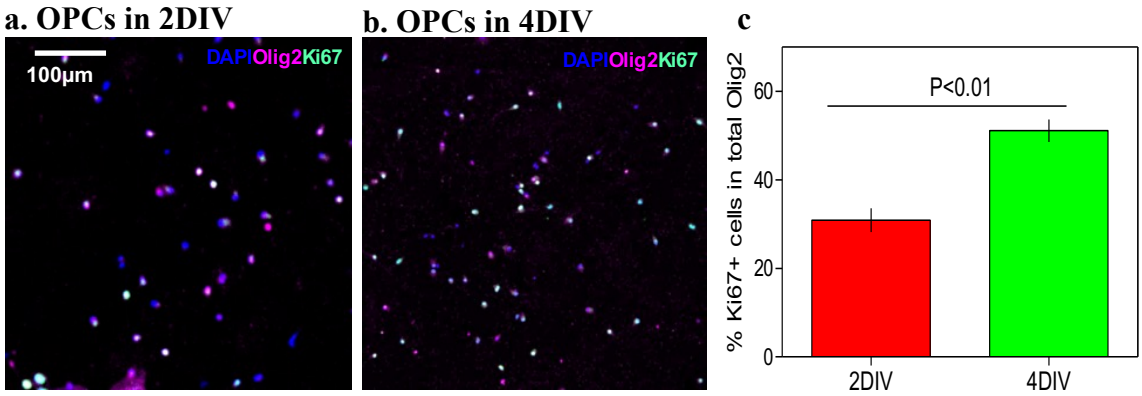

Figure 7.2 Maintaining OPCs in culture.

Representative images showing OPCs after (**a)** 2DIV and (**b)** 4DIV. OPCs lineage and newly formed OPCs were immune stained with antibodies olig2, and Ki67 respectively. **(c)** Histogram showing increasing of OPCs number at different days. Each value (mean ± SEM) was derived from 3 individual experiments. Two-tailed unpaired t-test was used to compare data between groups.

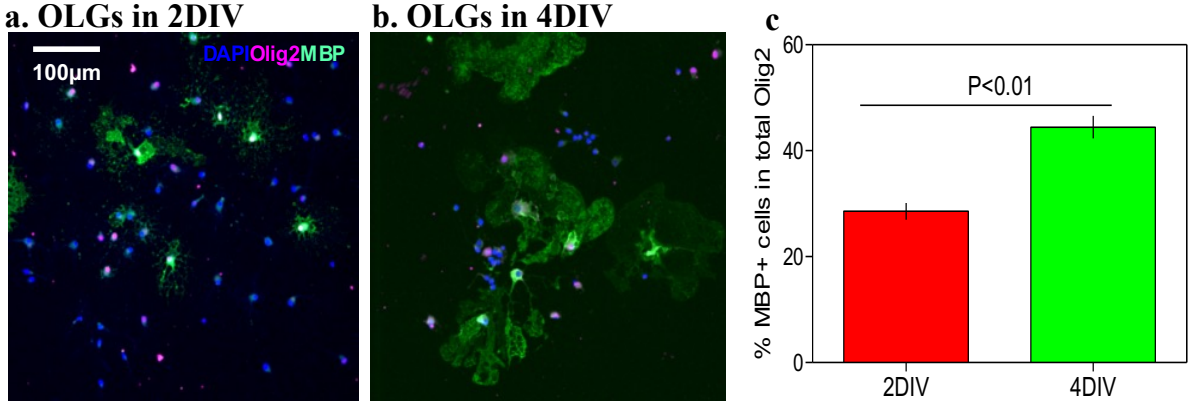

Figure 7.3 Generation of oligodendrocytes (OLGs).

Representative images showing OLGs after (**a)** 2DIV and (**b)** 4DIV. OPCs lineage and mature oligodendrocytes (OLGs) were immune stained with antibodies olig2, and MBP respectively. **(c)** Histogram showing increasing of OLGs number at different days. Each value (mean ± SEM) was derived from 3 individual experiments. Two-tailed unpaired t-test was used to compare data between groups.

7.2.3 Characterization of SOCE in OPCs

7.2.3.1 SOCE activation in OPCs via pharmacological mean

To study SOCE, OPCs were obtained from 4DIV culture maintained in proliferation medium. Extracellular Ca^{2+} entry was observed in OPCs loaded with 4µM fura-2/AM, stimulated by 2µM Tg (**Fig. 7.3**). Known SOCE inhibitors, BTP2 and AncoA4, were included as positive control group and each of the compounds was preincubated for ~15 min prior to executing single cell Ca^{2+} imaging experiment. As expected, known inhibitors supressed SOCE in OPCs significantly when compared to control group (**Fig. 7.3**).

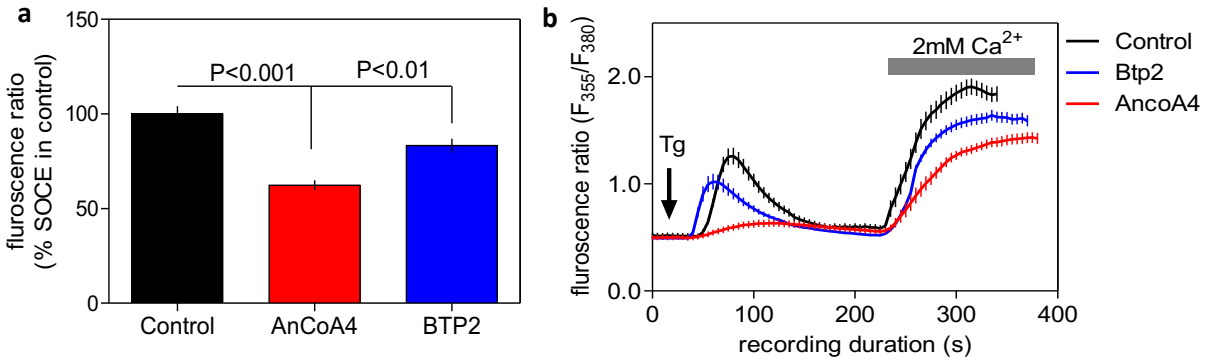

Figure 7.4 Pharmacological activation of SOCE in OPCs.

(a) Histograms showing the highest peak SOCE levels triggered by Tg (2µM) in control cells and cells pre-treated with AncoA4:10µM, and BTP2:2µM. **(b)** Sample traces representing Ca^{2+} signals triggered by adding Tg to cells with or without pre-treatment of the chosen compound. Each value (mean ± SEM) was derived from 3-5 independent experiments done in different days with 35-50 cells. One-way ANOVA followed by Dunnett's test was used for statistical comparison.

7.2.3.2 SOCE activation in OPCs via physiological mean

To see whether physiological ligands could activate SOCE in OPCs obtained from 4DIV culture, similar protocol was used except Tg was replaced by PDGF-AA. As can be seen in **Fig. 7.5,** SOCE was activated in OPCs by addition of 40nl/ml PDGF-AA as well suppressed upon preincubation of BTP2, a known SOCE inhibitor

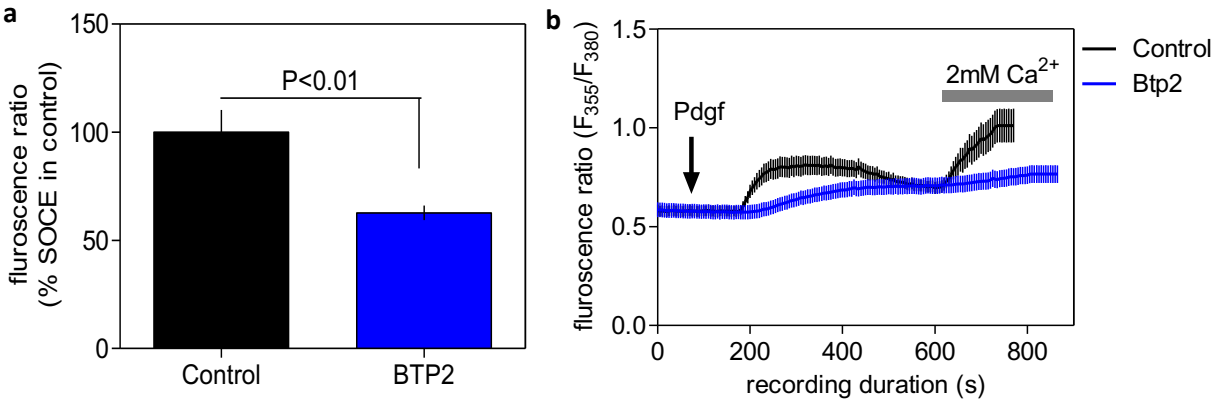

Figure 7.5 SOCE triggered in OPCs via physiological mean.

(a) Histograms showing the highest peak SOCE levels triggered by PDGF-AA at 40ng/ml in control cells and cells pre-treated with BTP2 at 2μM dose. **(b)** Sample traces representing Ca^{2+} signals triggered by adding PDGF-AA to cells with or without pre-treatment of BTP2. Each value (mean ± SEM) was derived from 3-5 independent experiments done in different days with 35-50 cells. Two-tailed unpaired t-test was used to compare data between groups.

7.2.3.3 Evaluation of teriflunomide on SOCE in OPCs

As mentioned earlier, teriflunomide which is an approved drug for MS, was found to be inhibiting SOCE in immune (RBL-1H and human jurkat T cells) and human neuroblastoma cells (SHSY-5Y). After basic characterisation of SOCE in OPCs (see above), I was sought out to know, using standard experimental protocol, whether this drug could affect SOCE in OPCs as well. As can be seen in **Fig.7.6**, acute incubation (15min) of OPCs with 10µM teriflunomide indeed significantly suppressed Tg-evoked SOCE in OPCs when compared to control.

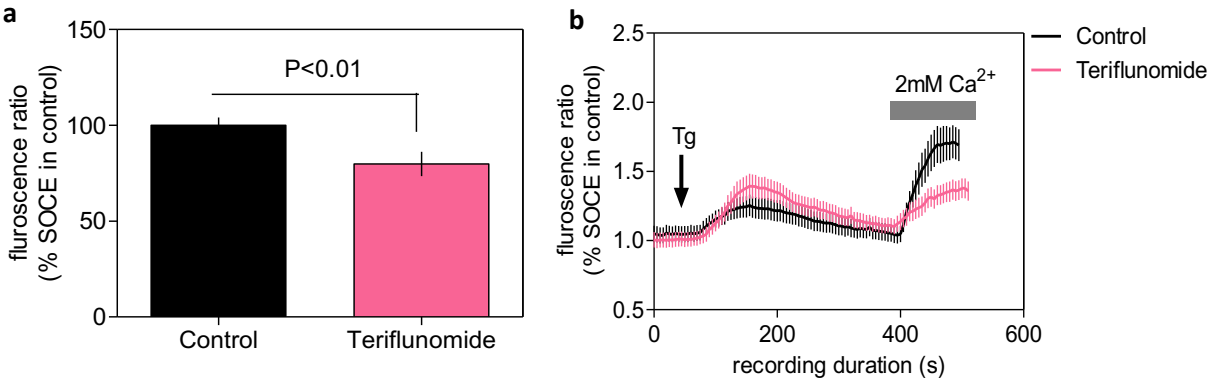

Figure 7.6 Teriflunomide on SOCE in OPCs.

(a) Histograms showing the highest peak SOCE levels triggered by Tg:2µM in control cells and cells pre-treated with 10µM teriflunomide. **(b)** Sample traces representing Ca^{2+} signals triggered by adding Tg to cells with or without pre-treatment of teriflunomide. Each value (mean ± SEM) was derived from 3-5 independent experiments done in different days with 50–60 cells. Two-tailed unpaired t-test was used to compare data between groups.

7.2.3.4 TRPC channel mediated Ca^{2+} entry in OPCs

There have been few reports about the existence of TRPC channels in OPCs (Paez et al. 2011). Therefore, next experiment was executed to investigate TRPC mediated Ca^{2+} entry in OPCs obtained from 4 DIV culture and for this, standard Ca^{2+}-imaging protocol was used but Tg was replaced by OAG. As can be seen in **Fig. 7.7**, OPCs exhibited robust rise in cytoplasmic Ca^{2+} concentrations upon application of 150µM OAG in the bath solution. The signal represented Ca^{2+} entry since it was discernible only after adding Ca^{2+} to the bath solution. Since the known TRPC blocker, SKF96365 at 15µM almost abolished the Ca^{2+} signal, it indicated that the OAG-evoked Ca^{2+} signal observed in OPCs was attributed to TRPC-mediated Ca^{2+} entry in these cells (**Fig. 7.7)**.

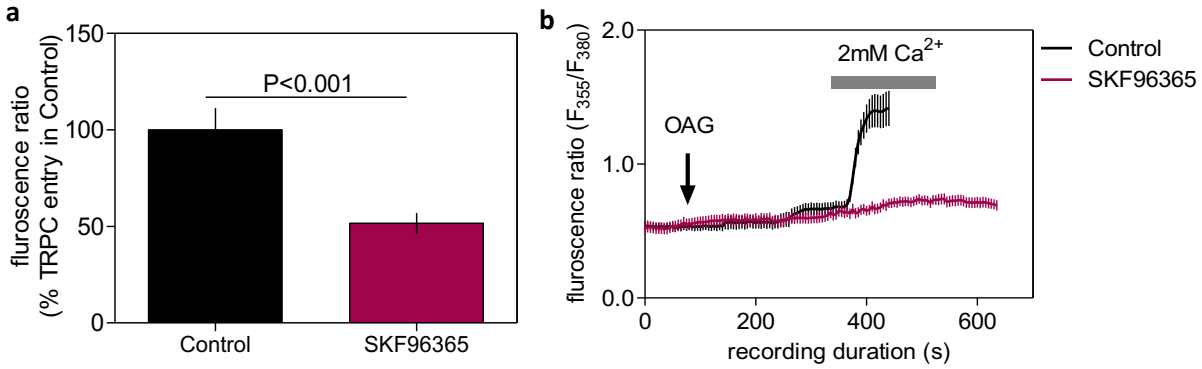

Figure 7.7 TRPC mediated Ca^{2+} entry in OPCs.

(a) Histograms showing the peak OAG-activated Ca^{2+} entry in control cells and cells treated with 15µM SKF96365. **(b)** Sample traces representing Ca^{2+} signals triggered by adding 150µM of OAG to OPCs with or without pre-treatment of SKF96365. Each value (mean ± SEM) was derived from 3-5 independent experiments done in different days with 40-45 cells. Two-tailed unpaired t-test was used to compare data between groups.

7.2.3.5 SOCE differences between OPCs and OLGs

OPCs and OLGs were obtained from 4DIV culture maintained in presence and in absence of growth factors respectively to investigate difference of SOCE between OPCs and OLGs. SOCE was triggered in both cell types through pharmacological mean, Tg and data from single cell Ca^{2+} imaging experiment demonstrated no significant difference in the magnitude of SOCE (**Fig. 7.8**).

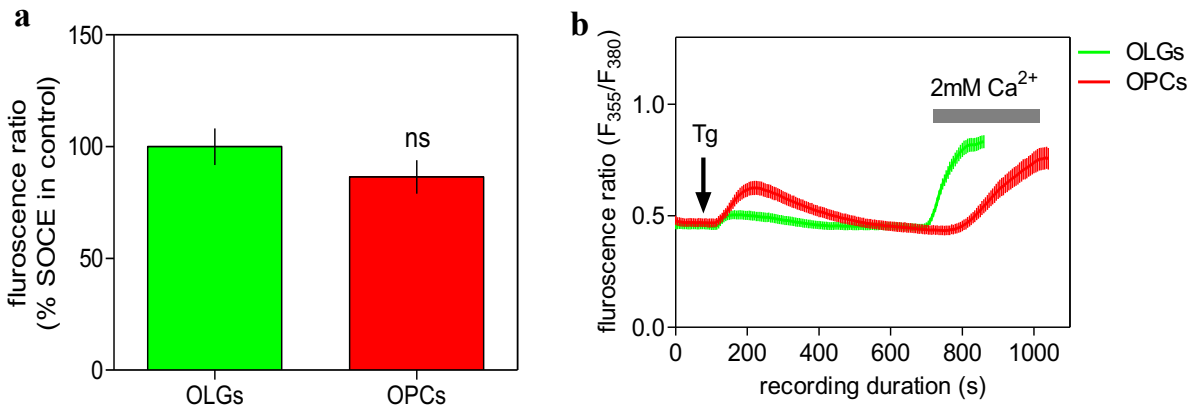

Figure 7.8 SOCE differences between OPCs and OLGs cells.

(a) Histograms showing the highest peak SOCE levels triggered by Tg (2µM) in OPCs and OLGs cells **(b)** Sample traces representing Ca^{2+} signals triggered by adding Tg to both OPCs and OLGs cells. Each value (mean ± SEM) was derived from 3-5 independent experiments done in different days with 40-45 cells. Two-tailed unpaired t-test was used to compare data between groups.

7.2.4 Investigation of voltage-gated Ca^{2+} channel (VGCC) entry in OPCs

In order to test whether OPCs could also support Ca^{2+} entry via voltage-gated Ca^{2+} channel (VGCC), KCl-evoked depolarization experiment was carried out in OPCs generated from 4DIV culture. Upon addition of high concentration of KCl (70mM) cells became depolarized which then triggered extra cellular calcium entry. Data extracted from single cell Ca^{2+} imaging showing OPCs allow voltage gated channel mediated Ca^{2+} entry since nifedipine - a known VGCC inhibitor could block it (**Fig. 7.9**).

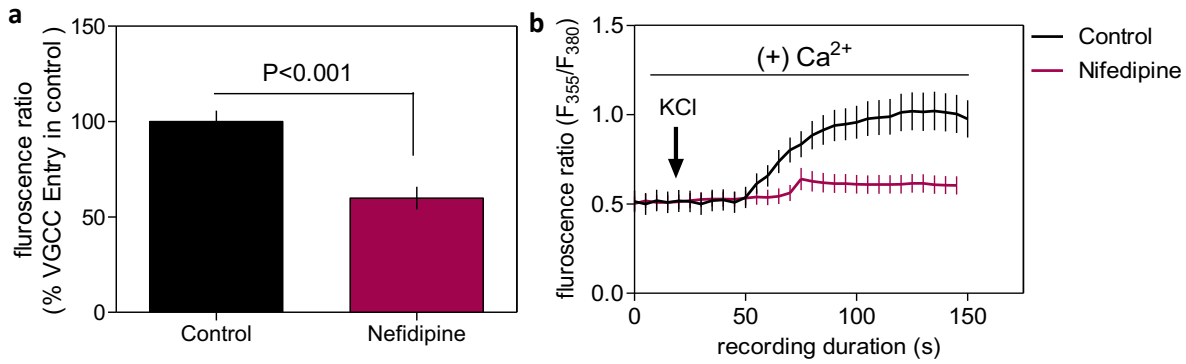

Figure 7.9 Voltage-gated Ca^{2+} entry in OPCs.

(a) Bar diagram shows fluorescence peak ratio of voltage-gated Ca^{2+} entry triggered by 70mM KCl in control cells and cells pre-treated with nifedipine at 3µM. **(b)** Sample trace representing voltage-gated Ca^{2+} entry signal in OPCs with or without pre-treatment of nifedipine. Each value (mean ± SEM) was derived from 3-5 independent experiments done in different days with 45-60 cells. Two-tailed unpaired t-test was used to compare data between groups.

7.2.5 SOCE in OPCs differentiation

7.2.5.1 OPCs differentiation upon SOCE inhibition triggered by BTP2

To investigate any possible role of SOCE on OPCs differentiation, one of the widely used known SOCE inhibitors, BTP2 (Ishikawa et al. 2003; Zitt et al. 2004; He et al. 2005) was used. OPCs maintained in differentiation medium without T_3 hormone, were treated with vehicle or BTP2 for 2 days. BTP2 was used at concentration ranging from 1µM to 10nM. Afterwards, cells were immune stained against respective antibodies. **Fig. 7.10** demonstrated a significant increase of myelin basic protein (MBP) positive cells only at 100nM of BTP2. MBP is expression marker for differentiated cells (Pfeiffer et al. 1993).

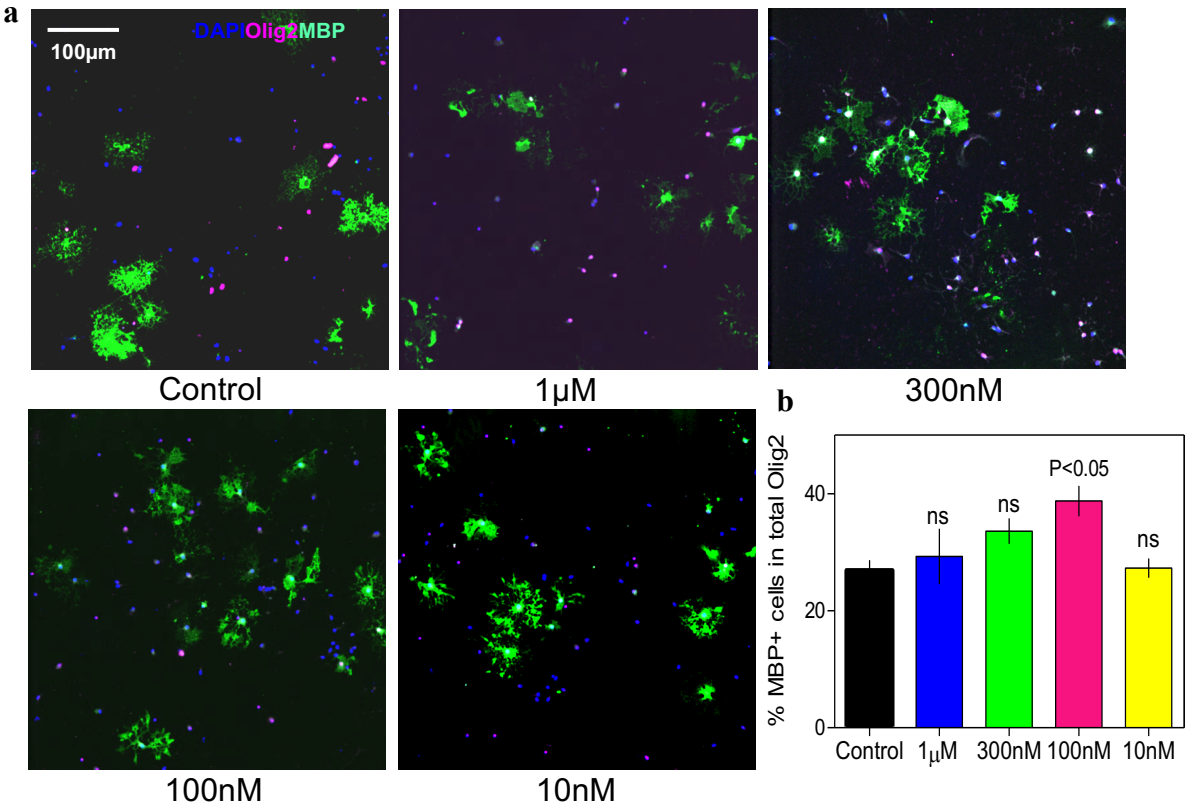

Figure 7.10 OPCs differentiation upon SOCE inhibition triggered by BTP2.

(a) Representative images of MBP-positive OPCs treated with vehicle or BTP2 at concentrations ranging from 10nM to 1µM. Olig2 and MBP expression are the markers for OPCs lineage and differentiation respectively. **(b)** Bar graph evaluating OPCs differentiation-promoting efficacy in the presence or absence of BTP2 at concentrations ranging from 10nM to 1µM after 2 days. Each value (mean ± SEM) was derived from 3 individual experiments. One-way ANOVA followed by Dunnett's test was used for statistical comparison.

7.2.5.2 OPCs differentiation upon SOCE inhibition triggered by AnCoA4

To see whether any SOCE channel protein had any involvement on OPCs differentiation, Orai1, (SOCE channel protein) inhibitor, AnCoA4 (Sadaghiani et al. 2014) was included to test this hypothesis. OPCs maintained in differentiation medium without T_3 hormone were treated with vehicle and AncoA4 at concentrations used ranging from 50nM to 3µM for 48 hrs. At 300nM dose, AncoA4 showed most differentiation whereas it was lesser at 1µM, both cases were significant though when compared to control group (**Fig. 7.11**).

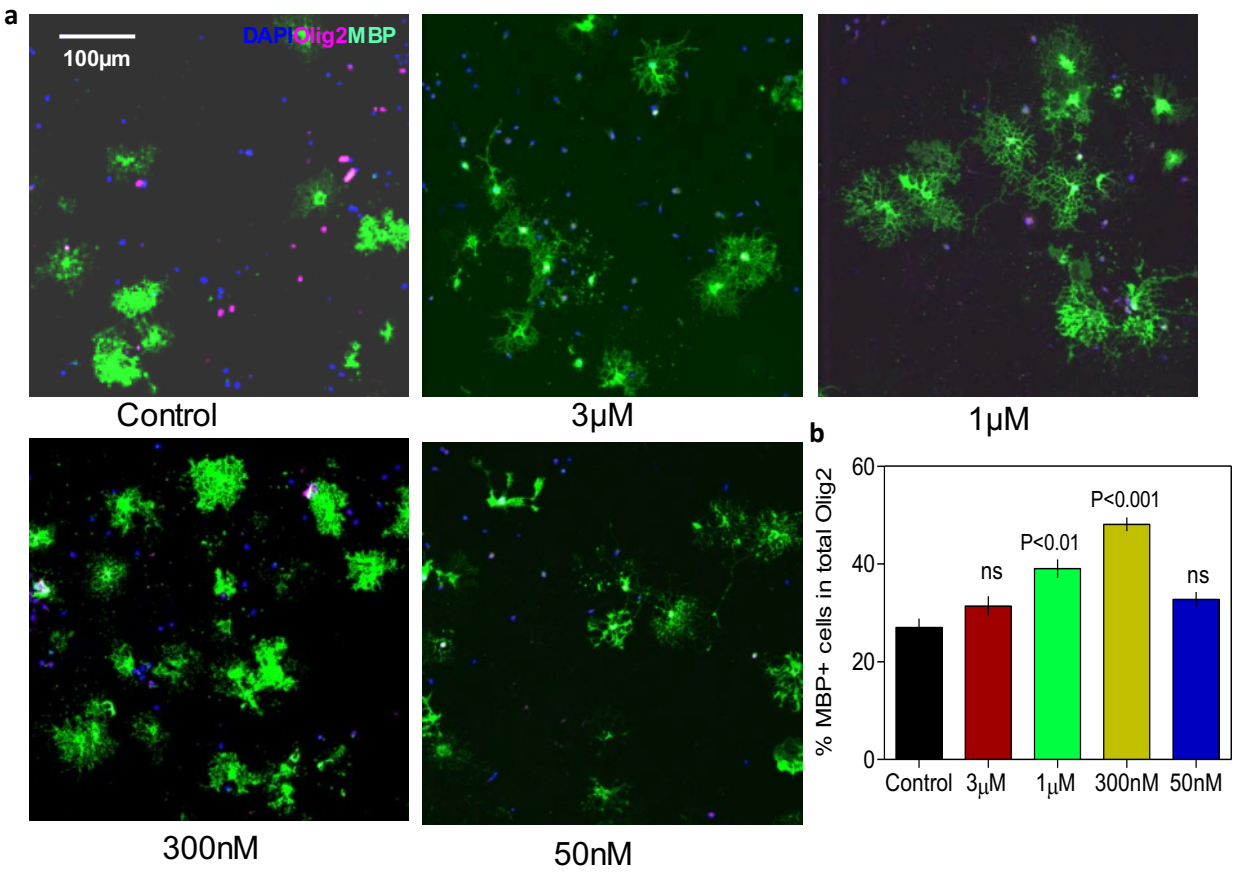

Figure 7.11 OPCs differentiation upon SOCE inhibition triggered by AnCoA4.

(a) Representative images of MBP-positive OPCs treated with vehicle or AnCoA4 at concentrations ranging from 50nM to 3µM. Olig2 and MBP expression are the markers for OPCs lineage and differentiation respectively. **(b)** Bar graph evaluating OPCs differentiation-promoting efficacy in the presence or absence of AnCoA4 at concentrations ranging from 50nM to 3µM after 2 days. Each value (mean ± SEM) was derived from 3 individual experiments. One way ANOVA followed by Dunnett's test was used for statistical comparison.

7.2.5.2 Effect of TRPC channel inhibition on OPCs differentiation

Next step was to test any effect of TRPC channel inhibition on OPCs differentiation, for this OPCs maintained in differentiation medium without T_3 hormone were treated with vehicle control and different doses of TRPC channel inhibitor, SKF96365, ranging from 50nM to 3µM for 48 hrs. Immunostaining data revealed that TRPC channel blocker enhanced OPCs differentiation at both 300nM and 3µM doses (**Fig. 7.12**).

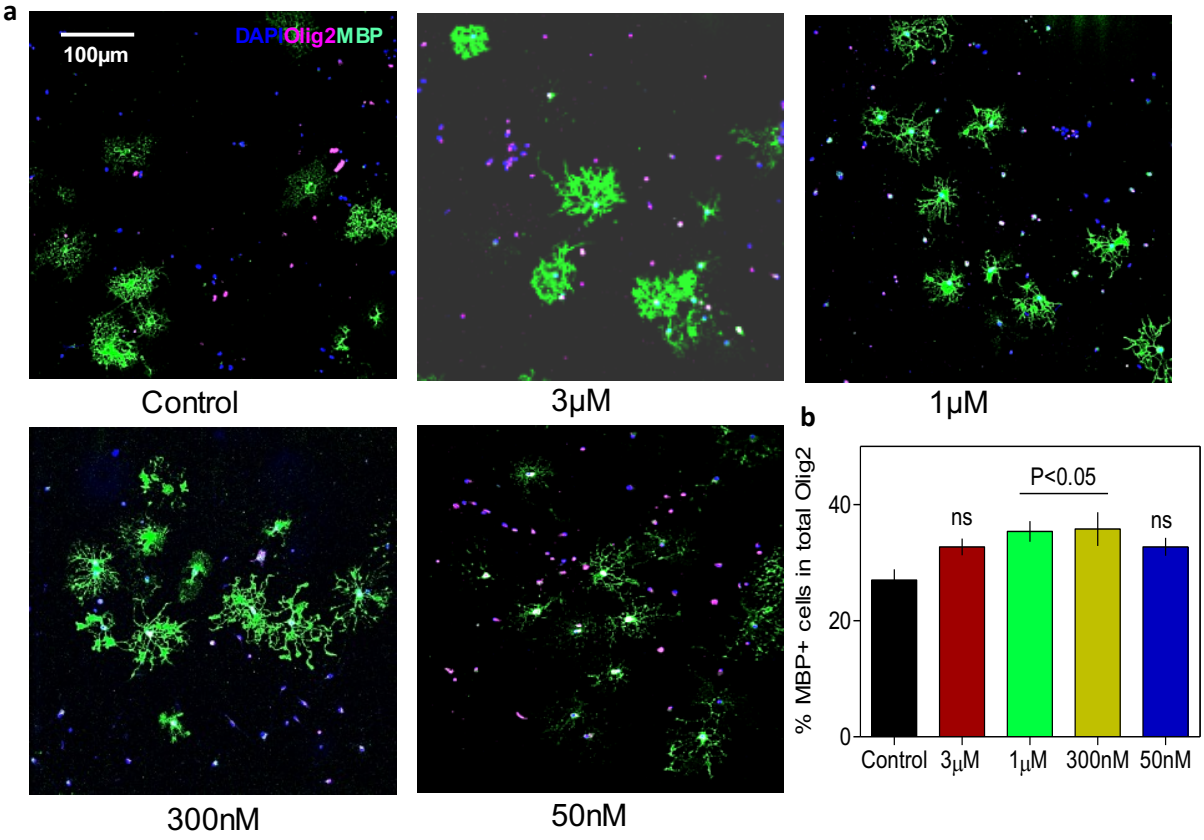

Figure 7.12 Effect of OPCs differentiation on TRPC channel inhibition.

(a) Representative images of MBP-positive OPCs treated with vehicle or SKF96365 at concentrations ranging from 50nM to 3µM. Olig2 and MBP expression are the markers for OPCs lineage and differentiation respectively. **(b)** Bar graph evaluating OPCs differentiation-promoting efficacy in the presence or absence of SKF96365 at concentrations ranging from 50nM to 3µM after 2 days. Each value (mean ± SEM) was derived from 3 individual experiments. One-way ANOVA followed by Dunnett's test was used for statistical comparison.

7.2.5.3 Effect of teriflunomide on OPCs differentiation

As mentioned earlier, teriflunomide, a drug for MS, was found to block SOCE, therefore effect of this drug on OPCs differentiation was further investigated. OPCs maintained in differentiation medium without T_3 hormone were treated with vehicle or different doses of teriflunomide for 48 hrs to test this hypothesis. As can be seen in **Fig. 7.13**, teriflunomide treated at 3µM increased MBP positive cells significantly compared to vehicle treatment group.

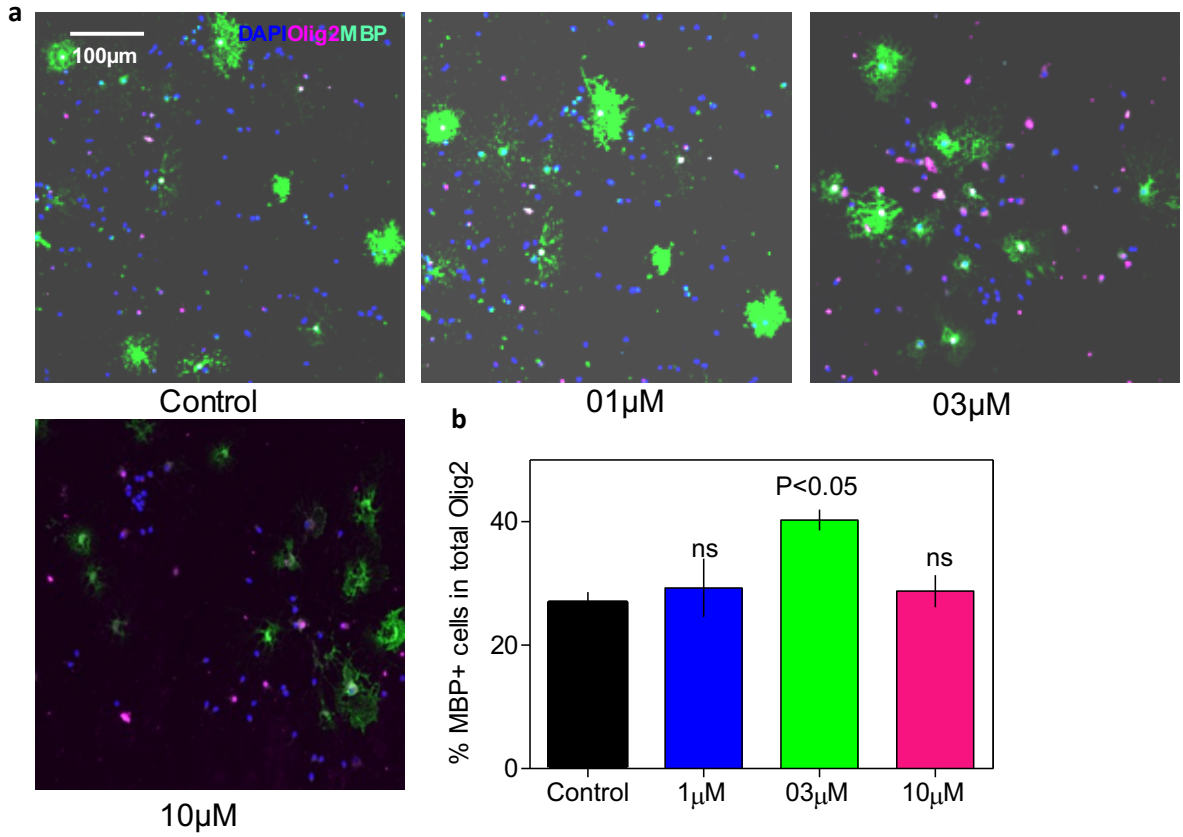

Figure 7.13 Effect of teriflunomide on OPCs differentiation.

(a) Representative images of MBP-positive OPCs treated with vehicle or teriflunomide at concentrations ranging from 1µM to 10µM. Olig2 and MBP expression are the markers for OPCs lineage and differentiation respectively. **(b)** Bar graph evaluating OPCs differentiation-promoting efficacy in the presence or absence of teriflunomide at concentrations ranging from 1µM to 10µM after 2 days. Each value (mean ± SEM) was derived from 3 individual experiments. One-way ANOVA followed by Dunnett's test was used for statistical comparison.

7.2.6 Effect of the SOCE and TRPC channel inhibitors on OPCs proliferation

Since SOCE and TRPC channel inhibitors have shown to enhance OPCs differentiation therefore any potential role of these compounds on OPCs proliferation at differentiation-promoting dose was taken into consideration for further investigation. OPCs maintained in proliferation medium were treated with BTP2, AnoCA4 and SKF96365 for 48 hrs, no growth factor was added, whereas vehicle control was maintained for the same time period with daily addition of 10ng/ml growth factors; PDGF-AA and bFGF. Data extracted from immune stained images showing none of the compounds had any ability to increase proliferation at differentiation-promoting dose compare to growth factors treated group (**Fig. 7.14**). Compound treated group has got significantly a smaller number of Ki67 positive cells than control (**Fig 7.14**). Ki67 is a marker newly formed OPCs (Scholzen and Gerdes 2000).

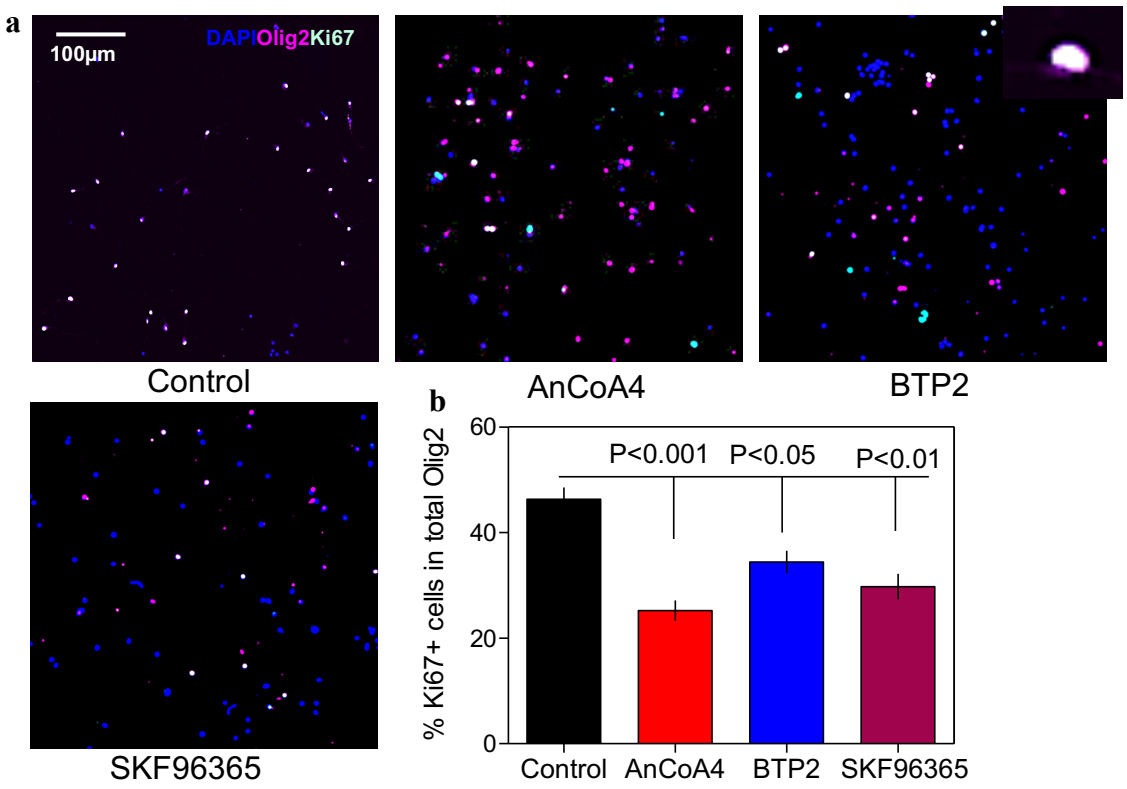

Figure 7.14 SOCE and TRPC channel inhibitors on OPCs proliferation.

(a) Representative images of Ki67-positive OPCs treated with vehicle or BTP2, AnCoA4 and SKF96365 at differentiation promoting doses. Olig2 and Ki67 expression are the markers for OPCs lineage and newly formed OPCs respectively. Inset picture depicts co-localization of Olig2 and Ki67 protein expression **(b)** Bar graph evaluating effect of differentiation-promoting dose of AnCoA4: 300nM, BTP2:100nM and SKF96365:300nM on OPCs proliferation. Each value (mean ± SEM) was derived from 3 individual experiments. One-way ANOVA followed by Dunnett's test was used for statistical comparison.

7.2.7 Cell death assessment

To assess cytotoxicity, compounds were tested against OPCs at differentiation-promoting dose. Propidium iodide-based assay (de la Fuente et al. 2015) showed compounds were not toxic to the cells at the dose which yielded highest differentiated OPCs (**Fig. 7.15**).

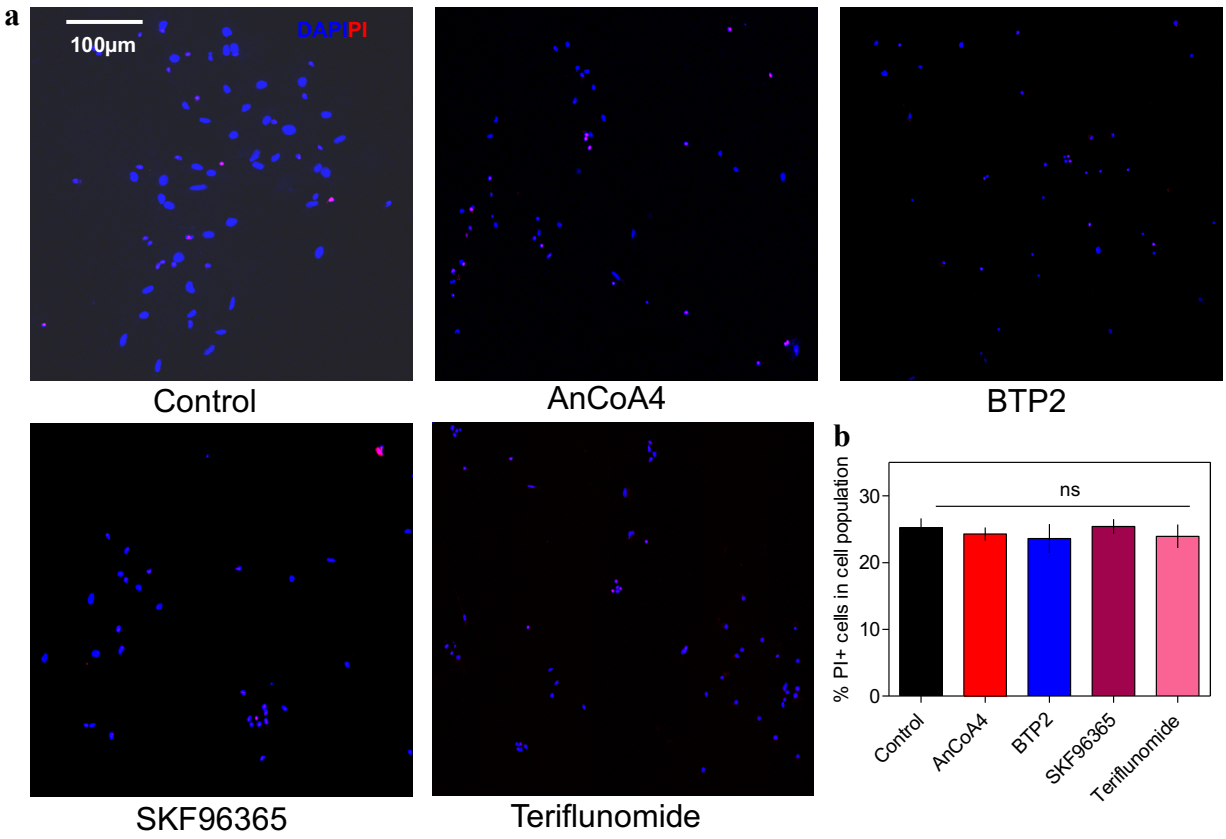

Figure 7.15 Cytotoxicity of the compounds.

(a) Images representing PI (propidium iodide) staining for the control cells as well as well cells exposed to AnCoA4: 300nM, BTP2:100nM, SKF96365:300nM and teriflunomide:3µM for ~15min. **(b)** Histogram showing the percentage of dead cells within each treatment group. Each value (mean ± SEM) was derived from 3 individual experiments and a total of 30-80 cells. One-way ANOVA followed by Dunnett's test was used for statistical comparison.

7.2.8 SOCE alteration in OPCs at differentiation-promoting dose of the compounds

To investigate whether the compounds can inhibit SOCE at concentrations that promoted differentiation, OPCs obtained from 4DIV culture maintained in proliferation medium were chosen for single cell Ca^{2+} imaging experiment. Cells were preincubated for ~15 min with compounds at differentiation-promoting dose. SOCE triggered by Tg showed compounds were incapable of suppressing SOCE at such dose (**Fig. 7.16**).

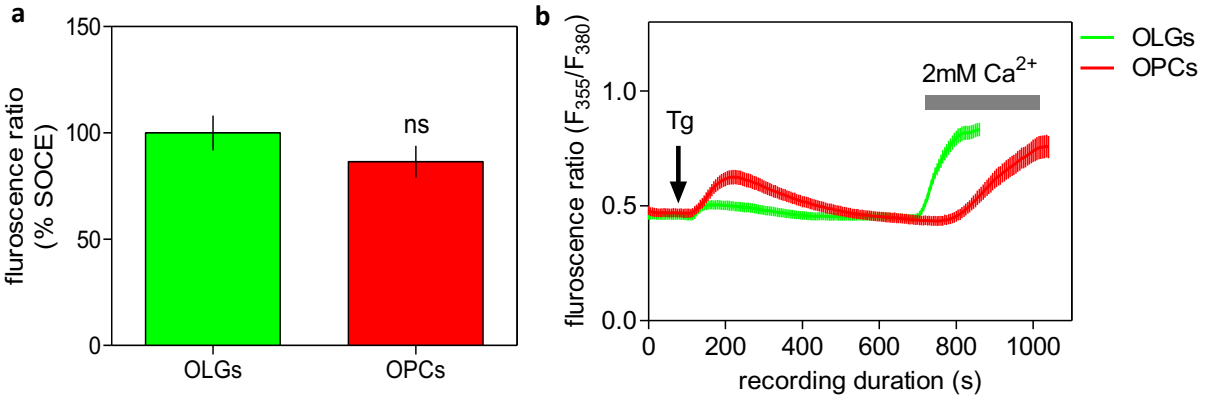

Figure 7.16 SOCE inhibition through differentiation-promoting dose of the compounds. **(a)** Histograms showing the highest peak SOCE levels triggered by Tg (2μM) in control cells and cells pre-treated with BTP2:100nM, and AnCoA4: 300nM. **(b)** Sample traces representing Ca^{2+} signals to cells with or without pre-treatment of BTP2 and AnCoA4. Each value (mean ± SEM) was derived from 3-5 independent experiments done in different days with 60-70 cells. One-way ANOVA followed by Dunnett's test was used for statistical comparison.

7.3 Discussion

SOCE regulates numerous cellular processes, including survival, motility, apoptosis and differentiation as well as a critical role in proliferation (Putney 2005; Kar and Parekh 2013). Although Ca^{2+} is a ubiquitous physiological characteristic of glial cells, but the mechanisms of SOCE that is an essential part of Ca^{2+} signalling in glial cell, particularly in OPCs remain uncharacterized.

Isolation of OPCs

Several methods for isolation of rat OPCs from the CNS have been developed till date, such as immunopanning, fluorescence-activated cell sorting (FACS) by exploiting cell surface specific antigens, differential gradient centrifugation or shaking method. In this project, OPCs were isolated from neonatal rat brain using two different methods. OPCs isolation was started with conventional shaking method, MGC (McCarthy and de Vellis 1980). Later on another newly developed OPCs isolation method, MACS procedure (Baror et al. 2019) was introduced. In terms of purity, there was no significant difference between the methods, although slightly higher purity rate was noticed in OPCs population isolated through MACS procedure (**Fig. 7.1**).

MACS procedure has several advantages over MGC method, former can generate cells much quicker than MGC, potentially in a day whereas the latter requires more than a week. Another important benefit that MACS procedure could provide is healthy yield of OPCs from neonatal to postnatal animal while isolating OPCs from adult brain is more critical when shaking method is used.

Isolated OPCs were then maintained in proliferation medium supplemented with growth factors, PDGF and FGF (Calver et al. 1998), on the other hand OLGs were generated through growing OPCs in differentiation medium supplemented T_3 hormone (Bartel 2004). Usually 4 to 5 DIV results the differentiation/maturation of OPCs (Butts et al. 2008)**.**

SOCE in OPCs

Activation of SOCE was triggered via both pharmacological (for example, using Tg) and physiological (for example, using growth factors) means. SOCE signal was recorded in OPCs stimulated by pharmacological mean, Tg. BTP2 and AnCoA4 which are two well-known SOCE inhibitors, attenuated such signal (**Fig. 7.4**), indicating expression of functional SOCE channel in OPCs. This agrees with other studies (Paez et al. 2009; Paez et al. 2011; Papanikolaou et al. 2017).

SOCE inhibitors, used in this study, have their own distinct SOCE inhibitory mechanisms. BTP2 is well-known to inhibit SOCE but it's mechanism of action remains poorly understood and it does not affect Stim or Orai protein individually but may affect their interaction (Ishikawa et al. 2003; Zitt et al. 2004; He et al. 2005) whereas AnCoA4 was identified as a small molecule that physically bind to fragment of Orai1 protein and was functionally characterised to inhibit Orai1-mediated SOCE (Sadaghiani et al. 2014). These features played a great role to identify the target sites in SOCE channel when SOCE was studied on OPCs differentiation.

SOCE was also monitored when triggered by physiological agent; PDGF (**Fig. 7.5**). Growth factor like PDGF, is already known to activate SOCE in OPCs (Paez et al. 2009). PDGF is the best characterized and the most active proliferative factor for OPCs. It can interacts with receptors tyrosine kinase which then activates Ca^{2+} signals resultant SOCE activation (Taniguchi 1995; Paez et al. 2009).

Thereafter, teriflunomide, drug for MS and one of the best SOCE inhibitors discovered in this study, also tested against SOCE in OPCs. It came as no surprise when SOCE suppression by teriflunomide was noted also in OPCs (**Fig. 7.6**), since the SOCE-inhibitory property of teriflunomide was already established to be cell-type independent in early phase of the work (Chapter 3).

Although the best characterised SOCE is well-established to be due to activation of Orai1 channels (also known as CRAC channels) by Stim proteins, several studies have indicated that in some cells, TRPC channels can also be activated by STIM proteins following store depletion (Liao et al. 2008; Ong and Ambudkar 2017). So, it is also likely that if a cell expresses both Orai and TRPC proteins, the SOCE it would manifest may have Ca^{2+} entry occurring via both the Orai and TRPC channels. It was therefore imperative to assess whether OPCs have functional TRPC channels present in their membrane. Previously TRPC mediated Ca^{2+} entry

was characterized in OPCs using pharmacological means, Tg (Paez et al. 2011) however, this agent activates both Orai and TRPC- mediated SOCE. Therefore, TRPC- mediated Ca^{2+} entry was characterized using OAG instead of Tg. The former is a membrane permeable, synthetic analogue of diacylglycerol (DAG), well known to activate members of the TRPC family of ion channels (Hofmann et al. 1999).

SOCE difference was anticipated between OPCs and OLGs because certain Ca^{2+} channel expression decreases as oligodendrocytes mature (Fulton et al. 2010). However, no discrepancy of SOCE signalling noticed between OPCs and OLGs (**Fig. 7.8**).

Voltage-gated Ca^{2+} channel (VGCC) in OPCs

In addition to SOCE, Ca^{2+}-entry via VGCCs was also characterized in OPCs. Despite of having numerous reports on expression of VGCC in oligodendrocytes, there was unsettled argument whether OPCs expressed VGCC or not. Studies are available on favour of non-existence of this channel in OPCs (Barres et al. 1990; Tong et al. 2009) whilst few other reports their existence in OPCs (Fulton et al., 2010; Paez et al., 2010). Such controversy therefore encouraged to investigate VGCC mediated Ca^{2+} entry in OPCs. High dose of KCl evoked depolarization have shown the permeability of Ca^{2+} entry from extracellular environment (**Fig. 7.9**) which indicated the expression of VGCC in OPCs.

SOCE in OPCs proliferation

SOCE, TRPC channel inhibitors as well as teriflunomide have shown to enhance OPCs differentiation therefore any effect of these compounds except teriflunomide, on OPCs proliferation was explored. Since, teriflunomide was already proven not to enhance proliferation (Göttle et al. 2018) therefore it was decided not to investigate this drug further on OPCs proliferation. As can be seen in **Fig. 7.14**, at differentiation- promoting dose, none of these inhibitors promoted proliferation although this result contradicted with studies carried out by others who have shown SOCE and/or TRPC channel regulate/modulate OPCs proliferation (Paez et al. 2009; Paez et al. 2011).

However current result could be supported by a widely-accepted notion that describes Ca^{2+} channel expression tends to decrease as oligodendrocytes mature (Fulton et al., 2010) which again indicated inhibition of such channels could accelerate differentiation process, not proliferation.

SOCE in OPCs differentiation

Identification of small molecules, or a signalling pathway that selectively induce differentiation of OPCs always have a significant impact on the future treatments of demyelinating disease like MS. Despite of having a wide range of effective role on biological process, SOCE was not well studied in the context of OPCs differentiation. Present study showed pharmacological inhibition of Ca^{2+}-entry via SOCE and TRPC channel potentially upregulated OPCs differentiation (**Fig. 7.10, Fig. 7.11,** and **Fig. 7.12**). However, others have shown otherwise; SOCE and TRPC channel regulate/modulate OPCs proliferation, not differentiation, by golli–MBP proteins (Paez et al. 2009; Paez et al. 2011).

It was somewhat surprising to find AnCoA4 being more potent than BTP2 in promoting differentiation of OPCs when both are well-established as SOCE inhibitors. This could explain whether the inhibitors promoted OPCs differentiation acting through inhibiting the Ca^{2+} signals stemming from the SOCE pathway or inhibiting the protein players underlying SOCE namely STIM and Orai.

To unwrap this puzzle, compounds were tested against SOCE to investigate whether they can inhibit SOCE at differentiation-promoting dose, however, neither BTP2 at 100nM dose or AnCoA4 at 300nM dose showed any significant effect on SOCE (**Fig. 7.16**). Such observation ruled out the possible effect of Ca^{2+} signals generated via SOCE on OPCs differentiation and hint a possible non-Ca^{2+} signalling associated role of STIM and/or Orai proteins. AnCoA4 is already known to bind to the Orai1 protein at an intracellular site and this explains its ability to inhibit SOCE (Sadaghiani et al. 2014) while BTP2 is not experimentally proven to physically bind to STIM or Orai protein but is believed to allosterically affect Orai pore geometry only when applied extracellularly (Ishikawa et al. 2003; Zitt et al. 2004). Therefore, given the ability to promote differentiation and incapacity to inhibit SOCE at differentiation promoting dose, both AnCoA4 and BTP2 enhanced OPCs differentiation probably through inhibiting Orai protein or blocking the formation of STIM-Orai complex. However, small molecules including drugs often have off target effects and this aspect could not be entirely ruled out for the observed effect of BTP2 and AnCoA4 in OPC differentiation.

The concept of exploring SOCE in OPCs context appeared through teriflunomide, the latter was found to block SOCE as well as relevant to MS therefore its effect on OPCs differentiation was further investigated. Teriflunomide emerged to promote differentiation at micromolar concentration (**Fig. 7.1.13**). While my study was undergoing, another group published a work showing pulsed application of teriflunomide promoted OPCs differentiation (Göttle et al. 2018). However, present study demonstrated such effect can be achieved at lower dose than the dose used in existing study.

Chapter 8

Final discussion

8.1 Summary of findings

Discovering the drug molecules that mimic few known SOCE inhibitors structurally and functionally, was one of the major goals of my doctoral study. Using ligand-based *in silico* screening, from existing FDA approved drug library, 10 drugs were selected, and purchased followed by testing against SOCE using single cell Ca^{2+} imaging technique. Out of ten drugs, five drugs, namely, leflunomide, teriflunomide, tolvaptan, lansoprazole and roflumilast found to inhibit SOCE most at ≤10 μM dose when tested in RBL-1 cells (**Fig. 3.4**). Of these 5 drugs, roflumilast was the most potent SOCE inhibitor drug with lowest IC50 dose (~4.5μM) (**Fig. 3.5)**. Drugs also retained their ability to inhibit SOCE in SHSY-5Y cells, indicating that the observed effect was not cell type specific (**Fig. 3.6**). SOCE- inhibitory concentration found in this study were achievable from the clinically-used doses of these drugs (**table 3.2**) which makes this finding more significant.

NFAT translocation assay was then executed to determine whether the chosen drugs could affect SOCE-dependent cell signalling and it was satisfying to see their complementary ability to retard nuclear translocation of NFAT1(1–460)-GFP in HeLa cells (**Fig. 3.10**) except leflunomide which was proven not to affect NFAT signalling. That could be due to an off-target effect of leflunomide that requires further experimentation. Whether these drugs had any effect on STIM1 oligomerisation and/or STIM1-Orai1 coupling when inhibit SOCE, experiments were executed using confocal microscopy with a HEK293 cell line with an inducible mCherry-STIM1-T2A-Orai1-eGFP. None of the drugs as well as the known SOCE-inhibitor BTP2 showed any efficiency on either STIM1 puncta formation or Orai1 puncta formation (**Fig. 3.11**). This indicated that SOCE-inhibitory properties of these drugs could be due mechanisms other than STIM/Orai clustering. Of the five drugs, leflunomide and its active metabolite teriflunomide are already known to inhibit DHODH enzyme resulting the reduction of activated lymphocytes proliferation, therefore these are being used as an immunosuppressive drug (Yara and Bidin 2015). The observed SOCE inhibitory properties might contribute significantly to the therapeutic benefits of these immunosuppressive drugs.

Tolvaptan, another drug with SOCE-inhibitory property reveal in this study, is orally and intravenously effective non-peptide antagonists for the arginine vasopressin (AVP) receptor subtypes. However, tolvaptan is unlikely to affect SOCE at therapeutic doses as the reported C_{max} of this drug is at sub-micromolar level. Similar to tolvaptan, omeprazole - a gastric proton pump inhibitor, inhibited SOCE at concentration that is much higher than what is possible in

clinically used oral doses (Shin and Kim 2013).

Roflumilast, an orally administered drug, selective inhibitor of PDE4 was the best SOCE inhibitor among the 5 drugs found in this study. However, given its known C_{max} (Rabe 2011) being much lower than what is needed to inhibit SOCE, this drug is unlikely to affect SOCE in clinical uses (Rabe 2011).

With a view to finding agents with more potent SOCE-inhibitory potency, few more drugs/compounds from each of the total 4 different pharmacological classes (DHODH inhibitor, PDE inhibitors, AVR antagonists and PPIs were purchased and tested against SOCE as an extended investigation. Since the best performing drugs inhibited SOCE at ~10 μM dose in the earlier studies therefore the goal of the extended study was to find out any drug or compound that potentially could inhibit SOCE at concentrations lower than 10μM. However, the starting dose for evaluating these molecules were decided to be 10μM so that agents without any effect on SOCE at this dose was not considered for testing at lower doses.

Among the additionally-purchased drugs, none of AVR antagonists and proton pump inhibitors (PPI) showed any SOCE suppression at 10 μM dose in RBL-1 cells (**Fig. 4.1** and **Fig. 4.2**). Among the PDE and PDE4-specific inhibitors class, only roflumilast N oxide and trequinsin supressed SOCE at 3 μM (**Fig. 3.4** and **Fig. 4.4**). From DHODH inhibitor family, vidofludimus was found to be the most potent inhibitor of SOCE as it could suppress SOCE significantly at nanomolar dose (**Fig. 4.9**) Thus, as a whole, the follow up work with extended members of the 4 pharmacological classes led to the finding of three candidates namely trequinsin, roflumilast N oxide and vidofludimus as more potent inhibitors of SOCE than the 5 drugs found in the early phase of the work. Similar to other drugs with SOCE inhibitory property, all these three drugs from extended investigation could suppress SOCE in few other cell types, indicating non-cell type specific effect and also in agreement with their effect on SOCE, they could significantly retard translocation of the NFAT to the nucleus. Like BTP2 and other initially-found drugs with SOCE-inhibitory property, the three new drugs also were devoid of any effect on STIM-Orai clustering.

Whether these compounds could affect other Ca^{2+} signalling pathways, for instances, IP_3 evoked ER-Ca^{2+} release (Vaughan et al. 1995) or voltage dependent Ca^{2+} entry (Di Virgilio et al. 1987) pathway, were subsequently investigated for . None of the compounds affected these channels except vidofludimus which showed some inhibition of IP_3 evoked Ca^{2+} release (**Fig. 5.3**).

Next, the selected SOCE inhibitors were evaluated for any possible effect on biological processes like cancer cell proliferation and neuroblastoma cell differentiation. Cell proliferation assay showed tested compounds had diverse effect on lungs cancer cell proliferation and such effect was cell type specific (**table 6.1**). Almost every compound inhibited SOCE in lung cancer cells at the dose of anti-proliferation (**Fig. 6.2**) which indicated SOCE inhibitory properties of these compounds might at least partially account for the observed antiproliferative effects of these drugs. None of the compounds exhibited any differentiation effect when experimented against SHSY-5Y cell (**Fig. 6.4**).

The main reason of exploring of SOCE in OPCs was derived from the fact that teriflunomide (along with its prodrug, leflunomide) was found to be able to suppress SOCE in immune and other cell types at doses that is clinically-achievable. This led to the hypothesis that apart from acting on the immune cells and thus reducing inflammation in the periphery as well as in the central nervous system, these drugs may also have significant effect on the biology of the OPCs. It was therefore logical to first characterise SOCE in OPCs and then evaluate the effect of these drugs. The critical aspect of this part of the work was reliable isolation of OPCs in good yields. For this, two isolation methods, MGC and MACS were exploited. SOCE was observed in OPCs stimulated through both pharmacological and physiological means using single cell Ca^{2+} imaging technique (**Fig. 7.4** and **Fig. 7.5**). Most importantly, no difference in SOCE was noticed between OPCs and mature OPCs (**Fig. 7.8**). In addition to SOCE, voltage-gated Ca^{2+} entry was also characterized in OPCs (**Fig. 7.9**).

To see the role of SOCE on OPCs differentiation, known pharmacological blockers of SOCE and TRPC (also part of SOCE (Liao et al. 2008)) as well as teriflunomide were tested aginst OPCs. Result showed pharmacological inhibition of SOCE and TRPC channel potentially upregulated OPCs differentiation (**Fig. 7.10, Fig. 7.11** and **Fig. 7.12**) although this result contradicted with related existing study (Paez et al. 2009; Paez et al. 2011). Afterwards, these compounds were tested to see their role on proliferation, as expected, inhibition of SOCE halted OPCs proliferation (**Fig. 7.14).** This result was believable because in general, Ca^{2+} channel expression tends to decrease as oligodendrocytes mature (Fulton et al., 2010), however, few other studies reported differently (Paez et al. 2009; Paez et al. 2011).

8.2 Future directions

The key results of this thesis have revealed that some of the FDA approved drugs and their analogues could modulate SOCE, additionally, these modulators could inhibit lung cancer cell proliferation. Another important aspect of this study was characterization of SOCE in OPCs. Further, it was also discovered that pharmacological inhibition of SOCE enhanced OPCs differentiation. However, despite of having some important findings from this study, few suggestions need to be taken into consideration for further study.

Firstly, compounds have shown their ability to restrict NFAT translocation into nucleus, Since NFAT is important for IL-2 gene expression, as well as also contribute to the expression of other cytokines, including IL-3, IL-4, IL-5 (Chow, Rincón, and Davis 1999) therefore it would be interesting to see if there any effect these compounds have on cytokines production.

Secondly, when the compounds were evaluated to see their biological impact, some of the compounds have shown anti-proliferative activity on lung cancer cell. Whether the observed anti-proliferative effect of these drugs stemmed from their SOCE- modulatory properties or inhibition of their known targets or action on any other off target, could not be clearly discerned and this need to be investigated in future.

Thirdly, SOCE was thoroughly characterised in OPCs but expression of SOCE channel proteins, STIM, Orai, (Prakriya et al. 2006) remain uncharacterized. Pharmacological modulation of SOCE in OPCs led to differentiation which was probably due to inhibition of Orai protein that needs to be further investigated through knocking down respective gene.

Given the SOCE modulatory ability of few PDE inhibitors found in this study, it could have been interesting to see the effect of these inhibitors on OPCs differentiation as inhibition of PDE4 reported to promote OPCs differentiation (Syed et al. 2013). Recently it was discovered that adult OPCs are the cells that are mainly responsible for generating new oligodendrocytes during the regenerative process of remyelination (Franklin and Ffrench-Constant 2017) therefore OPCs differentiation due to SOCE inhibition found in this study could be re-evaluated through testing against OPCs isolated from aged animal.

8.3 Conclusion

Finding the drug molecules that mimic few known SOCE inhibitors structurally and functionally, was the major goal of the present study. Using computational and experimental techniques, several drugs and their analogues have been found to suppress SOCE significantly, with no such prior records. It was interesting to see some existing drugs eventually could supress SOCE at clinically relevant doses, therefore any future reuse of these drugs might not be required additional study for pharmacokinetic properties as such properties for these agents are already been established.

Aberrant SOCE in various diseases appear to be an attractive therapeutic target for treating several diseases. SOCE inhibitors found in this study showed reduced proliferation in lung cancer cell which could open a new target to develop therapy for lung cancer.

Identification of small molecules, or a signalling pathway that selectively induce differentiation of OPCs always have a significant impact on the future treatments of MS. OPCs differentiation due to pharmacological inhibition of SOCE observed in this study certainly has novelty, which could help to identify new target to develop therapeutic for demyelinating diseases.

Chapter 9

Bibliography

Aditya, Suruchi and Aditya Rattan. 2012. “Vaptans: A New Option in the Management of Hyponatremia.” *Int J App Basic Med Res* 2(2):77.

Alicia, S., Angelica, Z., Carlos, S., Alfonso, S. and Vaca, L. 2008. “STIM1 converts TRPC1 from a receptor-operated to a store-operated channel: moving TRPC1 in and out of lipid rafts.” *Cell Calcium* 44(5):479-491.

Angela Dziedzic, Elzbieta Miller, Joanna Saluk-Bijak and Michal Bijak. 2020. The GPR17 Receptor-A Promising Goal for Therapy and a Potential Marker of the Neurodegenerative Process in Multiple Sclerosis. *Int J Mol Sci* 21:1852.

Armesilla, a L., E. Lorenzo, P. Gómez del Arco, S. Martínez-Martínez, Alfranca, and J. M. Redondo. 1999. “Vascular Endothelial Growth Factor Activates Nuclear Factor of Activated T Cells in Human Endothelial Cells: A Role for Tissue Factor Gene Expression.” *Mol Cell Biol* 19(3):2032-2043.

Bai, Hui, Chenchen Wang, Yu Qi, Jin Xu, Nan Li, Lili Chen, Bin Jiang, Xudong Zhu, Hanwen Zhang, Xiaoyu Li, Qing Yang, Junqing Ma, Yong Xu, Jingjing Ben, and Qi Chen. 2019. “Major Vault Protein Suppresses Lung Cancer Cell Proliferation by Inhibiting STAT3 Signaling Pathway.” *BMC Cancer* 19(1):1-13.

Bakowski, D., M. D. Glitsch, and a B. Parekh. 2001. “An Examination of the Secretion-like Coupling Model for the Activation of the Ca^{2+} Release-Activated Ca^{2+} Current I(CRAC) in RBL-1 Cells.” *J Physiol* 532(1):55-71.

Bansal R, Kumar M, Murray K, Morrison RS, and Pfeiffer SE. 1996. “Regulation of FGF receptors in the oligodendrocyte lineage.” *Mol Cell Neurosci* 7:263-275.

Baror, Roey, Björn Neumann, Michael Segel, Kevin J. Chalut, Stephen P. J. Fancy, Dorothy P. Schafer, and Robin J. M. Franklin. 2019. “Transforming Growth Factor-Beta Renders Ageing Microglia Inhibitory to Oligodendrocyte Generation by CNS Progenitors.” *Glia* 67(7):1374-84.

Barres BA, Lazar MA, and Raff MC. 1994a. “A novel role for thyroid hormone, glucocorticoids and retinoic acid in timing oligodendrocyte development.” *Development* 120:1097-1108.

Barres BA, Raff MC, Gaese F, Bartke I, Dechant G, and Barde YA. 1994b. “A crucial role for neurotrophin-3 in oligodendrocyte development.” *Nature* 367:371-375.

Bartel DP. 2004. “MicroRNAs: genomics, biogenesis, mechanism, and function.” *Cell* 116:281-297.

Berridge, M. J. 1993. “Inositol Trisphosphate and Calcium Signalling.” *Nature* 361:315-325.

Berridge, M. J. 1995. “Capacitative Calcium Entry.” *Biochem J* 312:1-11.

Berridge, M. J., P. Lipp, and M. D. Bootman. 2000. “The Versatility and Universality of Calcium Signalling.” *Nat Rev Mol Cell Biol* 1(1):11-21.

Berridge, Michael J., Martin D. Bootman, and H. Llewelyn Roderick. 2003. “Calcium: Calcium Signalling: Dynamics, Homeostasis and Remodelling.” *Nat Rev Mol Cell Biol* 4(7):517-29.

Bhatt, Purav, Elizabeth McNeely, Tess Lin, Kirkwood Adams, and J. Patterson. 2014. “Review of Tolvaptan’s Pharmacokinetic and Pharmacodynamic Properties and Drug Interactions.” *J Clin Med* 3(4):1276-90.

Biedler, June L., Lawrence Helson, and Barbara a Spengler. 1973. “Morphology and Growth, Tumorigenicity, and Cytogenetics of Human Neuroblastoma Cells in Continuous Culture.” *Cancer Res* 33(11):2643-52.

Bird, Gary S., Wayne I. DeHaven, Jeremy T. Smyth, and James W. Putney. 2008. “Methods for Studying Store-Operated Calcium Entry.” *Methods* 46(3):204-212.

Bootman, Martin D., Tony J. Collins, Claire M. Peppiatt, Larissa S. Prothero, Lauren MacKenzie, Patrick De Smet, Marianne Travers, Stephen C. Tovey, Jeong T. Seo, Michael J. Berridge, Francesca Ciccolini, and Peter Lipp. 2001. “Calcium Signalling—an Overview.” *Semin Cell Dev Biol* 12(1):3-10.

Butts, B. D., C. Houde, and H. Mehmet. 2008. “Maturation-Dependent Sensitivity of Oligodendrocyte Lineage Cells to Apoptosis: Implications for Normal Development and Disease.” *Cell Death Differ* 15(7):1178-1186.

Cai R, Ding X, Zhou K, Shi Y, Ge R, Ren G, Jin Y, and Wang Y. 2009. Blockade of TRPC6 channels induced G2/M phase arrest and suppressed growth in human gastric cancer cells. *Int J Cancer* 125(10):2281-2287.

Calver AR, Hall AC, Yu WP, Walsh FS, Heath JK, Betsholtz C, and Richardson WD. 1998 “Oligodendrocyte population dynamics and the role of PDGF in vivo.” *Neuron* 20:869-882.

Carafoli, Ernesto. 2002. “Calcium Signaling: A Tale for All Seasons.” *PNAS* 99(3):1115-1122.

Catterall, William A. 2011. “Voltage-Gated Calcium Channels.” *Cold Spring Harb Perspect Biol* 3(8):3947.

Cerpnjak K, Zvonar A, Gašperlin M, Vrečer F. 2013. Lipid-based systems as a promising approach for enhancing the bioavailability of poorly water-soluble drugs. *Acta Pharm* 63(4):427-445.

Chen, Gang, Sandip Panicker, Kai-Yeung Lau, Subramaniam Apparsundaram, Vaishali A. Patel, Shiow-Ling Chen, Rothschild Soto, Jimmy K. C. Jung, Palanikumar Ravindran, Dayne Okuhara, Gary Bohnert, Qinglin Che, Patricia E. Rao, John D. Allard, Laura Badi, Hans-Marcus Bitter, Philip A. Nunn, Satwant K. Narula, and Julie A. DeMartino. 2013. “Characterization of a Novel CRAC Inhibitor That Potently Blocks Human T Cell Activation and Effector Functions.” *Mol Immunol* 54(3-4):355-67.

Chen, Y. F., W. T. Chiu, Y. T. Chen, P. Y. Lin, H. J. Huang, C. Y. Chou, H. C. Chang, M. J. Tang, and M. R. Shen. 2011. “Calcium Store Sensor Stromal-Interaction Molecule 1-Dependent Signaling Plays an Important Role in Cervical Cancer Growth, Migration, and Angiogenesis.” *PNAS* 108(37):15225-15230.

Cheng, K. T., Liu, X., Ong, H. L. and Ambudkar, I. S. 2008. “Functional requirement for Orai1 in store-operated TRPC1-STIM1 channels.” *J Biol Chem* 283(19):12935-12940.

Chigurupati S, Venkataraman R, Barrera D, Naganathan A, Madan M, Paul L, Pattisapu JV, Kyriazis GA, Sugaya K, Bushnev S, Lathia JD, Rich JN, and Chan SL. 2010. Receptor channel TRPC6 is a key mediator of Notch-driven glioblastoma growth and invasiveness. *Cancer Res* 70(1):418-427.

Chow, Chi-Wing, Mercedes Rincón, and Roger J. Davis. 1999. “Requirement for Transcription Factor NFAT in Interleukin-2 Expression.” *Mol Cell Biol* 19(3):2300-2307.

Claussen, Malte C. and Thomas Korn. 2012. “Immune Mechanisms of New Therapeutic Strategies in MS - Teriflunomide.” *J Clin Immunol* 142(1):49-56.

Confavreux, Christian, O'Connor, Paul Comi, Giancarlo Freedman, Mark S. Miller, Aaron E. Olsson, Tomas P. Wolinsky, Jerry S. Bagulho, Teresa Delhay, Jean Luc Dukovic, Deborah Truffinet, and Philippe Kappos, Ludwig. 2014. “Oral teriflunomide for patients with relapsing

multiple sclerosis (TOWER): A randomised, double-blind, placebo-controlled, phase 3 trial." *Lancet Neurol* 13(3):247-256.

Cox, Jennifer H., Scott Hussell, Henrik Søndergaard, Kirstine Roepstorff, John-Vu Bui, Jen Running Deer, Jun Zhang, Zhan-Guo Li, Kasper Lamberth, Peter Helding Kvist, Søren Padkjær, Claus Haase, Stefan Zahn, and Valerie H. Odegard. 2013. "Antibody-Mediated Targeting of the Orai1 Calcium Channel Inhibits T Cell Function." *PloS One* 8(12):e82944.

David T. Hsieh and Elizabeth A. 2013. Efficacy and safety of rufinamide in pediatric epilepsy. *Ther Adv Neurol Disord* 6(3):189-198.

Dawson MR, Polito A, Levine JM, and Reynolds R. 2003. "NG2-expressing glial progenitor cells: an abundant and widespread population of cycling cells in the adult rat CNS." *Mol Cell Neurosci* 24:476-488.

Darbellay, Basile, Serge Arnaudeau, Stéphane König, Hélène Jousset, Charles Bader, Nicolas Demaurex, and Laurent Bernheim. 2009. "STIM1- and Orai1-Dependent Store-Operated Calcium Entry Regulates Human Myoblast Differentiation." *J Biol Chem* 284(8):5370-5380.

De Biase LM, Nishiyama A, and Bergles DE. 2010. "Excitability and synaptic communication within the oligodendrocyte lineage." *J Neurosci* 30:3600-3611.

DeHaven, W. I., Smyth, J. T., Boyles, R. R. and Putney, J. W., Jr. 2007. "Calcium inhibition and calcium potentiation of Orai1, Orai2, and Orai3 calcium release-activated calcium channels." *J Biol Chem* 282(24):17548-17556.

De la Fuente, Alerie Guzman, Oihana Errea, Peter van Wijngaarden, Ginez A. Gonzalez, Christophe Kerninon, Andrew A. Jarjour, Hilary J. Lewis, Clare A. Jones, Brahim Nait-Oumesmar, Chao Zhao, Jeffrey K. Huang, Charles Ffrench-Constant, and Robin J. M. Franklin. 2015. "Vitamin D Receptor-Retinoid X Receptor Heterodimer Signaling Regulates Oligodendrocyte Progenitor Cell Differentiation." *J Cell Biol* 211(5):975-985.

De Waal, Luc, Timothy A. Lewis, Matthew G. Rees, Aviad Tsherniak, Xiaoyun Wu, Peter S. Choi, Lara Gechijian, Christina Hartigan, Patrick W. Faloon, Mark J. Hickey, Nicola Tolliday, Steven A. Carr, Paul A. Clemons, Benito Munoz, Bridget K. Wagner, Alykhan F. Shamji, Angela N. Koehler, Monica Schenone, Alex B. Burgin, Stuart L. Schreiber, Heidi Greulich, and Matthew Meyerson. 2016. "Identification of Cancer-Cytotoxic Modulators of PDE3A by Predictive Chemogenomics." *Nat Chem Biol* 12(2):102-8.

Decaux, Guy, Alain Soupart, and Gilbert Vassart. 2008. “New Drug Class Non-Peptide Arginine-Vasopressin Antagonists : The Vaptans.” *Lancet* 371(9624):1624-1632.

Derler, Isabella, Rainer Schindl, Reinhard Fritsch, Peter Heftberger, Maria Christine Riedl, Malcolm Begg, David House, and Christoph Romanin. 2013. “The Action of Selective CRAC channel blockers is affected by the Orai pore geometry.” *Cell Calcium* 53(2):139-151.

Derler I, Jardin I, and Romanin C. 2016. Molecular mechanisms of STIM/Orai communication. *Am J Physiol Cell Physiol* 310(8):643-662.

Deshmukh, V.A., Tardif, V., Lyssiotis, C.A., Green, C.C., Kerman, B., Kim, H.J., Padmanabhan, K., Swoboda, J.G., Ahmad, I., Kondo, T. 2013. “A regenerative approach to the treatment of multiple sclerosis.” *Nature* 502:327-332.

Di Capite, Joseph, Charmaine Nelson, Grant Bates, and Anant B. Parekh. 2009. “Targeting Ca^{2+} Release-Activated Ca^{2+} Channel Channels and Leukotriene Receptors Provides a Novel Combination Strategy for Treating Nasal Polyposis.” *J Allergy Clin Immunol* 124(5):1014-1021.

Di Virgilio, F., D. Milan, A. Leon, J. Meldolesi, and T. Pozzan. 1987. “Voltage-Dependent Activation and Inactivation of Calcium Channels in PC12 Cells.” *J Biol Chem* 262:9189-9195.

Dorasamy, Mathura Subangari, Bhavesh Choudhary, Kavitha Nellore, Hosahalli Subramanya, and Pooi Fong Wong. 2017. “Dihydroorotate Dehydrogenase Inhibitors Target C-Myc and Arrest Melanoma, Myeloma and Lymphoma Cells at S-Phase.” *J Cancer* 8(15):3086-3098.

Dugas JC, Cuellar TL, Scholze A, Ason B, Ibrahim A, Emery B, Zamanian JL, Foo LC, McManus MT, and Barres BA. 2010. “Dicer1 and miR-219 Are required for normal oligodendrocyte differentiation and myelination.” *Neuron* 65:597-611.

Earl W. Sutherland and T. W. Rall. 1958. “Fractionation and characterization of a cyclic adenine ribonucleotide formed by tissue particles.” *J Biol Chem* 232:1077-1092.

Eccleston, Enid, Brian J. Leonard, John S. Lowe, and Hilary J. Welford. 1973. “Basophilic Leukaemia in the Albino Rat and a Demonstration of the Basopoietin.” *Nat New Biol* 244:73-76.

Faouzi M, Kischel P, Hague F, Ahidouch A, Benzerdjeb N, Sevestre H, Penner R, and Ouadid Ahidouch H. 2013. ORAI3 silencing alters cell proliferation and cell cycle progression via c-myc pathway in breast cancer cells. *Biochim Biophys Acta* 1833(3):752-760.

Fasolato, C., P. Pizzo, and T. Pozzan. 1998. “Delayed Activation of the Store-Operated Calcium Current Induced by Calreticulin Overexpression in RBL-1 Cells.” *Mol Biol Cell* 9(6):1513-1522.

Feske, Stefan. 2019. “CRAC Channels and Disease – From Human CRAC Channelopathies and Animal Models to Novel Drugs.” *Cell Calcium* 80:112-16.

Feske, Stefan, Yousang Gwack, Murali Prakriya, Sonal Srikanth, Sven-Holger Puppel, Bogdan Tanasa, Patrick G. Hogan, Richard S. Lewis, Mark Daly, and Anjana Rao. 2006. “A Mutation in Orai1 Causes Immune Deficiency by Abrogating CRAC Channel Function.” *Nature* 441(7090):179-185.

Feske, Stefan, Murali Prakriya, Anjana Rao, and Richard S. Lewis. 2005. “A Severe Defect in CRAC Ca^{2+} Channel Activation and Altered K^{+} Channel Gating in T Cells from Immunodeficient Patients.” *J Exp Med* 202(5):651-662.

Fierro, L. and A. B. Parekh. 1999. “Fast Calcium-Dependent Inactivation of Calcium Release-Activated Calcium Current (CRAC) in RBL-1 Cells.” *J Membr Biol* 168(1):9-17.

Fitzpatrick, Leo R., Ludwig Deml, Claudia Hofmann, Jeffrey S. Small, Manfred Groeppel, Svetlana Hamm, Sylvia Lemstra, Johann Leban, and Aldo Ammendola. 2010. “4SC-101, a Novel Immunosuppressive Drug, Inhibits IL-17 and Attenuates Colitis in Two Murine Models of Inflammatory Bowel Disease.” *Inflamm Bowel Dis* 16(10):1763-1777.

Fitzpatrick, Leo R., Jeffrey S. Small, and Aldo Ammendola. 2011. “Inhibition of IL-17 Release by the Novel Anti-Inflammatory Drug Vidofludimus Involves Attenuation of STAT3 and NF-Kappa B Signaling Pathways in Murine Splenocytes and Hapten-Induced Colitis.” *Gastroenterology* 140(5):S-837.

Franklin, Robin J. M. 2002. “Why does remyelination fail in multiple sclerosis?” *Nat Rev Neurosci* 3(9):705-714.

Franklin, Robin J. M. and Charles Ffrench-Constant. 2008. “Remyelination in the CNS: from biology to therapy.” *Nat Rev Neurosci* 9(11):839-855.

Franklin, Robin J. M. 2015. “Regenerative Medicines for Remyelination: From Aspiration to Reality.” *Cell Stem cell* 16(6):576-577.

Franklin, Robin J. M. and Charles Ffrench-Constant. 2017. “Regenerating CNS Myelin - From Mechanisms to Experimental Medicines.” *Nat Rev Neurosci* 18(12):753-769.

Franzius, D., M. Hoth, and R. Penner. 1994. “Non-Specific Effects of Calcium Entry Antagonists in Mast Cells.” *Pflug Arch Eur J Phy* 428(5-6):433-438.

Fünfschilling Ursula, Supplie Lotti, Mahad Don, Boretius Susann, Saab Aiman, Edgar Julia, Brinkmann Bastian, Kassmann Celia, Tzvetanova Iva, Möbius, Wiebke Diaz, Francisca Meijer, Dies Suter, Ueli Hamprecht, Bernd Sereda, Michael W. Moraes, Carlos T. Frahm, Jens Goebbels, Sandra and Nave, Klaus Armin. 2012. “Glycolytic oligodendrocytes maintain myelin and long-term axonal integrity.” *Nature* 485(7399):517-521.

Fulton D, Paez PM, Fisher R, Handley V, and Colwell CS, Campagnoni AT. 2010. “Regulation of L-type Ca^{++} currents and process morphology in white matter oligodendrocyte precursor cells by golli-myelin proteins.” *Glia* 58:1292-1303.

Goodman, Marc, James Gurney, Malcolm Smith, and Andrew Olshan. 1985. “Sympathetic Nervous System - SEER Pediatric Monograph.” *J Natl Canc Inst Monogr* 65-72.

Gopurappilly, Renjitha, Bipan Kumar Deb, Pragnya Chakraborty, and Gaiti Hasan. 2018. “Stable STIM1 Knockdown in Self-Renewing Human Neural Precursors Promotes Premature Neural Differentiation.” *Front Mol Neurosci* 11:1-19.

Goretzki L, Burg MA, Grako KA and Stallcup WB. 1999. “High-affinity binding of basic fibroblast growth factor and platelet-derived growth factor-AA to the core protein of the NG2 proteoglycan.” *J Biol Chem* 274:16831-16837.

Goto, Jun-Ichi, Akinobu Z. Suzuki, Shoichiro Ozaki, Nagisa Matsumoto, Takeshi Nakamura, Etsuko Ebisui, Andrea Fleig, Reinhold Penner, and Katsuhiko Mikoshiba. 2010. “Two Novel 2-Aminoethyl Diphenylborinate (2-APB) Analogues Differentially Activate and Inhibit Store-Operated Ca^{2+} Entry via STIM Proteins.” *Cell Calcium* 47(1):1-10.

Göttle, Peter, Anastasia Manousi, David Kremer, Laura Reiche, Hans Peter Hartung, and Patrick Küry. 2018. “Teriflunomide Promotes Oligodendroglial Differentiation and Myelination.” *J Neuroinflammation* 15(1):1-12.

Gwack, Yousang, Sonia Sharma, Julie Nardone, Bogdan Tanasa, Alina Iuga, Sonal Srikanth, Heidi Okamura, Diana Bolton, Stefan Feske, Patrick G. Hogan, and Anjana Rao. 2006. “A Genome-Wide Drosophila RNAi Screen Identifies DYRK-Family Kinases as Regulators of NFAT.” *Nature* 441(7093):646-50.

Hao, Baixia, Yingying Lu, Qian Wang, Wenjing Guo, King Ho Cheung, and Jianbo Yue. 2014. "Role of STIM1 in Survival and Neural Differentiation of Mouse Embryonic Stem Cells Independent of Orai1-Mediated Ca^{2+} Entry." *Stem Cell Res* 12(2):452-466.

He, Li Ping, Thamara Hewavitharana, Jonathan Soboloff, Maria a. Spassova, and Donald L. Gill. 2005. "A Functional Link between Store-Operated and TRPC Channels Revealed by the 3,5-Bis(Trifluoromethyl)Pyrazole Derivative, BTP2." *J Biol Chem* 280(12):10997-11006.

Hendron, Eunan, Xizhuo Wang, Yandong Zhou, Xiangyu Cai, Jun Ichi Goto, Katsuhiko Mikoshiba, Yoshihiro Baba, Tomohiro Kurosaki, Youjun Wang, and Donald L. Gill. 2014. "Potent Functional Uncoupling between STIM1 and Orai1 by Dimeric 2-Aminodiphenyl Borinate Analogs." *Cell Calcium* 56(6):482-492.

Hernández, G. L., O. V Volpert, M. A. Iñiguez, E. Lorenzo, S. Martínez-Martínez, R. Grau, M. Fresno, and J. M. Redondo. 2001. "Selective Inhibition of Vascular Endothelial Growth Factor-Mediated Angiogenesis by Cyclosporin A: Roles of the Nuclear Factor of Activated T Cells and Cyclooxygenase 2." *J Exp Med* 193(5):607-620.

Hofmann, Thomas, Alexander G. Obukhov, M. Schaefer, C. Harteneck, T. Gudermann, and G. Schultz. 1999. "Direct Activation of Human TRPC6 and TRPC3 Channels by Diacylglycerol." *Nature* 397(6716):259-263.

Hogan, Patrick G. and Anjana Rao. 2007. "Dissecting ICRAC, a Store-Operated Calcium Current." *Trends Biochem Sci* 32(5):235-245.

Hoth, M. and R. Penner. 1992. "Depletion of Intracellular Calcium Stores Activates a Calcium Current in Mast Cells." *Nature* 355(6358):353-356.

Hoth, M. and R. Penner. 1993. "Calcium Release-Activated Calcium Current in Rat Mast Cells." *J Physiol* 465:359-386.

Huang, Yi and J. W. Putney. 1998. "Relationship between Intracellular Calcium Store Depletion and Calcium Release-Activated Calcium Current in a Mast Cell Line (RBL-1)." *J Biol Chem* 273(31):19554-19559.

Huang, G. N., Zeng, W., Kim, J. Y., Yuan, J. P., Han, L., Muallem, S. and Worley, P. F. 2006. "STIM1 carboxyl-terminus activates native SOC, Icrac and TRPC1 channels." *Nat Cell Biol* 8(9):1003-1010.

Irvine KA, Blakemore WF. 2008. “Remyelination protects axons from demyelination-associated axon degeneration.” *Brain* 131(6):1464-1477.

Ishikawa, Jun, Keiko Ohga, Taiji Yoshino, Ryuichi Takezawa, Atsushi Ichikawa, Hirokazu Kubota, and Toshimitsu Yamada. 2003. “A Pyrazole Derivative, YM-58483, Potently Inhibits Store-Operated Sustained Ca^{2+} Influx and IL-2 Production in T Lymphocytes.” *J Immunol* 170(9):4441-4449.

Jairaman, Amit and Murali Prakriya. 2013. “Molecular Pharmacology of Store-Operated CRAC Channels.” *Channels* 7(5):402-414.

Joshi, Amita S., Shang Ying P. King, Barbara A. Zajac, Leonard Makowka, Linda S. Sher, Barry D. Kahan, Alan H. Menkis, Calvin R. Stiller, Brigitte Schaefle, and David M. Kornhauser. 1997. “Phase I Safety and Pharmacokinetic Studies of Brequinar Sodium after Single Ascending Oral Doses in Stable Renal, Hepatic, and Cardiac Allograft Recipients.” *J Clin Pharmacol* 37(12):1121-1128.

Kar, Pulak and Anant B. Parekh. 2013. “STIM Proteins, Orai1, and Gene Expression.” *Channels* 7(5):374-378.

Karadottir R, Hamilton NB, Bakiri Y, Attwell D. 2008. “Spiking and nonspiking classes of oligodendrocyte precursor glia in CNS white matter.” *Nat Neurosci* 11:450-456.

Korn, Thomas, Tim Magnus, Klaus Toyka, and Stefan Jung. 2004. “Modulation of Effector Cell Functions in Experimental Autoimmune Encephalomyelitis by Leflunomide- Mechanisms Independent of Pyrimidine Depletion.” *J Leukoc Biol* 76(5):950-960.

Kotter Mark R.,Christine Stadelmann, and Hans-Peter Hartung. 2011. “Enhancing remyelination in disease - Can we wrap it up?” *Brain* 134(7):1882-1900.

Kreideweiss, S., C. Ahlers, a Nordheim, and a Rühlmann. 1999. “Ca2+-Induced P38/SAPK Signalling Inhibited by the Immunosuppressant Cyclosporin A in Human Peripheral Blood Mononuclear Cells.” *FEBS* 265(3):1075-1084.

Kucharova K and Stallcup WB. 2010. “The NG2 proteoglycan promotes oligodendrocyte progenitor proliferation and developmental myelination.” *Neuroscience* 166:185-194.

Kukley M, Nishiyama A, and Dietrich D. 2010. “The fate of synaptic input to NG2 glial cells: neurons specifically downregulate transmitter release onto differentiating oligodendroglial cells.” *J Neurosci* 30:8320-8331.

Kulkarni, Onkar P., Sufyan G. Sayyed, Claudia Kantner, Mi Ryu, Max Schnurr, Miklós Sárdy, Johann Leban, Ruediger Jankowsky, Aldo Ammendola, Robert Doblhofer, and Hans Joachim Anders. 2010. "4SC-101, a Novel Small Molecule Dihydroorotate Dehydrogenase Inhibitor, Suppresses Systemic Lupus Erythematosus in MRL-(Fas)Lpr Mice." *Am J Pathol* 176(6):2840-2847.

Langedijk, Joris, Aukje K. Mantel-Teeuwisse, Diederick S. Slijkerman, and Marie-Hélène D. B. Schutjens. 2015. "Drug Repositioning and Repurposing: Terminology and Definitions in Literature." *Drug Discov Today* 20(8):1027-1034.

Leban, Johann, Martin Kralik, Jan Mies, Michael Gassen, Karin Tentschert, and Roland Baumgartner. 2005. "SAR, Species Specificity, and Cellular Activity of Cyclopentene Dicarboxylic Acid Amides as DHODH Inhibitors." *Bioorg Med Chem* 15(21):4854-4857.

Lecoeur H. 2002. Nuclear apoptosis detection by flow cytometry: influence of endogenous endonucleases. *Exp Cell Res* 277(1):1-14.

Lewis, R. S. and M. D. Cahalan. 1989. "Mitogen-Induced Oscillations of Cytosolic Ca^{2+} and Transmembrane Ca^{2+} Current in Human Leukemic T Cells." *Cell Regul* 1(1):99-112.

Liao, Yanhong, Christian Erxleben, Joel Abramowitz, Veit Flockerzi, Michael Xi Zhu, and David L. Armstrong. 2008. "STIM1 Suggest a STIM-Regulated Heteromeric Orai / TRPC Model for SOCE / Icrac Channels." *PNAS* 105(8):2895-2900.

Liao, Y., Plummer, N. W., George, M. D., Abramowitz, J., Zhu, M. X. and Birnbaumer, L. 2009. "A role for Orai in TRPC-mediated Ca^{2+} entry suggests that a TRPC: Orai complex may mediate store and receptor operated Ca^{2+} entry." *PNA*S 106(9):3202-3206.

Li G, Zhang Z, Wang R, Ma W, Yang Y, Wei J, and Wei Y. 2013. Suppression of STIM1 inhibits human glioblastoma cell proliferation and induces G0/G1 phase arrest. *J Exp Clin Cancer Res* 32:20.

Li, Shiliang, Guoqin Luan, Xiaoli Ren, Wenlin Song, Liuxin Xu, Minghao Xu, Junsheng Zhu, Dong Dong, Yanyan Diao, Xiaofeng Liu, Lili Zhu, Rui Wang, Zhenjiang Zhao, Yufang Xu, and Honglin Li. 2015. "Rational Design of Benzylidenehydrazinyl-Substituted Thiazole Derivatives as Potent Inhibitors of Human Dihydroorotate Dehydrogenase with in Vivo Anti-Arthritic Activity." *Sci Rep* 5:1-19.

Li, Wenjun, Minhong Zhang, Lei Xu, Danmiao Lin, Shaoxi Cai, and Fei Zou. 2013. "The Apoptosis of Non-Small Cell Lung Cancer Induced by Cisplatin through Modulation of STIM1." *Exp Toxicol Pathol* 65(7-8):1073-1081.

Lievremont, Jean-philippe, Gary S. Bird, James W. Putney, and North Carolina. 2005. "Mechanism of Inhibition of TRPC Cation Channels by 2- Aminoethoxydiphenylborane." *Mol Pharmacol* 68(3):758-762.

Lin, Fen-Fen, Robin Elliott, Anne Colombero, Kevin Gaida, Laura Kelley, Angelica Moksa, Shu-Yin Ho, Ekaterina Bykova, Min Wong, Palaniswami Rathanaswami, Sylvia Hu, John K. Sullivan, Hung Q. Nguyen, and Helen J. McBride. 2013. "Generation and Characterization of Fully Human Monoclonal Antibodies against Human Orai1 for Autoimmune Disease." *J. Pharmacol Exp Ther* 345(2):225-238.

Liou, Jen, Man Lyang Kim, Won Do Heo, Joshua T. Jones, Jason W. Myers, James E. Ferrell, and Tobias Meyer. 2005. "STIM Is a Ca^{2+} Sensor Essential for Ca^{2+}-Store-Depletion-Triggered Ca^{2+} Influx." *Curr Biol* 15(13):1235-1241.

Liou, Jen, Marc Fivaz, Takanari Inoue, and Tobias Meyer. 2007. "Live-Cell Imaging Reveals Sequential Oligomerization and Local Plasma Membrane Targeting of Stromal Interaction Molecule 1 after Ca^{2+} Store Depletion." *PNAS* 104(22):9301-9306.

Liu, Ying, Yuanyuan Wu, Jeffrey C. Lee, Haipeng Xue, Larysa H. Pevny, Zaven Kaprielian, and Mahendra S. Rao. 2002. "Oligodendrocyte and Astrocyte Development in Rodents: An in Situ and Immunohistological Analysis during Embryonic Development." *Glia* 40(1):25-43.

Luik, R. M., Wu, M. M., Buchanan, J. and Lewis, R. S. 2006. "The elementary unit of store-operated Ca^{2+} entry: local activation of CRAC channels by STIM1 at ER-plasma membrane junctions." *J Cell Biol* 174(6):815-825.

Liu, X., Cheng, K. T., Bandyopadhyay, B. C., Pani, B., Dietrich, A., Paria, B. C., Swaim, W. D., Beech, D., Yildrim, E., Singh, B. B., Birnbaumer, L. and Ambudkar, I. S. 2007. "Attenuation of store-operated Ca2+ current impairs salivary gland fluid secretion in TRPC1(-/-) mice." *PNAS* 104(44):17542-17547.

Lopez, J. J., Salido, G. M., Pariente, J. A. and Rosado, J. A. 2006. "Interaction of STIM1 with endogenously expressed human canonical TRP1 upon depletion of intracellular Ca^{2+} stores." *J Biol Chem* 281(38):28254-28264.

Lytton, J., M. Westlin, and M. R. Hanley. 1991. “Thapsigargin Inhibits the Sarcoplasmic or Endoplasmic Reticulum Ca-ATPase Family of Calcium Pumps.” *J Biol Chem* 266:17067-17071.

Macián, Fernando, Francisco García-Cózar, Sin Hyeog Im, Heidi F. Horton, Michael C. Byrne, and Anjana Rao. 2002. “Transcriptional Mechanisms Underlying Lymphocyte Tolerance.” *Cell* 109(6):719-731.

Martin, A. C. L. 2006. “Capacitative and 1-Oleyl-2-Acetyl-Sn-Glycerol-Activated Ca^{2+} Entry Distinguished Using Adenylyl Cyclase Type 8.” *Mol Pharmacol* 70(2):769-777.

Matthews, B. Y. Gary, Erwin Neher, and Reinhold Penner. 1989. “Second Messenger-Activated Calcium Influx in Rat Peritoneal Mast Cells.” *J Physiol* 418:105-130.

McCarthy Ken D and de Vellis J. 1980. “Preparation of separate astroglial and oligodendroglial cell cultures from rat cerebral tissue.” *J Cell Biol* 85(3):890-902.

Mehta, Vandana, Saurav Kisalay, and C. Balachandran. 2009. “Leflunomide.” *Indian J Dermatol Venereol Leprol* 75(4):422.

Mercer, J. C., Dehaven, W. I., Smyth, J. T., Wedel, B., Boyles, R. R., Bird, G. S. and Putney, J. W., Jr. 2006. “Large store-operated calcium selective currents due to co-expression of Orai1 or Orai2 with the intracellular calcium sensor, Stim1.” *J Biol Chem* 281(34):24979-24990.

Mei, F., Fancy, S.P.J., Shen, Y.A., Niu, J., Zhao, C., Presley, B., Miao, E., Lee, S., Mayoral, S.R., Redmond, S.A. 2014) “Micropillar arrays as a high- throughput screening platform for therapeutics in multiple sclerosis.” *Nat Med* 20:954-960.

Mignen, O., Thompson, J. L. and Shuttleworth, T. J. 2008. “Both Orai1 and Orai3 are essential components of the arachidonate-regulated Ca^{2+}-selective (ARC) channels.” *J Physiol* 586(1):185-195.

Muik, Martin, Marc Fahrner, Isabella Derler, Rainer Schindl, Judith Bergsmann, Irene Frischauf, Klaus Groschner, and Christoph Romanin. 2009. “A Cytosolic Homomerization and a Modulatory Domain within STIM1 C Terminus Determine Coupling to ORAI1 Channels.” *J Biol Chem* 284(13):8421–8426.

Mukherjee, Sreya and Wesley H. Brooks. 2014. “Stromal Interaction Molecules as Important Therapeutic Targets in Diseases with Dysregulated Calcium Flux.” *Biochim Biophys Acta Mol Cell Res* 1843(10):2307-2314.

Najm, F.J., Madhavan, M., Zaremba, A., Shick, E., Karl, R.T., Factor, D.C., Miller, T.E., Nevin, Z.S., Kantor, C., Sargent, A. 2015. "Drug-based modulation of endogenous stem cells promotes functional remyelination in vivo." *Nature* 522:216-220.

Nakanishi, Shigetada and Okazawa, Makoto. 2006. "Membrane potential-regulated Ca2+ signalling in development and maturation of mammalian cerebellar granule cells." *J Physiol* 575(2):389-395

Naylor, Edmund, Abdelilah Arredouani, Sridhar R. Vasudevan, Alexander M. Lewis, Raman Parkesh, Akiko Mizote, Daniel Rosen, Justyn M. Thomas, Minoru Izumi, a Ganesan, Antony Galione, and Grant C. Churchill. 2009. "Identification of a Chemical Probe for NAADP by Virtual Screening." *Nat Chem Biol* 5(4):220-226.

Neumann, Björn, Baror, Roey, Zhao, Chao, Segel, Michael, Dietmann, Sabine, Rawji, Khalil S. Foerster, Sarah, McClain, Crystal R. Chalut, Kevin, van Wijngaarden, Peter, Franklin, Robin J.M. 2019. "Metformin Restores CNS Remyelination Capacity by Rejuvenating Aged Stem Cells." *Cell stem cell* 25(4):473-485.

Ng, Siaw Wei, Joseph di Capite, Karthika Singaravelu, and Anant B. Parekh. 2008. "Sustained Activation of the Tyrosine Kinase Syk by Antigen in Mast Cells Requires Local Ca^{2+} Influx through Ca^{2+} Release-Activated Ca^{2+} Channels." *J Biol Chem* 283(46):31348-31355.

Ng, L. C., McCormack, M. D., Airey, J. A., Singer, C. A., Keller, P. S., Shen, X. M. and Hume, J. R. 2009. "TRPC1 and STIM1 mediate capacitative Ca^{2+} entry in mouse pulmonary arterial smooth muscle cells." *J Physiol* 587(11):2429-2442.

Nishiyama A, Komitova M, Suzuki R, and Zhu X. 2009. "Polydendrocytes (NG2 cells): multifunctional cells with lineage plasticity." *Nat Rev Neurosci* 10:9-22.

Ong, H. L., Cheng, K. T., Liu, X., Bandyopadhyay, B. C., Paria, B. C., Soboloff, J., Pani, B., Gwack, Y., Srikanth, S., Singh, B. B., Gill, D. L. and Ambudkar, I. S. 2007. "Dynamic assembly of TRPC1-STIM1-Orai1 ternary complex is involved in store-operated calcium influx. Evidence for similarities in store-operated and calcium release-activated calcium channel components." *J Biol Chem* 282(12):9105-9116.

Ong H. L., and Ambudkar I. S. 2017. "STIM-TRP Pathways and Microdomain Organization: Contribution of TRPC1 in Store-Operated Ca^{2+} Entry: Impact on Ca^{2+} Signaling and Cell Function." *Adv Exp Med Biol* 993:159-188.

Oh, J. and P. W. O'Connor. 2014. "Teriflunomide in the Treatment of Multiple Sclerosis: Current Evidence and Future Prospects." *Ther Adv Neurol Diso* 7(5):239-252.

Oh, Jiwon and Paul W. O'Connor. 2013. "Teriflunomide for the Treatment of Multiple Sclerosis." *Semin Neurol* 33(1):45-55.

Paez, Pablo M., Daniel J. Fulton, Vilma Spreuer, Vance Handley, Celia W. Campagnoni, and Anthony T. Campagnoni. 2009. "Regulation of Store-Operated and Voltage-Operated Ca^{2+} Channels in the Proliferation and Death of Oligodendrocyte Precursor Cells by Golli Proteins." *ASN Neuro* 1(1):25-41.

Paez, Pablo M., Daniel Fulton, Vilma Spreuer, Vance Handley, and Anthony T. Campagnoni. 2011. "Modulation of Canonical Transient Receptor Potential Channel 1 in the Proliferation of Oligodendrocyte Precursor Cells by the Golli Products of the Myelin Basic Protein Gene." *J Neurosci* 31(10):3625-3637.

Papanikolaou M, Lewis A, and Butt AM. 2017. "Store-operated calcium entry is essential for glial calcium signalling in CNS white matter." *Brain Struct Funct* 222(7):2993-3005.

Parekh, A. B., A. Fleig, and R. Penner. 1997. "The Store-Operated Calcium Current I(CRAC): Nonlinear Activation by InsP3 and Dissociation from Calcium Release." *Cell* 89(6):973–80.

Parekh, a. B. and J. W. Putney Jr. 2005. "Store-Operated Calcium Channels." *Physiol Rev* 85(2):757-810.

Parekh, Anant B. 2010. "Store-Operated CRAC Channels: Function in Health and Disease." *Nat Rev Drug Discov* 9(5):399-410.

Park, Chan Young, Paul J. Hoover, Franklin M. Mullins, Priti Bachhawat, Elizabeth D. Covington, Stefan Raunser, Thomas Walz, K. Christopher Garcia, Ricardo E. Dolmetsch, and Richard S. Lewis. 2009. "STIM1 Clusters and Activates CRAC Channels via Direct Binding of a Cytosolic Domain to Orai1." *Cell* 136(5):876-890.

Peinelt, Christine, Annette Lis, Andreas Beck, Andrea Fleig, and Reinhold Penner. 2008. "2-Aminoethoxydiphenyl Borate Directly Facilitates and Indirectly Inhibits STIM1-Dependent Gating of CRAC Channels." *J Physiol* 586(13):3061-3073.

Peters-Golden, M., M. M. Gleason, and A. Togias. 2006. "Cysteinyl Leukotrienes: Multi-Functional Mediators in Allergic Rhinitis." *Clin Exp Allergy* 36(6):689-703.

Pfeiffer, S., Warrington,a and Bansal, R.,1993. “The oligodendrocyte and its many cellular processes.” *Trends Cell Biol* 3(6):191-197.

Pihan, E., L. Colliandre, J. F. Guichou, and D. Douguet. 2012. “E-Drug3D: 3D Structure Collections Dedicated to Drug Repurposing and Fragment-Based Drug Design.” *Bioinformatics* 28(11):1540-1541.

Pozzan, T., R. Rizzuto, P. Volpe, and J. Meldolesi. 1994. “Molecular and Cellular Physiology of Intracellular Calcium Stores.” *Physiol Rev* 74(3):595-636.

Prakriya, M. and R. S. Lewis. 2001. “Potentiation and Inhibition of Ca^{2+} Release-Activated Ca^{2+} Channels by 2-Aminoethyldiphenyl Borate (2-APB) Occurs Independently of IP(3) Receptors.” *J Physiol* 536(1):3-19.

Prakriya, Murali, Stefan Feske, Yousang Gwack, Sonal Srikanth, Anjana Rao, and Patrick G. Hogan. 2006. “Orai1 Is an Essential Pore Subunit of the CRAC Channel.” *Nature* 443(7108):230-233.

Prakriya, Murali and Richard S. Lewis. 2015. “Store-Operated Calcium Channels Pharmacology.” *Physiol Rev* 95(307):1383-1436.

Psachoulia K, Jamen F, Young KM, and Richardson WD. 2009. “Cell cycle dynamics of NG2 cells in the postnatal and ageing brain.” *Neuron Glia Biol* 5:57-67.

Putney, J. W. Jr. 1986. “A Model for Receptor-Regulated Calcium Entry.” *Cell Calcium* 7(1):1-12.

Putney, James W. 2005. “Capacitative Calcium Entry.” *J Cell Biol* 169(3):381-382.

Putney, James W., Lisa M. Broad, Franz Josef Braun, Jean Philippe Lievremont, and Gary St J. Bird. 2001. “Mechanisms of Capacitative Calcium Entry.” *J Cell Sci* 114(12):2223-2229.

Putney, James W. 2009. “Capacitative Calcium Entry: From Concept to Molecules.” *Immunol Rev* 231(1):10-22.

Putney, James W. 2010. “Store-Operated Calcium Channels.” *Mol Interv* 10(4):209-218.

Rabe, Klaus F. 2011. “Update on Roflumilast, A phosphodiesterase 4inhibitor for the Treatmentof Chronic Obstructive pulmonary Disease.” *Br J Pharmacol* 163:53-67.

Ribeiro, Carla M. Pedros., Jeffrey Reece, and James W. Putney. 1997. “Role of the Cytoskeleton in Calcium Signaling in NIH 3T3 Cells. An Intact Cytoskeleton is Required for

Agonist-Induced [Ca^{2+}], Signaling, but Not for Capacitative Calcium Entry." *J Biol Chem* 272(42):26555-26561.

Rivers LE, Young KM, Rizzi M, Jamen F, Psachoulia K, Wade A, Kessaris N, and Richardson WD. 2008. "PDGFRA/NG2 glia generate myelinating oligodendrocytes and piriform projection neurons in adult mice." *Nat Neurosci* 11:1392-1401.

Roberts-Thomson, Sarah J., Amelia a Peters, Desma M. Grice, and Gregory R. Monteith. 2010. "ORAI-Mediated Calcium Entry: Mechanism and Roles, Diseases and Pharmacology." *Pharmacol Ther* 127(2):121-130.

Roos, J., DiGregorio, P. J., Yeromin, A. V., Ohlsen, K., Lioudyno, M., Zhang, S., Safrina, O., Kozak, J. A., Wagner, S. L., Cahalan, M. D., Velicelebi, G. and Stauderman, K. A. 2005. "STIM1, an essential and conserved component of store-operated Ca^{2+} channel function." *J Cell Biol* 169(3):435-445.

Ross, R. a, B. a Spengler, and J. L. Biedler. 1983. "Coordinate Morphological and Biochemical Interconversion of Human Neuroblastoma Cells." *J Natl Cancer Inst* 71(4):741-747.

Ross, P. E. and M. D. Cahalan. 1995. "Ca^{2+} Influx Pathways Mediated by Swelling or Stores Depletion in Mouse Thymocytes." *J Gen Physiol* 106(3):415-444.

Roy K, Murtie JC, El-Khodor BF, Edgar N, Sardi SP, Hooks BM, Benoit-Marand M, Chen C, Moore H, O'Donnell P, Brunner D, and Corfas G. 2007. "Loss of erbB signaling in oligodendrocytes alters myelin and dopaminergic function, a potential mechanism for neuropsychiatric disorders." *PNAS* 104:8131-8136.

Sadaghiani, Amir Masoud, Sang Min Lee, Justin I. Odegaard, Dennis B. Leveson-Gower, Olivia M. McPherson, Paul Novick, Mi Ri Kim, Angela N. Koehler, Robert Negrin, Ricardo E. Dolmetsch, and Chan Young Park. 2014. "Identification of Orai1 Channel Inhibitors by Using Minimal Functional Domains to Screen Small Molecule Microarrays." *Chem Biol* 21(10):1278-1292.

Sainas, Stefano, Agnese C. Pippione, Marta Giorgis, Elisa Lupino, Parveen Goyal, Cristina Ramondetti, Barbara Buccinnà, Marco Piccinini, Rodolpho C. Braga, Carolina H. Andrade, Mikael Andersson, Ann Christin Moritzer, Rosmarie Friemann, Stefano Mensa, Salam Al-Kadaraghi, Donatella Boschi, and Marco L. Lolli. 2017. "Design, Synthesis, Biological

Evaluation and X-Ray Structural Studies of Potent Human Dihydroorotate Dehydrogenase Inhibitors Based on Hydroxylated Azole Scaffolds." *Eur J Med Chem* 129:287-302.

Schein, Catherine H. 2019. "Repurposing Approved Drugs on the Pathway to Novel Therapies." *Med Res Rev* 40:1–20.

Schmidt S, Liu G, Liu G, Yang W, Honisch S, Pantelakos S, Stournaras C, Hönig A, and Lang F. 2014. Enhanced Orai1 and STIM1 expression as well as store operated Ca2+ entry in therapy resistant ovary carcinoma cells. *Oncotarget* 5(13):4799-4810.

Scholzen T, and Gerdes J. 2000. "The Ki-67 protein: from the known and the unknown." *J Cell Physiol* 182(3):311-322.

Shafiee Nick, Reza, Amir R. Afshari, Seyed Hadi Mousavi, Abbasali Rafighdoust, Vahid Reza Askari, Hamid Mollazadeh, Sahar Fanoudi, Elmira Mohtashami, Vafa Baradaran Rahimi, Moein Mohebbi, and Mohammad Mahdi Vahedi. 2017. "A Comprehensive Review on the Potential Therapeutic Benefits of Phosphodiesterase Inhibitors on Cardiovascular Diseases." *Biomed Pharmacother* 94:541-555.

Shin, Jai Moo, Michel Homerin, Florence Domagala, Hervé Ficheux, and George Sachs. 2006. "Characterization of the Inhibitory Activity of Tenatoprazole on the Gastric H^+,K^+ -ATPase in Vitro and in Vivo." *Biochem Pharmacol* 71(6):837-849.

Shin, Jai Moo and Nayoung Kim. 2013. "Pharmacokinetics and Pharmacodynamics of the Proton Pump Inhibitors." *J Neurogastroenterol Motil* 19(1):25-35.

Shoaf, Susan E., Patricia Bricmont, and Suresh Mallikaarjun. 2014. "Pharmacokinetics and Pharmacodynamics of Oral Tolvaptan in Patients with Varying Degrees of Renal Function." *Kidney Int* 85(4):953-961.

Sidell N. 1982. "Retinoic Acid-Induced Growth Inhibition and Morphologic Differentiation of Human Neuroblastoma Cells in Vitro." *J Natl Cancer Inst* 68(4):589-596.

Simons, Mikael and Lyons, David A. 2013. "Axonal selection and myelin sheath generation in the central nervous system." *Curr Opin Cell Biol* 25(4):512-519.

Siraganian, Reuben P. and William A. Hook. 1975. "Ionophore A-23187 Induced Histamine Release from Rat Mast Cells and Rat Basophil Leukemia (RBL-1) Cells." *J Immunol* 115:1599-1602.

Smyth, Jeremy T., Wayne I. Dehaven, Gary S. Bird, and James W. Putney. 2008. "Ca^{2+}-Store-Dependent and -Independent Reversal of Stim1 Localization and Function." *J Cell Sci* 121(6):762-772.

Smyth, Jeremy T., Sung-Yong Hwang, Takuro Tomita, Wayne I. DeHaven, Jason C. Mercer, and James W. Putney. 2010. "Activation and Regulation of Store-Operated Calcium Entry." *J Cell Mol Med* 14(10):2337-2349.

Snaidero N, Möbius W, Czopka T, Hekking LH, Mathisen C, Verkleij D, Goebbels S, Edgar J, Merkler D, Lyons DA, Nave KA, and Simons M. 2014. "Myelin membrane wrapping of CNS axons by PI(3,4,5)P3-dependent polarized growth at the inner tongue." *Cell* 156(2):277-290.

Somasundaram, Agila, Andrew K. Shum, Helen J. Mcbride, John A. Kessler, Stefan Feske, and Richard J. Miller. 2014. "Store-Operated CRAC Channels Regulate Gene Expression and Proliferation in Neural Progenitor Cells." *J Neurosci* 34(27):9107-9123.

Squire LR, Bloom FE, McConnel SK, Roberts JL, Spitzer NC, Zigmond M. 2003. "Fundamental neuroscience." In: Squire LR, editor. San Diego: Elsevier. 61-70.

Stathopulos, Peter B., Le Zheng, Guang-Yao Li, Michael J. Plevin, and Mitsuhiko Ikura. 2008. "Structural and Mechanistic Insights into STIM1-Mediated Initiation of Store-Operated Calcium Entry." *Cell* 135(1):110-122.

Strand, Daniel S., Daejin Kim, and David A. Peura. 2017. "25 Years of Proton Pump Inhibitors: A Comprehensive Review." *Gut Liver* 11(1):27-37.

Syed, Yasir A., Alexandra Baer, Matthias P. Hofer, Ginez A. González, Jon Rundle, Szymon Myrta, Jeffrey K. Huang, Chao Zhao, Moritz J. Rossner, Matthew W. B. Trotter, Gert Lubec, Robin J. M. Franklin, and Mark R. Kotter. 2013. "Inhibition of Phosphodiesterase-4 Promotes Oligodendrocyte Precursor Cell Differentiation and Enhances CNS Remyelination." *EMBO Mol Med* 5(12):1918–1934.

Takezawa, Ryuichi, Henrique Cheng, Andreas Beck, Jun Ishikawa, Pierre Launay, Hirokazu Kubota, Jean-Pierre Kinet, Andrea Fleig, Toshimitsu Yamada, and Reinhold Penner. 2006. "A Pyrazole Derivative Potently Inhibits Lymphocyte Ca^{2+} Influx and Cytokine Production by Facilitating Transient Receptor Potential Melastatin 4 Channel Activity." *Mol Pharmacol* 69(4):1413-1420.

Taniguchi T. 1995. “Cytokine signaling through nonreceptor protein tyrosine kinases.” *Science* 268(5208):251-255.

Temple S and Raff MC.1986. “Clonal analysis of oligodendrocyte development in culture: evidence for a developmental clock that counts cell divisions.” *Cell* 44:773-779.

Thibonnier M, Coles P, Thibonnier A, and Shoham M. 2001. “The basic and clinical pharmacology of nonpeptide vasopressin receptor antagonists.” *Annu Rev Pharmacol Toxicol* 41:175-202.

Tong XP, Li XY, Zhou B, Shen W, Zhang ZJ, and Xu TL, Duan S. 2009. “Ca^{2+} signaling evoked by activation of Na^{+} channels and Na^{+}/Ca^{2+} exchangers is required for GABA-induced NG2 cell migration.” *J Cell Biol* 186:113-128.

Toth, Anna B., Shum, Andrew K. and Prakriya, Murali. 2016. “Regulation of neurogenesis by calcium signalling.” *Cell Calcium* 59:124-134.

Tsujii T. 2000. Comparison of prazosin, terazosin and tamsulosin in the treatment of symptomatic benign prostatic hyperplasia: a short-term open, randomized multicenter study. *Int J Urol* 7(6):199-205.

Umemura M, Baljinnyam E, Feske S, De Lorenzo MS, Xie LH, Feng X, Oda K, Makino A, Fujita T, Yokoyama U, Iwatsubo M, Chen S, Goydos JS, Ishikawa Y, and Iwatsubo K. 2014. Store-operated Ca2+ entry (SOCE) regulates melanoma proliferation and cell migration. *PLoS One* 9(2):e89292.

Van't Veer A, Du Y, Fischer TZ, Boetig DR, Wood MR, and Dreyfus CF. 2009. “Brain-derived neurotrophic factor effects on oligodendrocyte progenitors of the basal forebrain are mediated through trkB and the MAP kinase pathway.” *J Neurosci Res* 87:69-78.

Vasudevan SR, Moore JB, Schymura Y, and Churchill GC. 2012. Shape-based reprofiling of FDA-approved drugs for the H_1 histamine receptor. *J Med Chem* 55(16):7054-7060.

Vaughan, P. F., C. Peers, and J. H. Walker. 1995. “The Use of the Human Neuroblastoma SH-SY5Y to Study the Effect of Second Messengers on Noradrenaline Release.” *Gen Pharmacol* 26(6):1191-1201.

Venkiteswaran G, and Hasan G. 2009. “Intracellular Ca^{2+} signaling and store- operated Ca^{2+} entry are required in Drosophila neurons for flight.” *PNAS* 106:10326-10331.

Victoria Boswell-Smith, Domenico Spina, and Clive P Page. 2017. “Phosphodiesterase Inhibitors.” *Br J Pharmacol* 147:252-257.

Vig, M., C. Peinelt, A. Beck, D. L. Koomoa, D. Rabah, M. Koblan-Huberson, S. Kraft, H. Turner, A. Fleig, R. Penner, and J. P. Kinet. 2006. “CRACM1 Is a Plasma Membrane Protein Essential for Store-Operated Ca^{2+} Entry.” *Science* 312(5777):1220-1223.

Vyas, Vivek K., Bhavesh Variya, and Manjunath D. Ghate. 2014. “Design, Synthesis and Pharmacological Evaluation of Novel Substituted Quinoline-2-Carboxamide Derivatives as Human Dihydroorotate Dehydrogenase (HDHODH) Inhibitors and Anticancer Agents.” *Eur J Med Chem* 82:385-393.

Wang, J. Y., J. Sun, M. Y. Huang, Y. S. Wang, M. F. Hou, Y. Sun, H. He, N. Krishna, S. J. Chiu, S. Lin, S. Yang, and W. C. Chang. 2015. “STIM1 Overexpression Promotes Colorectal Cancer Progression, Cell Motility and COX-2 Expression.” *Oncogene* 34(33):4358-4367.

Walsh, Ciara M, Doherty, Mary K, Tepikin, Alexei V, and Burgoyne, Robert D. 2010. “Evidence for an interaction between Golli and STIM1 in store-operated calcium entry.” *Biochem J* 430:453-460.

Williams, R. T., Manji, S. S., Parker, N. J., Hancock, M. S., Van Stekelenburg, L., Eid, J. P., Senior, P. V., Kazenwadel, J. S., Shandala, T., Saint, R., Smith, P. J. and Dziadek, M. A. 2001. “Identification and characterization of the STIM (stromal interaction molecule) gene family: coding for a novel class of transmembrane proteins.” *Biochem J* 357(3):673-685.

Wilson, A. P., C. E. Pullar, A. M. Camp, and B. A. Helm. 1993. “Human IgE Mediates Stimulus Secretion Coupling in Rat Basophilic Leukemia Cells Transfected with the Alpha Chain of the Human High-Affinity Receptor.” *Eur J Immunol* 23(1):240-244.

Wu, Minnie M., JoAnn Buchanan, Riina M. Luik, and Richard S. Lewis. 2006. “Ca2+ Store Depletion Causes STIM1 to Accumulate in ER Regions Closely Associated with the Plasma Membrane.” *J Cell Biol* 174(6):803-813.

Xie, Jiansheng, Hongming Pan, Junlin Yao, Yubin Zhou, and Weidong Han. 2016. “SOCE and Cancer: Recent Progress and New Perspectives.” *Int J Cancer* 138(9):2067-2077.

Yamashita, Megumi and Murali Prakriya. 2014. “Divergence of Ca^{2+} Selectivity and Equilibrium Ca^{2+} Blockade in a Ca^{2+} Release-Activated Ca^{2+} Channel.” *J Gen Physiol* 143(3):325-343.

Yan, X., C. Liao, Z. Liu, Hagler At, Q. Gu, and J. Xu. 2016. “Chemical Structure Similarity Search for Ligand-Based Virtual Screening : Methods and Computational Resources .” *Curr Drug Targets* 17(14):1580-1585.

Yang, Ning, Ying Tang, Fang Wang, Haibin Zhang, Dan Xu, Yafeng Shen, Shuhan Sun, and Guangshun Yang. 2013. “Blockade of Store-Operated Ca^{2+} Entry Inhibits Hepatocarcinoma Cell Migration and Invasion by Regulating Focal Adhesion Turnover.” *Cancer Lett* 330:163-169.

Yang SL, Cao Q, Zhou KC, Feng YJ, and Wang YZ. 2009. Transient receptor potential channel C3 contributes to the progression of human ovarian cancer. *Oncogene* 28(10):1320-1328.

Yang, Shengyu, J. Jillian Zhang, and Xin Y. Huang. 2009. “Orai1 and STIM1 Are Critical for Breast Tumor Cell Migration and Metastasis.” *Cancer Cell* 15(2):124-134.

Yara Fragoso &Joseph Bidin. 2015. “Leflunomide and Teriflunomide: Altering the Metabolism of Pyrimidines for the Treatment of Autoimmune Diseases.” *Expert Rev Clin Pharmacol* 8(3):315-320.

Yazbeck, Pascal, Mohammad Tauseef, Kevin Kruse, Md Ruhul Amin, Rayees Sheikh, Stefan Feske, Yulia Komarova, and Dolly Mehta. 2017. “STIM1 Phosphorylation at Y361 Recruits Orai1 to STIM1 Puncta and Induces Ca^{2+} Entry.” *Sci Rep* 7:1-11.

Yeromin, A. V. 2004. “A Store-Operated Calcium Channel in Drosophila S2 Cells.” *J Gen Physiol* 123(2):167-182.

Yoshida J, Iwabuchi K, Matsui T, Ishibashi T, Masuoka T, and Nishio M. 2012. Knockdown of stromal interaction molecule 1 (STIM1) suppresses store-operated calcium entry, cell proliferation and tumorigenicity in human epidermoid carcinoma A431 cells. *Biochem Pharmacol* 84(12):1592-1603.

Yuan, J. P., Zeng, W., Huang, G. N., Worley, P. F. and Muallem, S. 2007. “STIM1 heteromultimerizes TRPC channels to determine their function as store-operated channels.” *Nat Cell Biol* 9(6):636-645.

Zagranichnaya, Tatiana K., Xiaoyan Wu, and Mitchel L. Villereal. 2005. “Endogenous TRPC1, TRPC3, and TRPC7 Proteins Combine to Form Native Store-Operated Channels in HEK-293 Cells.” J Biol Chem 280(33):29559-29569.

Zanto, Theodore P., Kelly Hennigan, Mattias Östberg, Wesley C. Clapp, and Adam Gazzaley. 2011. “Chemico-Genetic Identification of Drebrin as a Regulator of Calcium Responses.” *Int J Biochem Cell Biol* 46(4):564-574.

Zhang, Shenyuan L., Ying Yu, Jack Roos, J. Ashot Kozak, Thomas J. Deerinck, Mark H. Ellisman, Kenneth A. Stauderman, and Michael D. Cahalan. 2005. “STIM1 is a Ca^{2+} Sensor That Activates CRAC Channels and Migrates from the Ca^{2+} Store to the Plasma Membrane.” *Nature* 437(7060):902-905.

Zhao X, He X, Han X, Yu Y, Ye F, Chen Y, Hoang T, Xu X, Mi QS, Xin M, Wang F, Appel B, and Lu QR. 2010. “MicroRNA-mediated control of oligodendrocyte differentiation.” *Neuron* 65:612-626.

Zhu X, Bergles DE, Nishiyama A. 2008. “NG2 cells generate both oligodendrocytes and gray matter astrocytes.” *Development* 135:145-157.

Zitt, Christof, Bettina Strauss, Eva C. Schwarz, Nicola Spaeth, Georg Rast, Armin Hatzelmann, and Markus Hoth. 2004. “Potent Inhibition of Ca^{2+} Release-Activated Ca^{2+} Channels and T-Lymphocyte Activation by the Pyrazole Derivative BTP2.” J Biol Chem 279(13):12427-12437.

Zweifach, a and R. S. Lewis. 1993. “Mitogen-Regulated Ca^{2+} Current of T Lymphocytes Is Activated by Depletion of Intracellular Ca^{2+} Stores.” *PNAS* 90(13):6295-6299.